# SPECTROSCOPIC CHARACTERIZATION and CHARGING/DISCHARGING PROPERTIES of BIMETALLIC and CORE-SHELL Au-Ag NANOPARTICLES

**A THESIS**
**SUBMITTED TO THE DEPARTMENT OF CHEMISTRY**
**AND THE INSTITUTE OF ENGINEERING AND SCIENCES**
**OF BILKENT UNIVERSITY**
**IN PARTIAL FULFILLMENT OF THE REQUIREMENTS**
**FOR THE DEGREE OF**
**DOCTOR OF PHILOSOPHY**

**By**
**İLKNUR TUNÇ**

**May 2008**

I certify that I have read this thesis and that in my opinion it is fully adequate, in scope and quality, as a dissertation for the degree of doctor of philosophy.

_____

Prof. Dr. Şefik Süzer (Supervisor)

I certify that I have read this thesis and that in my opinion it is fully adequate, in scope and quality, as a dissertation for the degree of doctor of philosophy.

_____

Prof. Dr. Saim Özkar

I certify that I have read this thesis and that in my opinion it is fully adequate, in scope and quality, as a dissertation for the degree of doctor of philosophy.

_____

Prof. Dr. Ömer Dağ

I certify that I have read this thesis and that in my opinion it is fully adequate, in scope and quality, as a dissertation for the degree of doctor of philosophy.

_____

Assoc. Prof. Dr. Oğuz Gülseren

I certify that I have read this thesis and that in my opinion it is fully adequate, in scope and quality, as a dissertation for the degree of doctor of philosophy.

_____

Asst. Prof. Dr. Emrah Özensoy

Approved for the Institute of Engineering and Science:

_____

Prof. Dr. Mehmet Baray
Director of the Institute

## ABSTRACT

**SPECTROSCOPIC CHARACTERIZATION and CHARGING/DISCHARGING PROPERTIES of BIMETALLIC and CORE-SHELL Au-Ag NANOPARTICLES**

**İLKNUR TUNÇ**

**Ph.D. in Chemistry**

**Supervisor: Prof. Dr. Şefik Süzer**

**May 2008**

The purpose of this work, is to investigate optical and electrical properties of bimetallic alloy and core-shell Au and Ag nanoparticles by optical spectroscopy and XPS, respectively. Several objectives have been pursued in achievement of the goals. First goal is to investigate the tunability of optical properties of bimetallic Au and Ag alloy and core-shell nanoparticles due to changes in *composition* and *structure.* The second goal is to study the possibility of *charge-storage* on single metal particles, especially on Au and Ag, and bimetallic alloy forms of the corresponding nanoparticles in solution. Within this framework, bimetallic Au-Ag alloy and core-shell particles are synthesized, then their electron-storage capacities in aqueous media by introduction of sodium borohydride is followed by spectral shifts in their surface

plasmon resonance bands. Moreover, the parameters like composition, structure, affecting the charging ability of particles are reported by means of optical spectroscopy as well. In addition, electron storing/releasing capacities of Au and Ag nanoparticles and their kinetics are investigated.

In the second part, main focus is to investigate optical and electric properties by surface modification through incorporating Au and Ag nanoparticles within dielectric shell (silica and titania). Therefore, small $Au@SiO_2$, $Ag@SiO_2$, and $Ag@TiO_2$ core-shell nanoparticles with the metal core size ca. 5-7.5 nm and the shell size ca. 3-7.5 nm are synthesized and optical properties of these nanoparticles are studied. These nanoparticles are also analyzed by XPS under external biasing to get further understanding of their charging capacities. Additionally, we investigated incorporating metal nanoparticles within titania shell to provide enhanced photoactivity through the metal core by means of increased charging capacity.

**Key words:** Au-Ag Alloy Nanoparticles, Au-Ag Core-Shell Nanoparticles, Electron Storing/Releasing, Surface Plasmon Resonance, Metal@Dielectric Core-Shell Nanoparticles, Charging/Discharging of Core-Shell Nanoparticles, XPS Characterization of Core-Shell Nanoparticles.

# ÖZET

## BİMETALİK ve ÇEKİRDEK-KABUK Au-Ag NANOPARÇACIKLARIN SPEKTROSKOPİK KARAKTERİZASYONU ve YÜKLENME/YÜK BOŞALMASI ÖZELLİKLERİ

**İLKNUR TUNÇ**
**Danışman: Prof. Dr. Şefik Süzer**
**Mayıs 2008**

Bu çalışmanın amacı; bimetalik alaşım ve çekirdek-kabuk Au ve Ag nanoparçacıklarının optik ve elektriksel özelliklerinin sırasıyla optik spektroskopisi ve XPS ile araştırılmasıdır. Bu amaca ulaşabilmek için birçok hedef ve yöntem izlenmiştir. İlk amaç, bimetalik Au ve Ag alaşım ve çekirdek-kabuk nanoparçacıklarının, bileşim ve yapısal değişimlerinden doğan optik özelliklerin değişimlerinin incelemesidir. İkinci amaç, tek metal nanoparçacıkların (özellikle Au ve Ag) ve bunların bimetalik alaşımlarının çözelti içerinde yük depolanma özelliklerinin çalışılmasıdır. Bu çerçevede bimetalik Au ve Ag alaşım ve çekirdek-kabuk nanoparçacıkları sentezlenmiş, bunların sulu ortamdaki elektron depolama kapasiteleri, sodyumborhidrür eklenmesiyle, yüzey plazma rezonans bantlarındaki spektral değişimlerle takip edilmiştir. Ek olarak, parçacıkların yüklenme yeteneklerini etkileyen parametrelerden bileşim ve yapı, optik spektroskopi yoluyla rapor

edilmiştir. İkinci kısımda, Au ve Ag nanoparçacıklarının elektron depolanma/bırakma kapasiteleri ve bunların kinetiği incelenmiştir.

İkinci bölümde, yüzey modifikasyonuyla hazırlanan, Au ve Ag nanoparçacıklarının dielektrik kabuk içerisindeki, optik ve elektrik özelliklerinin araştırılması ana amaçtır. Buna bağlı olarak, çekirdek yarıçapı 5-7.5 nm, kabuk kalınlığı 3-7.5 nm olan $Au@SiO_2$, $Ag@SiO_2$, and $Ag@TiO_2$ çekirdek-kabuk nanoparçacıkları sentezlenmiş ve bu parçacıkların yüklenme kapasitelerinin daha iyi anlaşılabilmesi için numuneye dışarıdan voltaj uygularak XPS analizleri yapılmıştır. Ek olarak, metal nanoparçacıkları titanya kabuk içerisine yerleştirildiğinde, metalin yüklenmesi yoluyla titanyanın foto aktivitesinin artırılması incelenmiştir.

**Anahtar Kelimeler**: Au-Ag Alaşım Nanoparçacıkları, Au-Ag Çekirdek-Kabuk Nanoparçacıkları, Yüzey Plazma Rezonans, Electron Depolama/Bırakma, Metal@Dielektrik Çekirdek-Kabuk Nanoparçacıkları, Yüklenme/Yük boşalma, Çekirdek-Kabuk Nanoparçacıklarının XPS Karakterizasyonu.

## ACKNOWLEDGEMENTS

I gratefully thank my supervisor Prof. Şefik Süzer for his supervision, suggestions and guidance throughout the development of this thesis.

I would like to thank Prof. Saim Özkar, Prof. Ömer Dağ, Assoc. Prof. Oğuz Gülseren, and Asst. Prof. Emrah Özensoy for reading and commenting on this thesis.

Also, I would like to thank the members of our lab; Dr. Gülay Ertaş, Can Pınar Cönger, Hacı Osman Güvenç, Hikmet Sezen, Eda Özkaraoğlu for their help and friendship.

I apperiate the moral support by dear friends; Emine Yiğit, Şerife Okur, Altuğ Poyraz, Mustafa Fatih Genişel, Cemal Albayrak, Halil İbrahim Okur, İlknur Çayırtepe, Olga Samarskaya, Sündüz Erbaş, Yurdanur Türker, and Elif Aydoğdu.

Finally, my deepest thank go to my dear husband Celal Alp Tunç, and my family; Hasan Kaya, Gül Kaya, Öznur Kaya, Emre Kaya, Fatma Şükran Tunç, Osman Tunç, Gökhan Tunç, Gülay Gülşen.

**TABLE OF CONTENTS**

**LIST OF FIGURES**

# 1. INTRODUCTION

## *1.1. Optical Response of Metal Nanoparticles*

Intelligent use of metal nanoparticles for decoration purposes dates back to Roman times. One of the famous examples is the *glass Lycurgus Cup (4$^{th}$ century AD),* exhibited in British Museum. Since it contains Au and Ag nanoparticles, it is wine-colored red in transmitted light, however, appears green in reflected light.[1, 2] Today especially Au and Ag nanoparticles have attracted the interest of many scientists because of their unique optical properties due to so-called the surface plasmon resonance.

### *1.1.1. Surface Plasmon Resonance (SPR)*

The origin of unique optical properties of metal nanoparticles is attributed to SPR, which involves the interaction between incident electromagnetic radiation and surface electrons of the metal nanoparticles. When the oscillation modes of incident electromagnetic radiation are coupled to oscillation of the collective oscillation of conduction electrons, surface plasmons are generated. They are characterized by strong field enhancement at the interface, while electrical fields decay away from the surface. When dimensions are decreased, boundary and surface effects become more significant so that optical properties of metal nanoparticles are dominated by such collective oscillations of conduction electrons in resonance with electromagnetic radiation.[3] For

metals such as, Pb, Hg, Sn, the plasmon frequency spans the UV region, as a result they do not show significant color. For noble metals such as Au, Ag, Cu plasmon frequency shifts into the visible region.[3] Therefore, surface plasmon experiments are mostly performed using them. Formation of a surface plasmon is simply explained as follows; the electrical field of the incoming radiation induces a polarization in the nanoparticle, and then restoring force exists which tries to compensate it in order that a unique resonance frequency matches these electron oscillation within the nanoparticle as seen in scheme 1.1[4]

Resonance frequency, $\omega_1$ is given by the following expression;

$$\omega_1 = \left(\frac{e^2}{\varepsilon_0 m_e 4\pi r_s^3}\right)^{1/2} \qquad (1.1)$$

where $r_s$ is the radius of a sphere whose volume is equal to the volume per conduction electron in the bulk, $m_e$ is the effective mass and $\varepsilon_0$ is the vacuum permittivity. Sometimes, $\omega_1$ is inferred as the classical surface plasmon frequency. The term surface comes from the fact that, though all electrons oscillate with respect to positive background, the main effect producing the restoring force is the surface polarization (Scheme 1.1).[3]

Though, interests mostly focus on the size effect, resonance frequency also depends on other additional parameters, such as particle shape, composition, surrounding medium etc. These parameters will be discussed extensively, in the following sections.

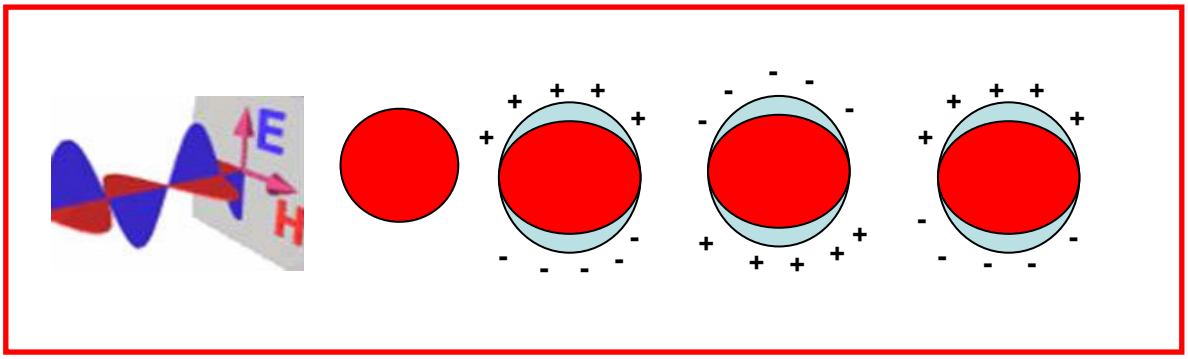


Scheme 1.1. Schematic drawing of the interaction of metal nanoparticles with incident electromagnetic radiation.

*1.1.1.1. Size Dependency*

Particularly, size dependence of the plasmon resonance band of gold nanoparticles has been extensively investigated.[5-17] Gold and silver nanoparticles smaller than 5 nm in diameter do not exhibit significant absorption in UV-vis region. However, particles of 5-50 nm show strong absorption bands around 390-420 and 520-560 nm for Ag and Au respectively.[10, 11] As the particles' sizes increase, absorption bands broaden and shift to higher wavelengths (red-shift).[5, 6, 14] When the particles' sizes increase, wavelength of the interacting light become comparable to the size of the nanoparticle. This brings about an inhomogeneous surface polarization by incident electrical field. The band broadening is then attributed to retardation effects during the surface polarization.[3]

*1.1.1.2. Composition Dependency*

The properties of combination of various metals in nanoscale can be very different from their own monometallic nanoparticles. This provides another point of view to tailor the properties of nanomaterials besides size and shape. For Instance, Au-Ag nanoalloys are more catalytically active than monometallic ones for the oxidation of CO.[18] Effect of alloying on optical dependency will be discussed in the next section.

*1.1.1.2.1. Bimetallic Au-Ag Alloy Nanoparticles*

When nanoparticles are composed of various metals, the resulting physicochemical properties of the materials, particularly optical properties are determined by both composition and actual distribution within the nanoparticles. Various nanoscale bimetallic systems have been investigated.[15, 19, 20] Particularly, combination of gold and silver is interesting, mainly for two reasons; i) both metals have intense and well-defined surface plasmon absorption bands in the visible region (around 400 and 520 nm for spherical nanoparticles of Ag and Au, respectively), and ii) they form fcc crystals with very similar lattice constants (4.078 Å for Au; 4.086 Å for Ag),[21] therefore, they are able to form bulk substitutional alloy of any composition. Combination of both metals as alloy in nanometric scale is also possible.[22]

Alloying is one of the synthetic routes for shifting the absorption band as was first shown by Papavassilio who prepared 10 nm Au-Ag Alloy nanoparticles in 2-butanol by evaporation and condensation of alloys.[23] Teo et al. prepared a 38 atom Au-Ag clusters

with the composition $Au_{18}Ag_{20}$ having single surface plasmon band at 495 nm.[24] Moreover, Sato et. al synthesized Au-Ag composite colloids (30-150 nm in diameter) consisting of Au and Ag domains by irradiation aqueous solution of Au and Ag ions with 253.7 nm UV-light.[25] Later on, Link et al. prepared bimetallic nanoparticles of gold and silver where the absorption band was shown to be tunable between 380-530 nm by varying only the composition.[22] Presence of a single absorption band and also change in its extinction coefficient, both of which shifted linearly with increasing mole fraction of the gold were taken as the evidence for alloy formation as opposed to core-shell type of a structure. These findings were later substantiated by additional structural (TEM) and other spectroscopic investigations.[26, 27]

Optical properties of both types of particles have been studied by various groups. Although results for alloys are well-accepted and agreed upon, different interpretations have been forwarded for the properties of core-shell structures. In the case of alloy nanoparticles, prepared by simultaneous reduction of metal salts, many authors reported that there is a linear relationship between the composition of the alloy and the position of the plasmon band in wavelength scale, which thus lies between those for pure silver and pure gold nanoparticles.[22, 28] Their colors changes yellow to red as Au content of alloy is increased. Assuming a linear combination of the dielectric data of pure silver and gold as input for Mie calculation, these shifts were modeled.

*1.1.1.3. Shape Dependency*

The metal particles of Au, Ag and Cu have distinct and well-defined surface plasmon absorption band in the visible region. The locations of well-defined plasmon absorption bands of silver and gold particles are shape-dependent. For example, as the shape of silver nanoparticles changes from spherical to trigonal prism, the band shifts from 400 nm to 670 nm.[29] This is related with altering resonance as a result of changing oscillations of conduction electrons that are induced by incident electromagnetic radiation. When spherical Au nanoparticles are elongated (such as nanorods) two distinct resonance modes are possible, as a function of their orientation with respect to direction of the electric field of incoming light. The resonance parallel to long axis of the rods determines the longtitutional surface plasmon absorption (SPL) whereas resonance perpendicular to long axis leads to transverse surface plasmon absorption (SPT). SPL band located at lower energies and with much higher absorption.

Another drastic change of surface plasmon is observed in the case of core-shell nanoparticles, which will discussed in the following.

*1.1.1.3.1. Bimetallic Au-Ag Core-Shell Nanoparticles*

Since optical properties of shell mostly determines the position of plasmon resonance band,[3] deposition of Ag on Au exhibits a drastic change in the position of the SPR band from 520 nm down to 420 nm depending on the thickness of the Ag shell.[28]

The radical change in the SPR band is again the result of altering oscillation mode of conduction electrons with respect to the incident electromagnetic light.[3]

Preparation of core-shell bimetallic nanoparticles has also been reported by several authors, generated by either sequential reduction of different metals or segregation during co-reduction. Extensive optical studies on bimetallic nanoparticle colloids performed during the eighties and early nineties, are summarized in the excellent review by Mulvaney.[15] Particularly, for core-shell nanoparticles containing gold and silver, the work of Morriss and Collins[30] was followed by Henglein et al[31, 32] using γ-radiolysis, and later by various groups using successive chemical reduction in solution. Rivas et al.[33] reported both Au@Ag and Ag@Au by citrate reduction while Srnová-Sloufová et al.[34] used hydroxylamine to grow Au on Ag seeds and Lu et al.[35] deposited silver shells on citrate stabilized gold nanoparticles using ascorbic acid as a reductant and cetyltrimethylammonium chloride (CTAC) as an additional stabilizer during the growth, which yielded moderately monodisperse core-shell particles with tunable shell thickness. Extensive optical studies on Au@Ag were also carried out by Kamat and co-workers.[36] Although the growth of Ag on Au is straightforward, formation of Au on Ag is difficult to achieve because of galvanic displacement with oxidation of $Ag^0$ and reduction of $Au^{3+}$ in solution since standard electrode potential of gold is relatively higher. The standard reduction potential of $Ag^+/Ag$ vs SHG is 0.8 V, whereas that of $AuCl_4^-/Au$ vs SHG is 1 V).[20] In fact, this process has been recently developed by Xia[37] and Mirkin[38] for producing bimetallic complex structures. Following wide-ranging works of Halas et al.[39] and Liz-Marzan et al.[40] are based on using silica as a spacer to obtain stable bimetallic gold and silver core-shell nanoparticles which have independent absorption of both core

and shell. However, silica is so thick to allow direct comparison with other structures. Current experiments illustrate that successive reduction of $AgNO_3$ and $HAuCl_4$ with ascorbic acid on preformed Au seeds (in the presence of CTAB) can be exploited towards the creation of onion-like multilayer bimetallic nanoparticles, which allows various effects with the same system to be studied.[28] Color of the dispersion changes dramatically when subsequent metal layers are deposited on the seeds, since the outermost layer is dominating the interaction with incoming light.[3] The TEM images show sufficient contrast to compare experiments with theoretical calculations using a model for multilayer concentric spheres developed by Quinten based on Mie calculations.[41] Liz-Marzan reported comparison between experimental and calculated optical spectra for sequential deposition of Ag(16 nm), Au(16.5 nm), and Ag(8 nm) layers on 17 nm Au spheres. Though the calculated data is similar to experimental one, deviation especially after third layer (Au) is observed. This is attributed to cumulative effects, including deviation from spherical geometry observed in TEM when third Au layer is grown. A second factor which effect deviation from theory is the assumption of well-defined shell structure. If the layers do not have well-defined structure, the use of dielectric values within the model may not be appropriate.[28] The observed metal distribution, deviates from core-shell structure, in TEM can be both related with galvanic displacement and interdiffusion of Ag atoms into the Au shell resulting to alloy formation exemplified by several groups[42, 43] Thus, all of these discussed results imply that synthesis of well-defined Ag@Au core-shell nanoparticles requires a firm control of the electrochemical potentials and reduction conditions.

*1.1.1.4. Environment Dependency*

Another important parameter affecting the plasmon absorption, is the surrounding environment. Solvent effect can be classified into two categories. i) solvent that alter the refractive index. ii) solvent that complex with the nanoparticle surface. Solvents such as cyclohexane, toluene, o-xylene , cholorobenzene, and o-dicholorobenzene do not have any active functional groups and nanoparticle remains inert. It means that there is no obvious chemical interaction between nanoparticle surface and solvent. The SPR band of TOAB-capped gold nanoparticles in these solvents gradually shifts to longer wavelength with the increasing refractive index of the solvent. The recent report on the effect of surrounding medium showed that refractive index increase[44] and complexation ability of the solvent with nanoparticles lead to red shift.[45]

The effect of surrounding medium on plasmon band can be discussed within the framework of Drude model, which states that plasmon band position is directly related to refractive index of surrounding medium

Similar dependence of solvent dielectric to plasmon band position of Au[46] and Ag[47] has been shown by independent workers. Underwood and Mulvaney observed 10 nm shift in the SPR band of gold nanoparticles, when refractive index of medium changed from 1.375(hexane) to 1.501(benzene).[46] On the contrary, Murray and et al. reported that surface plasmon band of alkenethiolate-protected clusters is almost unchanged with refractive index within such range. As a result of this, they concluded that organic shell influences dielectric environment more than bulk solvent does.[48, 49]

The maximum position of surface plasmon band of gold nanoparticles in solvents such as dimethylformamide (DMF), tetrahydrofuran(THF), dimethylsulfoxide,(DMSO) and acetone remains constant ($\lambda_{max=}$ 521 nm). These polar solvent complexes with Au surface with direct interaction. Stable colloids of Pt, Pd, Au have also been prepared in polar solvents like DMF, DMSO, acetone.[50] The metal clusters, especially gold, have high electron affinity and withdraw the electrons from solvent. These charged particles are stabilized by solvent molecules and repulsive forces between charged particles prevent aggregation.[51, 52] The complexation results change in electron density which directly affects surface plasmon absorption. Also, the surface plasmon absorption band is strongly affected by any absorbed species and dielectric of the medium. Adsorption of $I^-$, $SH^-$ ions induces red-shift in the plasmon band.[53]

*1.1.1.5. Presence of Electron Donor/Acceptor Species*

It is possible to predict shifts in the absorption spectrum of metallic nanoparticles by the Drude Model[15] using the factors which influence the plasmon absorption. The theory emphasizes on two factors; i) dielectric constant of the medium, and ii) density of the electrons. Accordingly, the bulk plasmon frequency of charged particles is proportional to square root of electron density (n) on the particles and inversely proportional to square root of effective mass ($m_{eff}$) and vacuum permittivity ($\varepsilon_0$), as shown in the equation ( $\omega_p^{\,2} = \frac{ne^2}{\varepsilon_0 m_{eff}}$ ). Hence storage of additional electrons on the

nanoparticles is expected to lead to a blue-shift in the spectrum, which was shown to be the case by Kamat et al. by following the extent of the band shift and correlating it with the electron density around particles when irradiated by UV light. [45, 54, 55]

Addition of reducing agents (electron donors) such as sodium borohydride ions also leads to electron storage in the nanoparticles as also evidenced by resulting blue shift.[15] Presence of electron acceptor agents such as nitrobenzene, methyl viologen, thionine prevents electron storage on metal nanoparticles by preferential capturing of the electrons by themselves.[56, 57] The corresponding positive-charge-storage was also reported by Mulvaney et al. by the observation of the red shift in the plasmon absorption band of colloidal silver particles when nucleophilic reagents were present in the solution.[58]

### *1.2. Chemical Reduction Methods for the Preparation of Au and Ag Nanoparticles*

Metal nanoparticles in nanometer sizes have potential applications in many areas. Moreover, size provides control of many of the physical and chemical properties of nanoscale materials including luminescence, conductivity, and catalytic activity.[59, 60] Colloidal particles of varying sizes and shapes have been synthesized using templates,[61] photochemistry,[62] seeds,[63] electrochemistry,[64] and radiolysis.[65]

Chemical reduction of metal salts is the simplest and the most commonly used bulk-solution synthetic method for metal nanoparticles. In this method, a soluble metal salt, a reducing agent, and a stabilizing agent are used for particle synthesis. The stabilizing agent caps the particle and prevents further growth or aggregation. Reducing

agents such as sodium borohydride[66, 67] alcohols,[68] hydrazine,[69] and hydroxylamine,[70] are commonly used for this purpose. The resulting particle size is strongly dependent on the strength of reducing agent. Generally, strong reducing agents yield small particles with narrow size distribution. Polymers and organic molecules bind to particle surface, serving as stabilizers. In the case of citrate reduction of gold and silver colloids, citrate ions serve as both reductant and stabilizer. It is also possible to manipulate the shape and size of the metal nanoparticles as one can control the growth process by the choice of the stabilizer. Whereas citrate reduction produces nearly spherical Au nanoparticles, the same reduction procedure yields relatively large 60-200-nm diameter Ag crystallites with a wide range of size and shape, which states different metals give particles with different size, even though used in the same synthetic route. Citrate is also an important factor for photoconversion of Ag nanospheres to trigonal nanoprism. Exact role of citrate in controlling size and shape of particles was thoroughly discussed by Kamat et al.[71] Henglein et al, investigated the early reduction steps using pulse radiolysis to understand the role of sodium citrate towards the growth of particles.[11] Deriving from colloid chemistry, development of the synthetic methods has allowed the researchers to control various other parameters which affect the properties of metal particles. Such parameters include composition (doping, alloying),[72] surface modification (dielectric or metal shell formation),[54, 73] surface charge,[74] and refractive index of the medium.[15]

### *1.2.1. Chemical Preparation of Bimetallic versus Core-Shell Au-Ag Nanoparticles*

Bimetallic alloy versus core-shell nanoparticles are prepared in different manners. While alloy nanoparticles are synthesized as single step by simultaneous reduction of metal salts, core-shell nanoparticles are generally synthesized by sequential reduction of metal salts as illustrated in Scheme 1.3. Details of synthetic procedures will be discussed specifically in the experimental part.

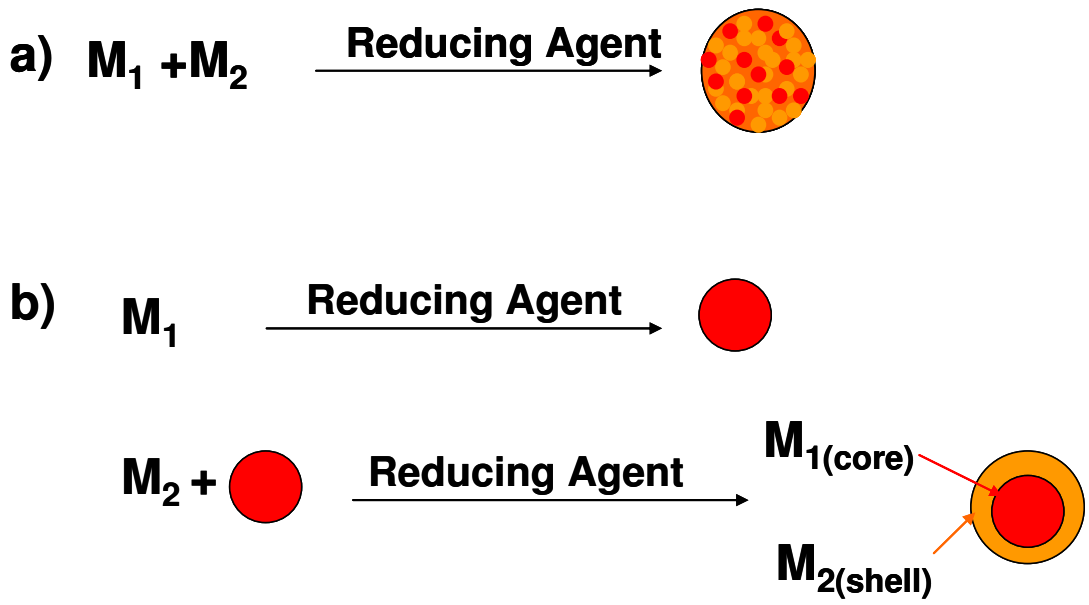


Scheme 1.3**.** Preparation of alloy versus core-shell nanoparticles

## **1.3.** ***Metal(core)@Dielectric(shell) Nanoparticles***

This part is separated into two parts as metal@$SiO_2$ and metal@$TiO_2$ core-shell nanoparticles, as discussed below.

### *1.3.1. Metal(core)@$SiO_2$(shell) Nanoparticles*

The wet chemical synthesis of metal particles offer more economic applications such as solar cells,[75] high density information storage systems,[76] and electrochromic devices.[77] Extremely small electronic capacitors, electrical switches can also be manipulated by chemically prepared metal particles.

The primary difficulty arises in the transfer of these materials out of their solution while keeping their size-dependent properties. In solution the particles are mobile and tend to coalesce due to van der Waals forces unless they are protected. Accordingly, the synthesis of small particles involves rapid nucleation, homogeneous growth, and finally encapsulation stage with polymers, ions, complexing ligands or surfactants to avoid the growth of larger, bulk crystals. Covalently bonded capping ligands are usually engaged with both semiconductor[78, 79] and metal particles.[80, 81] The ligands are chemisorbed to the particle surface terminating crystal growth and simultaneously confer stabilization against coagulation. Such particles can often be dried and redispersed in solvents without coalescence.[82] A number of publications reported that on these capped materials in the form of 2D lattices or 3D networks, possess unusual electronic properties.[83] An adverse complication is that the organic capping agents are susceptible to chemical oxidation, especially under photolysis. Particularly, mercaptans which have a strong affinity for metal chalcogenides and soft metals such as gold or silver are readily oxidized. Devices based on these capping functionalities are likely to be influenced by chemical degradation.

There are some important issues for preserving properties of these particles. Unless they are protected, transfer of the particles from solution causes coalescence, and organic or polymer capping agents, using to prevent aggregation lead to unusual electronic properties or chemical oxidation. To overcome these unfortunate complication, new capping materials, dielectrics (silica, titania, zirconia), have been searched in recent years. Coating metal particles with silicates leads to extra stability and multifunctionality. In particular, superiority of coating with silica over organic stabilizer can be given as follows; i) silica is chemically inert and does not affect redox reactions of core material, ii) silica shell is optically transparent, so that chemical reactions can be monitored spectroscopically, iii) shell can also be used to modulate the position and intensity of colloidal metal surface plasmon absorption bands,[15] iv) the most obvious is that, the shell prevents aggregation of the particles, hence provides protection. An added superiority of silica, is its tendency to form crystal structures which makes silica coating useful to generate 2D or 3D arrays of nanoparticle systems[84]

The usage of silica coating is not new. However, in all earlier work, employed particles were larger, and generally particle coalescence took place during silica deposition. The idea was extended by Furlong,[85] Matijevich,[86] and Philipse[87] who had reported many procedures for coating dispersions. But procedures have not been applied to materials, such as gold and silver dispersions.

A well-known synthetic procedure of silica coating of gold and silver colloids was reported by Liz-Marzan et al.[88] They stated the importance of many parameters which should be optimized during study of synthesis of $Ag@SiO_2$. These parameters are as

follows; pH of solution, concentration of surfactant (APS), concentration of $[SiO3]^{2-}$ etc.[88] (Detailed procedure is given in the experimental section)

*1.3.1.1. Optical Properties of Metal(core)@$SiO_2$(shell) Nanoparticles*

The exact position of this plasmon band is extremely sensitive both to particle size and shape and to the optical and electronic properties of the medium surrounding the particles.[3] Silica is electronically inert, but its refractive index is different from those of both water and ethanol (and of course from that of gold). The influence of the silica layer on the optical properties of the suspension was shown by Liz-Marzan et al.[88] firstly, as the shell thickness was increased, there was an increase in the intensity of the plasmon absorption band, as well as a red shift in the position of the absorption maximum. This is due to the increase in the local refractive index around the particles. However, when the silica shell was sufficiently large, scattering becomes significant, resulting in a strong increase in the absorbance at shorter wavelengths. This effect promotes blue shift of the surface plasmon band and weakening in the apparent intensity of the plasmon band. Finally with the shell thicknesses above 80 nm, the final colloid became very turbid and slightly pink in appearance since the scattering almost completely masks the surface plasmon band.[88]

*1.3.2. Metal(core)@$TiO_2$(shell) Nanoparticles*

Semiconductor-metal nanocomposites have been widely employed in photocatalysis. When a metal contacts with the semiconductor, it greatly enhances the

overall photocatalytic efficiency.[89] The role of which, dictating the charge-transfer processes, is yet to be understood fully. A better understanding of the energetics of such nanocomposite systems is important for tailoring the properties of next-generation nanodevices.

*1.3.2.1. Elementary processes in Dielectric $TiO_2$*

The principle terms involved in a photoactive semiconductor are conduction band (CB), valence band (VB), bandgap, traps sites and Fermi level. The bands are the allowed energy states that an electron can occupy in a material. The highest energy band occupied by an electron is called the valence band while the next available lowest empty energy level, next to valence band is called the conduction band. The bands are clearly differentiated in a semiconductor than in a metal. The Fermi level is usually defined as the top of the valance band. For an n-type semiconductor such as $TiO_2$ the Fermi level is close to the conduction band. A pictorial representation of an n-type semiconductor is shown in Scheme 1.4.

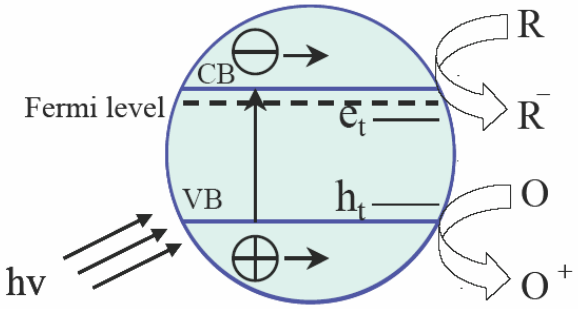


Scheme 1.4. Electron –hole pair generation in a photo illuminated n-type semiconductor nanoparticle.

A semiconductor demonstrates the following processes on photoillumination. Light of energy greater than the band gap of the semiconductor excites the electrons from the valence band to the conduction band leaving behind a hole in the valence band. $TiO_2$, for example, is a large band gap semiconductor and hence produces e-h pairs on illumination with UV light (reaction 1.1). The electrons (e) and holes (h) are available for carrying out redox activities at the semiconductor surface. Photogenerated e-h pairs are also delocalized in the semiconductor. In addition, there also exit localized traps which play important role in photocatalytic activity. These locations are called trap sites ($e_t$ and $h_t$). Both the e-h pairs and traps undergo recombinations which result in decreasing the photocatalytic efficiency of the semiconductor. The number of photogenerated electrons in $TiO_2$ is dictated by the ability of the surroundings to scavenge electrons and holes (reaction 1.2a and 1.2b) and the recombination between the photogenerated e-h pairs (reaction 1.3)

$$\mathbf{TiO_2 \rightarrow TiO_2(\mathit{e} + \mathit{h})} \qquad \mathbf{(1.1)}$$

$$\mathbf{TiO_2(\mathit{e} + \mathit{h}) + O \rightarrow TiO_2(\mathit{e}) + O^+} \qquad \mathbf{(1.2a)}$$

$$\mathbf{TiO_2(\mathit{e} + \mathit{h}) + R \rightarrow TiO_2(\mathit{e}) + R^-} \qquad \mathbf{(1.2b)}$$

$$\mathbf{TiO_2(\mathit{e}+\mathit{h}) \rightarrow TiO_2} \qquad \mathbf{(1.3)}$$

One of the major ideas behind designing composite nanoparticles is to improve the catalytic properties or to tune the luminescent or sensing properties (as given Scheme 1.5). For instance, single component semiconductor nanoparticles display relatively poor

photocatalytic efficiency (<5%) since the majority of the photogenerated charge carriers undergo recombination.[89]

In this framework, incorporating metal particles within titania shell provides interesting features to titania particles. For example, it should be possible to modulate charge transfer properties under band gap excitation so that, metal@$TiO_2$ nanoparticles might be used as superior catalysts or as light energy storage systems. Scheme 1.5 displays charge transfer process between $TiO_2$(shell) and Ag(core) when exposed to UV light.

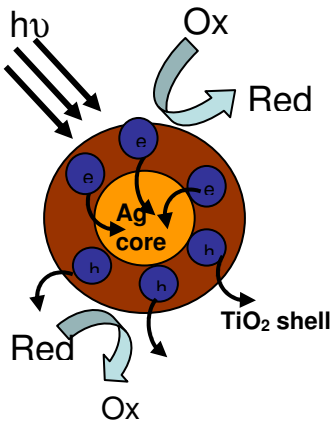


Scheme 1.5. Charge transfer between $TiO_2$(shell) and Ag (core) during photoillumination

Pastoriza-Santos et al. were first to prepare Ag@$TiO_2$ nanoparticles by combination of two procedures. They reported preparation of stable silver nanoparticles by reduction with N,N-dimethylformamide in the presence of a stabilizer.[90] In another study, by condensation polymerization of titanium(triethylaminoto)-isopropoxide in the presence of chelating agent, acetylacetone, formation of titania colloids were also reported.[91] As a result of combination of these two procedures formation of Ag@$TiO_2$

was carried out.[73] Later, modifying this procedure Kamat et al. also prepared $Ag@TiO_2$ nanoparticles which has plasmon band at 480 nm. They reported that large red-shift from 400 nm, which is the characteristic of the plasmon band of pure Ag nanoparticles, to 480 nm is the evidence of titania shell. High refractive index of titania shell leads to large shift in the plasmon absorption of the Ag core.[3] When there is no medium effect, $\lambda_p$ is expected at 136.3 nm, however, for Ag cluster dispersed in water or ethanol, $\lambda_p$ is observed around 390 nm due to the effect of medium. Since $n_{TiO2}(2.5)$ is much higher than $n_{EtOH}(1.359)$, the plasmon absorption band shows large shift. They calculated value of plasmon band as 463 nm. Accordingly, they stated that the slight difference between theoretical and experimental value must be related with some factors such as scattering effect or any absorbed chemical species.[55] They also reported the preparation of reverse case, gold coated titania nanoparticles.[92] Photoinduced charging properties of $Ag@TiO_2$ was reported by same group.[55, 93] When UV-Irradiated, even though $Ag@SiO_2$ displays no shift in the plasmon resonance band, $Ag@TiO_2$ shows large blue-shift (around 60 nm) in the SPR band due to large charge transfer from the shell to the silver core.

### *1.4. X-Ray Photoelectron Spectroscopy*

X-Ray Photoelectron Spectroscopy, XPS, is one of the most powerful surface probe techniques for analysis of solids, thin films and nanostructures. Surface analysis searches for determination of the elemental composition of the outermost layers of materials. Information about the chemical binding state and particular sites of atoms in the crystal structure, surface morphology and also the state of adsorbates can be obtained

by doing more detailed surface analysis.[94] The basic principle of XPS is that, when a sample is subjected to highly energetic X-Rays having energy greater or equal to the binding energy of an electron bound in the atom, a photoelectron, is emitted due to the Einstein equation given as follows; $BE = h\nu - E_K + \varphi$ where BE is the binding energy of the electron, $h\nu$ corresponds to energy of the X-ray, $E_K$ is the kinetic energy of the emitted photoelectron and $\varphi$ is the work function at spectrofotometer. Ultrahigh vacuum system ($<10^{-8}$ torr) is necessary for proper detection, since photoelectrons interact strongly with the atoms around because of their negative charges. Thus, electrons interact with the atoms of the sample during the emission process, then electrons created near the surface, will have greater possibility to leave the sample. Since photoelectrons travel through the sample, they undergo energy losses owing to inelastic scatterings with atoms of the sample. The surface sensitivity of the sample to photoelectrons can be determined by so-called term *inelastic mean free path* ($\lambda$). The electron inelastic mean free path (IMFP) is the average distance, measured along the trajectories that a particle with a given energy travels between following inelastic collisions in a substance. Electrons can travel only a distance of $3\lambda$ through the sample without any significant energy loss. Therefore, photoelectrons emitted from atoms close to surface (<10 nm) reach the detector as the mean free path range from 2 to 4 nm for different materials.[94]

Surface sensitivity of XPS measurements can be increased by reducing the take-off angle of the photoelectrons, down to 1-2 nm levels. It is also practical to determine the thicknesses of the layers and extracting information about the distribution of various atoms/clusters within different overlayers.[95, 96]

Since electrons are emitted from a sample, a positive charge is generated on the surface of the sample. When the sample is conducting, the positive charge due to the photoelectron emission is replenished immediately with an electron withdrawn from the ground. Whereas, when the sample is nonconducting, a positive voltage is generated on the surface with respect to the ground resulting in a decrease in the kinetic energy of the photoelectrons. When charging sets in on sample, the measured binding energy is equal to:

$$\mathbf{BE = h\nu - E_K - \varphi_S + C}$$

where $\varphi_S$ and C refer to the spectrometer work function and the change in the measured energy levels respectively, owing to charging. The positive charge increases on the sample resulting in an increase in the measured chemical shift. Contribution of C parameter to the measured chemical shift may possibly be different for the sample containing more than one layer according to the conducting behavior of the layer and the layer-substrate interaction. This difference could also appear between the same atoms of the sample due to the morphological variations in the system.[97] This is called differential charging. Chemical shift as a result of charging can be eliminated by exposing surface to neutralizing flux of low energy electrons by a 'flood gun' or choosing a suitable reference point to eliminate the contribution of charging to the measured chemical shift.[94] Additionally, application of external bias can be another method to examine the contribution of charging in the measured chemical shifts. When this method is applied to $Si/SiO_2$ system, although the observed overall shift is equal to the applied external bias, the measured binding energy difference between $Si^{4+}$ and $Si^0$ becomes larger when

negative bias is applied and smaller when positive voltage is applied. There also exist secondary electrons generated during the course of X-Ray generation and stray electrons falling onto the surface. Additionally, electrons, coming from a filament inserted to the set up in order to increase number of electrons falling to the surface, and all of these contribute to surface charge neutralization. When positive external bias is applied, these electrons are attracted by the surface for neutralization which causes binding energy difference between $Si^{4+}$ and $Si^{0}$ 2p peak to decrease. The same behavior will lead to increase in the binding energy difference when negative bias is applied.[98]

### *1.4.1 Characterization of Bimetallic Core-Shell Nanoparticles by XPS*

Many analytical techniques can be used for characterization of core-shell metal-dielectric nanoparticles, among which XPS is the most vital due to the perfect match of its probe length (~10 nm) to the size of these particles. Many reports have been published dealing with the use of XPS for characterization of various core-shell type nanostructures.[99-110]

When nanoparticles are deposited onto a smooth surface to perform XPS analysis, photoelectrons are attenuated throughout the core and the shell before they escape into the vacuum for their kinetic energy analysis. The well-known attenuation can be modeled to extract structural and morphological information from the XPS data. Wertheim and DiCenzo were the first to derive a formula relating the intensity of photoemission from spherical clusters.[108] Later on, to verify the core-shell structure Hoener and coworkers used relative attenuation of primary electrons and Auger signals[102]

Dabbousi et al. utilized XPS, together with other X-ray techniques, to determine chemical composition, size, shape, and internal structure of core-shell quantum dots.[101] Cao and Banin used XPS to demonstrate shell growth on core nanoparticles,[111] before Liu et al. showed that XPS provided the direct proof of the core-shell structure of shell cross-linked micelles.[105] In another work, Liu and Chuang characterized gold/polypyrrole core-shell nanocomposites with respect to naked Au nanoparticles according to their binding energy shifts.[106] Koktysh et al.[104] used XPS to analyze Ag/$TiO_2$ core-shell nanoparticle films before and after removing the silver core. Yang et al. also used XPS intensities and/or their angle-dependency to estimate the size and structure of Cu clusters on various surfaces.[107, 110] after Boyen et al. used angle-resolved XPS analysis for estimation of the size of the oxidation-resistant gold-55 clusters.[99] Recently, the Yang's group extended the formula, derived for a simple spherical particle, for application to particles with a spherical core and a uniform shell and studied the oxidation kinetics of Si-nanoparticles by XPS.[109] In most of the previous reports only one element was probed by XPS to extract information about the structure of the core-shell nanoparticles. It is, however, desirable to probe by XPS different elements belonging to the core and the shell separately in order to extract more accurate structural information, which eliminates many of the experimental sources of error.

The major idea behind XPS characterization of core-shell nanoparticles is not only to verify structure but also to gain information about charging properties. It is also possible to have information related with dielectric properties of surface structure by recording their charging/discharging behavior which was controlled by application of an external voltage stress either as dc or in pulse modes.[98, 112-114] Charging behavior is one of

the parameter that is attributed to affect the measured chemical shifts in XPS analysis. In a review article, Iwata and Ishizaka discussed these parameters and stated that for $SiO_2$/Si systems with different thickness the difference in measured chemical shifts comes from charging induced by the photoemission process.[115] Later on, Kobayashi et al. reported that deposition of thin palladium layer on oxide layer leads to disappearance of increasing on the energy shifts, as a result of elimination of the surface charging effect.[116] Surface charging on insulators caused by photoelectron emission, is usually overcome by using a low energy electron gun.[117] Lau and coworkers worked on using surface charging for extracting structural and electronic properties of ultrathin dielectric films on semiconductors.[118-120] Thomas et al. used charging to separate surface spectrum of oxide from that of the silicon substrate.[121]

Metal nanoparticles embedded within a dielectric shell can enhance surface charging capability on dielectric surfaces like the $SiO_2$/Si system. On the other hand no surface charging is expected in the bare metal nanoparticles on a conducting substrate because of the ease of discharging through the conductor surface.[113]

### *1.5. Objective of the Study*

This work comprises of optical and electrical characterization of bimetallic and core-shell Au and Ag nanoparticles by optical spectroscopy and XPS, respectively.

First of all, the tunability of optical properties of bimetallic Au and Ag alloy and core-shell nanoparticles is studied in terms of *composition change* and *structural change*, in the first part of this study. Later on, the possibility of *charge-storage* on single metal

particles, especially on gold and silver, and bimetallic alloy forms of corresponding nanoparticles in solution is discussed. Charge-storage of the silver-gold alloy nanoparticles and core-shells has not been reported to date. In this contribution, bimetallic silver-gold alloy and core-shell particles are synthesized, then electron-storage capacities in aqueous media by introduction of borohydride is followed by spectral shift in their surface plasmon resonance bands. It is extensively discussed in the first part of this report. Moreover, the parameters like composition and geometry affecting the charging ability of particles are reported by means of optical spectroscopy as well. Besides, electron storing/releasing capacities of Au and Ag nanoparticles and their kinetics are investigated.

In the second part of the work, we mainly focused on controlling and manipulating optical and electric properties by modification of surface with deposition of dielectric shell (silica and titania). Accordingly, the $Au@SiO_2$, $Ag@SiO_2$, and $Ag@TiO_2$ core-shell nanoparticles are synthesized and optical properties of these nanoparticles are investigated. The $Au@SiO_2$ and $Ag@SiO_2$ and $Ag@TiO_2$ nanoparticles are analyzed by XPS under external biasing to get further information about their charging capacities. In addition, we investigated incorporating the metal nanoparticles within titania shell to provide enhanced photocatalytic activity through the metal core by means of increased charging capacity.

# 2. EXPERIMENTAL SECTION

## *2.1. Materials*

[(3-Aminoproply)trimetoxysilane (APS), sodium silicate solution ($Na_2(SiO_2)$, 27 wt % $SiO_2$)], silver perchlorate ($AgClO_4$), silver nitrate ($AgNO_3$), etyltrimethylammonium bromide (CTAB), ascorbic acid, N,N-Dimethlyformamide (DMF), titanium(triethylaminoto)-isopropoxide, $[N((CH_2)_2O)_3TiOCH(CH_3)_2]$ were purchased from Aldrich. Tetracholoroauric acid ($HAuCl_4$), trisodium citrate dehydrate ($C_6H_5O_7Na_3.2H_2O$), Dowex (strongly acidic cation exchange resin 20-50 mesh) were purchased from Fluka and $NaBH_4$ was from BDH chemicals. Mili-Q water was used in all preparations.

## *2.2 Instrumentations*

KRATOS ES300 spectrometer with a $MgK\alpha$ (not monochromatized) source at 1253.6 eV was used to record XPS spectra. The base pressure was kept below $10^{-8}$ torr troughout the measurements. An angle of $90^o$ was used as take-off angle, unless otherwise mentioned. The sample rod is externally connected to either the ground or a DC power supply for recording XPS data under external bias. XPS peaks are fitted and deconvoluted by a third-party free program, XPSPEAK95 version 2.0. A representative XPS measurement under DC external bias bias is shown in Scheme 2.1.

UV-Vis absorption spectra were recorded by using the double beam Varian Cary 5E spectrophotometer and XRD patterns were recorded using a Rikagu Miniflex Difractometer with CuK$\alpha$ source operating at 30 kV/15 mA.

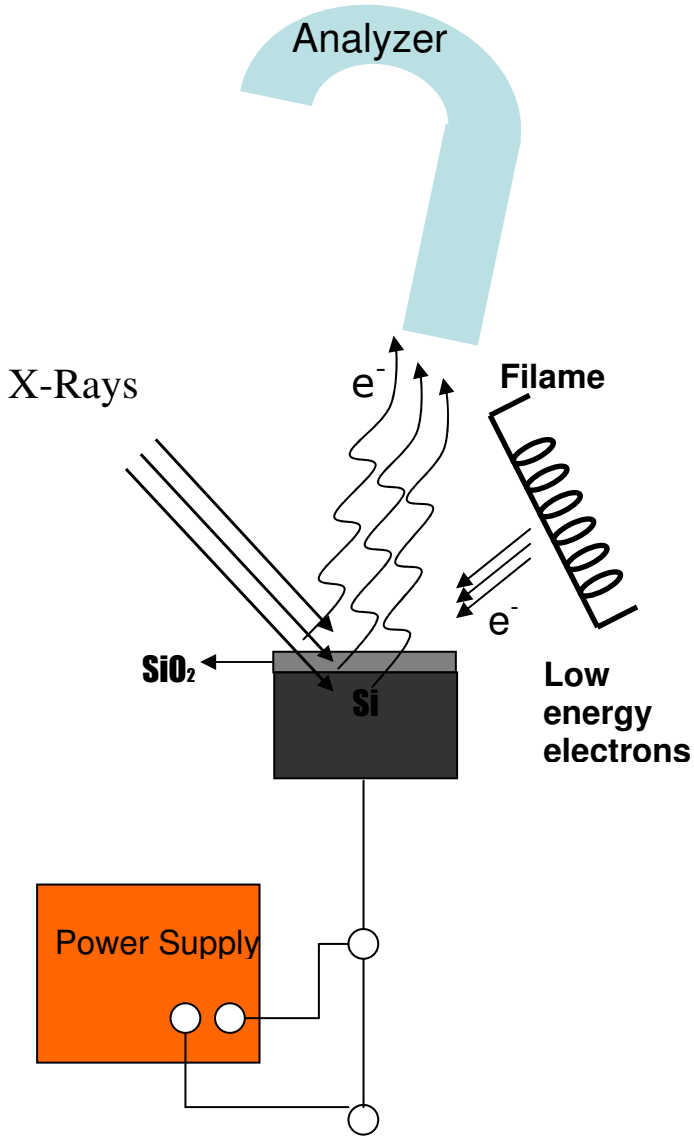


Scheme 2.1 A Schematic diagram of typical, DC biased XPS set-up.

## *2.3. Procedures*

### *2.3.1. Preparation of Bimetallic Alloy and Metal-Metal Core-Shell Nanoparticles*

#### *2.3.1.1. Preparation of Au-Ag Alloy Nanoparticles*

Keeping constant total metal concentration (0.5 mM), citrate capped Au-Ag alloy are prepared in different molar ratio (15, 25, 60, 80 %). To the 80 ml of boiling $HAuCl_4^-$ aqueous solution, 20 ml of hot $AgNO_3$ aqueous solution is added under vigorous stirring. (The problem is some AgCl might be precipitated, thus, silver solution should be hot). 5 ml of preheated citrate (1 wt %) solution is added fast, to the boiling mixed solution under vigorous stirring. 15 min later color changes which is evidence for the formation of citrate-capped alloy nanoparticles with various composition. The expected absorption maxima are around 400 nm (pure Ag) and 520 nm (pure Au).

#### *2.3.1.2. Preparation of Au(core)@Ag(shell) and Ag(core)@Au(shell) Nanoparticles*

The first step is preparation of spherical gold colloids using the standard gold colloid preparation method. Citrate-capped Au nanoparticles are prepared by following way; to 100 ml of boiling solution of $HAuCl_4^-$ (0.5 mM), preheated 5 ml of sodium citrate (1 wt %) is added under vigorous stirring. Fast color change from pale yellow to red wine is evidence of Au nanoparticles with the average particle size ca. 15 nm. For coating gold with a layer of silver, CTAB as cationic surfactant, and ascorbic acid as

reducing agent are used. To 20 ml of 50 mM CTAB solution, 1ml of 0.1 M ascorbic acid is added. After 5 min mixing under vigorous stirring, 0.5 ml 10 mM $AgNO_3$ solution and then 0.5 ml of Au colloids are slowly added. Finally 0.1 M NaOH is added dropwise very slowly to control growth of silver deposition, which leads to rapid change in color from pink to yellow. It means that the silver ions are reduced around gold particles and deposited. The average particle size of gold colloid is around 15 nm, if a standard preparation method is used and the expected silver thickness is around 15 nm. To obtain thinner shell, the silver nitrate concentration can be reduced. 3 and 5 mM silver solutions were used in the experiment. It is possible to synthesize Au(core)@Ag(shell) nanoparticles with any desired composition by changing concentration of added Au nanoparticle and $AgNO_3$ solutions. For the reverse case, formation of Ag(core)@Au(shell), first silver is reduced and then gold is reduced onto it. Preformed Ag nanoparticles are prepared by following way; To 99 ml of solution containing 0.3 mM sodium citrate and 1 mM $NaBH_4$ under vigorous stirring at room temperature, 1 ml solution of $AgNO_3$ (0.01 M) is added dropwise. The color of solution turns to yellow within a couple of minutes. Then, the exactly same procedure for the formation of Au@Ag is applied to form Ag@Au nanoparticles.

*2.3.1.3. Preparation of multishell Au-Ag Nanoparticles*

It is possible to increase the number of shells by sequential reduction of Au and Ag. For coating Au(core)@Ag(shell) with Au layer, 1 ml ascorbic acid solution is added to the preformed Au(core)@Ag(shell) solution. By addition of 0.05 ml $HAuCl_4$(aq.)

solution, color changes to blue which is an indication of Au shell. Finally, outer Ag shell is deposited on previously formed Au(core)@Ag(shell)@Au(shell) by mixing 20 ml of colloid with 0.5 ml 10 mM $AgNO_3$ followed by 0.2 ml NaOH solution.

### *2.3.2. Preparation of Metal(core)@Dielectric(shell) Nanoparticles*

#### *2.3.2.1. Preparation of Au(core)@$SiO_2$(shell) Nanoparticles*

Standard procedure for Au(core)@$SiO_2$(shell) is based on two steps. The first step is preparation of gold colloids using the standard citrate reduction method. The second one is polymerization of silica shell around the gold particles.

Preheated (≅ $30^o$ C) 5 ml of 1 wt % citrate solution is added quickly to the boiling gold solution (100 ml 0.5 mM) under vigorous stirring. The solution is boiled for 15-20 min. At last, stable deep-red wine colored dispersion of gold particles with diameter around 15 nm and 10% polydispersity is obtained. The fist step is completed by cooling down the mixture to room temperature. UV-Vis spectrum of above solution gives rise a sharp peak at 520 nm.

In the second step, to 100 ml of preformed aqueous solution of Au nanoparticles, freshly prepared 0,5 ml of 1 mM APS solution is added dropwise under vigorous stirring. (it is necessary to add the solution as slow as possible, if it is added fast gold colloids are aggregated and precipitated!). The solution is allowed to stand for 15 min to ensure complete bonding of the amine groups to gold particles. Then, 1 ml of active-silica solution (27 wt %) is diluted to 50 ml with water. Its initial pH (around 12) is reduced to 10-10.5 by adding Dowex-cation exchange resins to this solution, under stirring. The pH

of this solution is checked occasionally, until the pH is reduced to 10-10.5. 4 ml of this silica solution is added to the solution of APS-modified Au nanoparticles under vigorous magnetic stirring by careful dropwise addition. The pH of last solution is at 8.5, which is the most suitable pH to grow silicate shell around gold particles. Formation of 2-4 nm thickness of silicate layer is expected after 24 hours. Particles can be transferred to ethanol solution (water:ethanol ratio 1:4) to obtain thicker shell.

After reaching desired thickness the particles should be cleaned from excess citrate, silicate, impurities etc. by centrifugation. Then, particles are redispersed in water or ethanol to keep them stable.

For XPS characterization, the nanoparticles are deposited on a substrate, and after evaporation of solvent at room temperature, the XPS spectrum of the samples is taken. Scheme 2.2 represents the experimental preparation procedure.

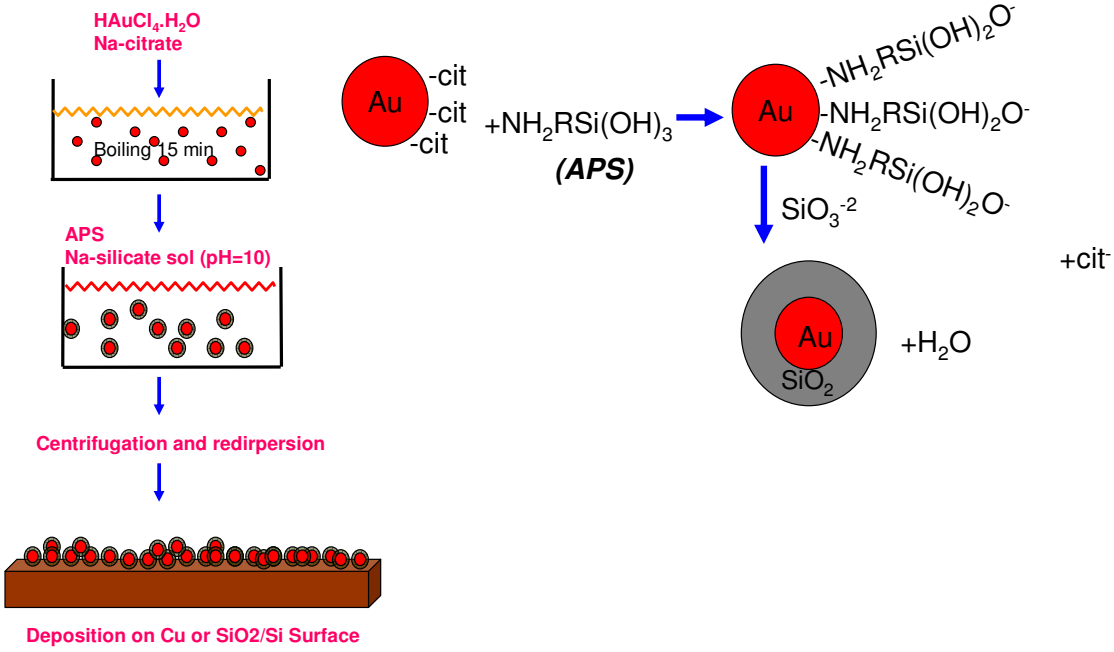


Scheme 2.2 Schematic representation of the experimental route for synthesis and characterization of Au@$SiO_2$ nanoparticles

*2.3.2.2. Preparation of Ag(core)@$SiO_2$(shell) Nanoparticles*

Preparation of Ag(core)@$SiO_2$(shell) Nanoparticles is as follows; in the first step silver colloids is prepared, then particles are covered by silicate. 99 ml solution of 0.3 mM citrate and 1mM $NaBH_4$ is cooled in 30 min, and then 1ml of cooled 0.01 M $AgNO_3$ solution is added to the vigorously stirred solution. $NaBH_4$ is added a minute before addition of the solution of $AgNO_3$. The solution turns yellow immediately. Eventually,

particles with diameter 10 nm give peak around 400 nm. In the second step, 0.15 ml APS solution (1mM) is added dropwise under vigorous stirring. 15 min is sufficient for completing amino groups to bind silver colloids. Then, 1.2 ml of active silica solution (pH≅10.5-11, 27 wt % silicate solution) is added under vigorous magnetic stirring by careful dropwise addition. 4-5 days later $Ag@SiO_2$ nanoparticles are obtained. The expected thickness of $SiO_2$ shell is ca. 5- 7 nm.

*2.3.2.3. Preparation of Ag(core)@$TiO_2$(shell)*

$Ag@TiO_2$ clusters are prepared by a method which is so-called one-pot synthesis. Both reduction of $AgNO_3$ and polymerization of titanium(triethanolaminato)-isopropoxide $[N((CH_2)_2O)_3TiOCH(CH_3)_2]$ are carried out in the same medium. *N*,*N*-dimethylformamide (DMF) is used as a reducing agent. A total of 2 mL of an aqueous $AgNO_3$ (15 mM) solution is mixed with 18 mL isopropanol solution of $[N((CH_2)_2O)_3TiOCH(CH_3)_2]$ (7.5mM) and 10 mL of DMF. Concentrations of $Ag^+$ and $TiO_2$ are 1 and 5 mM, respectively, in the reaction mixture. The mixture is heated at reflux temperature with vigorous stirring. After 90 min, color change towards dark brown is the evidence of formation of nanoparticles. The sample solution is cooled to room temperature, centrifuged and redispersed in ethanol and then deposited on a substrate for characterizing them with XPS.

Scheme 2.3 represents the experimental procedure for synthesis and characterization of Ag@$TiO_2$ nanoparticles.

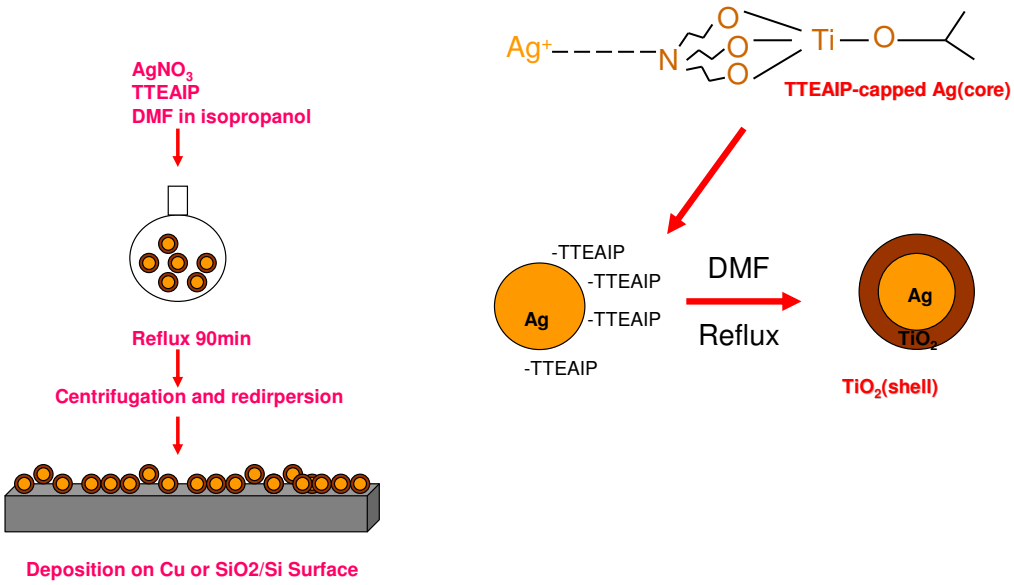


Scheme 2. 3 Schematic representation of experimental route for synthesis and characterization of Ag@$TiO_2$ nanoparticles

# 3. RESULT AND DISCUSSION

## *3.1. Au-Ag Alloy versus Core-Shell Nanoparticles*

### *3.1.1. Au-Ag Alloy Nanoparticles with Different Composition*

When gold and silver salts with different concentrations, are reduced simultaneously in the same mixture, gold and silver alloy nanoparticles with different compositions, are formed. The alloy formation can be confirmed by optical spectroscopy. Whereas an alloy with a certain Au and Ag concentration exhibits one single SPR band spaning the spectral range between those of isolated Au and Ag nanoparticles, two bands would be expected for the mixture of gold and silver nanoparticles. Figure 3.1 displays recorded SPR bands of gold-silver alloy nanoparticles with various gold contents (15, 25, 60, 80 % Au). Increased gold content of the nanoparticles results in a red-shift in the SPR band. When the maximum position of SPR band of alloys in those of pure Ag (25250 $cm^{-1}$, 3.13 eV) and Au colloids (19250 $cm^{-1}$, 2.39 eV), is plotted in wavelength scale versus gold mole fraction, a quasi-linear trend is reported by El-Sayed[22] and Gonzalez et al.[28] However, a non-linear relation is obtained when energy (wavenumber) scale is used, as shown in the inset of Figure 3.1. The wavenumber scale is used in all of our figures for more meaningful and direct visual comparison with the changes in the plasmon frequency, as 10 nm shift around 400 nm and 500 nm correspond to different extent of shift in the frequency scale.

A representative TEM image of the Au-Ag alloy nanoparticles with 0.8 gold mole fraction, is shown in Figure 3.2, The average particle size is about 25-30 nm. Nanoalloys with different compositions display similar size distribution (not shown in here), since the alloys are prepared by optimized synthetic procedures, nanoparticles with similar particle size are obtained in every synthesis.

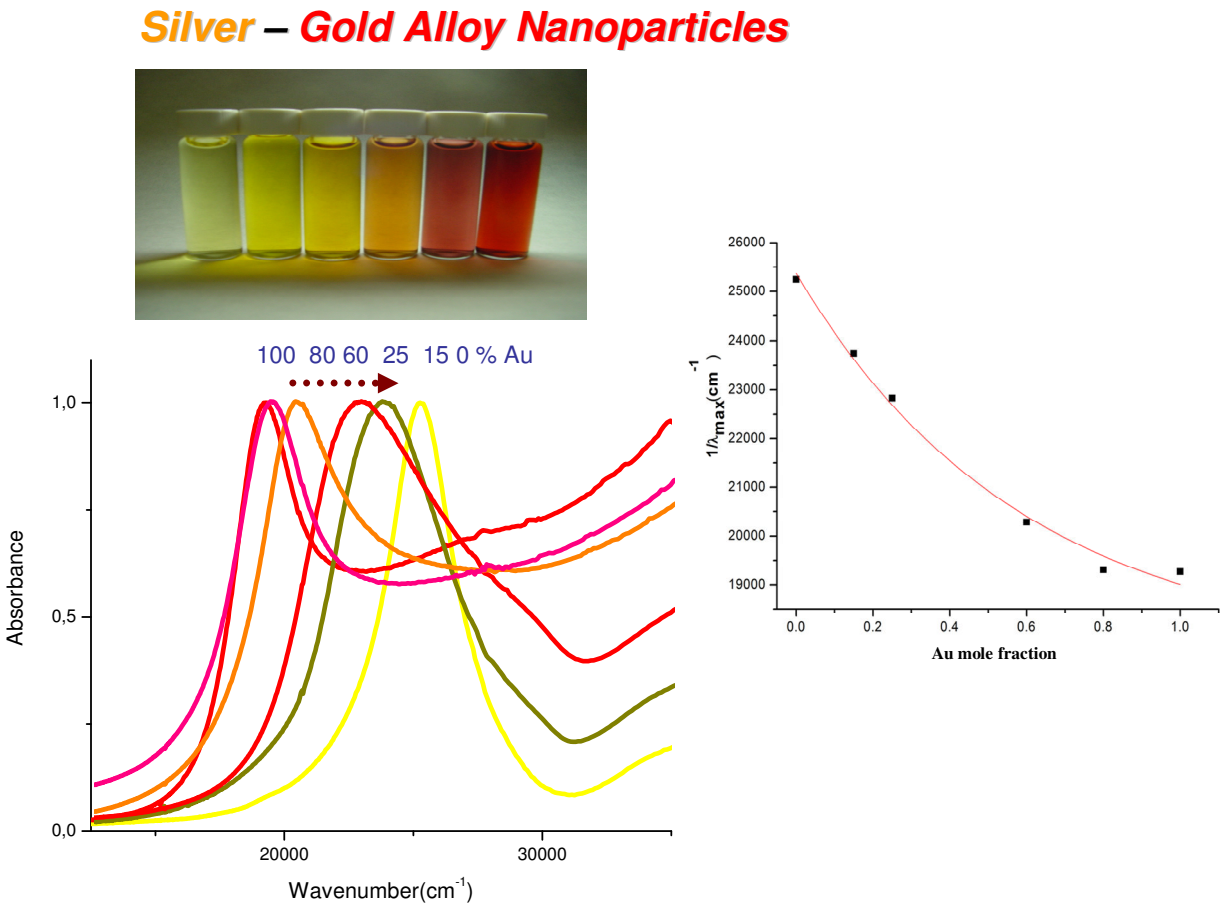


Figure 3.1 Normalized UV-Vis Spectra of Au-Ag Nanoalloys with varying composition.

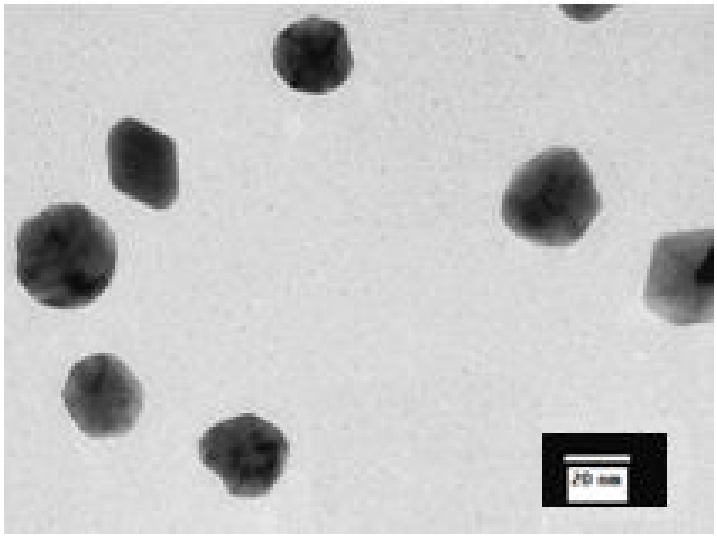

Figure 3.2 TEM Image of Au-Ag alloy nanoparticles with 80% Au content.

*3.1.2. Bimetallic Au-Ag Core-Shell Nanoparticles*

When the corresponding gold or silver salts are reduced sequentially on top of the preformed one, core-shell nanoparticles are obtained. The synthesis of Au@Ag and nanoparticles are carried out by modification of the method described by Srnová-Šloufová et al.[34] According to the method, a weak reducing agent, L-Ascorbic acid, is used to reduce $AgNO_3$ on preformed Au nanoparticles, so that reduction process only takes place on the surface of the Au nanoparticles. Also, for the deposition of both Ag and Au layers, the cationic surfactant (CTAB) which links two layers, is used. To start reduction of $AgNO_3$, the pH of the solution should be increased by using NaOH. Figure 3.3 displays time-evolved formation of Au@Ag and Ag@Au nanoparticles by UV-Vis Spectroscopy. The formation of Ag nanoshell onto preformed Au nanocore is

shown in Figure 3.3.(top). The large blue-shift in the SPR band of Au nanoparticles (520 nm) towards 400 nm which is the characteristic SPR band of Ag nanoparticles, is the evidence for the formation of Ag(shell), since conduction electrons of Ag(shell) are mostly responsible for the SPR band. The resultant SPR band displays the characteristic of Ag nanoparticles.

The lower part of Figure 3.3 shows the time-evaluated formation of Ag@Au nanoparticles. In this case, large red-shift from 400 nm to 520 nm is the evidence of presence of Au(shell).

In Figure 3.4, a representative TEM Image fo Au@Ag nanoparticles is shown. Ag shell can easily be distinguished by the color-contrast. The average particle size can be estimated as 25-30 nm.

It should be emphasized that they are in similar size with those of alloy nanoparticles previously discussed. Hence, when comparing the optical properties of Au-Ag nanoalloy versus core-shell, size related difference is eliminated.

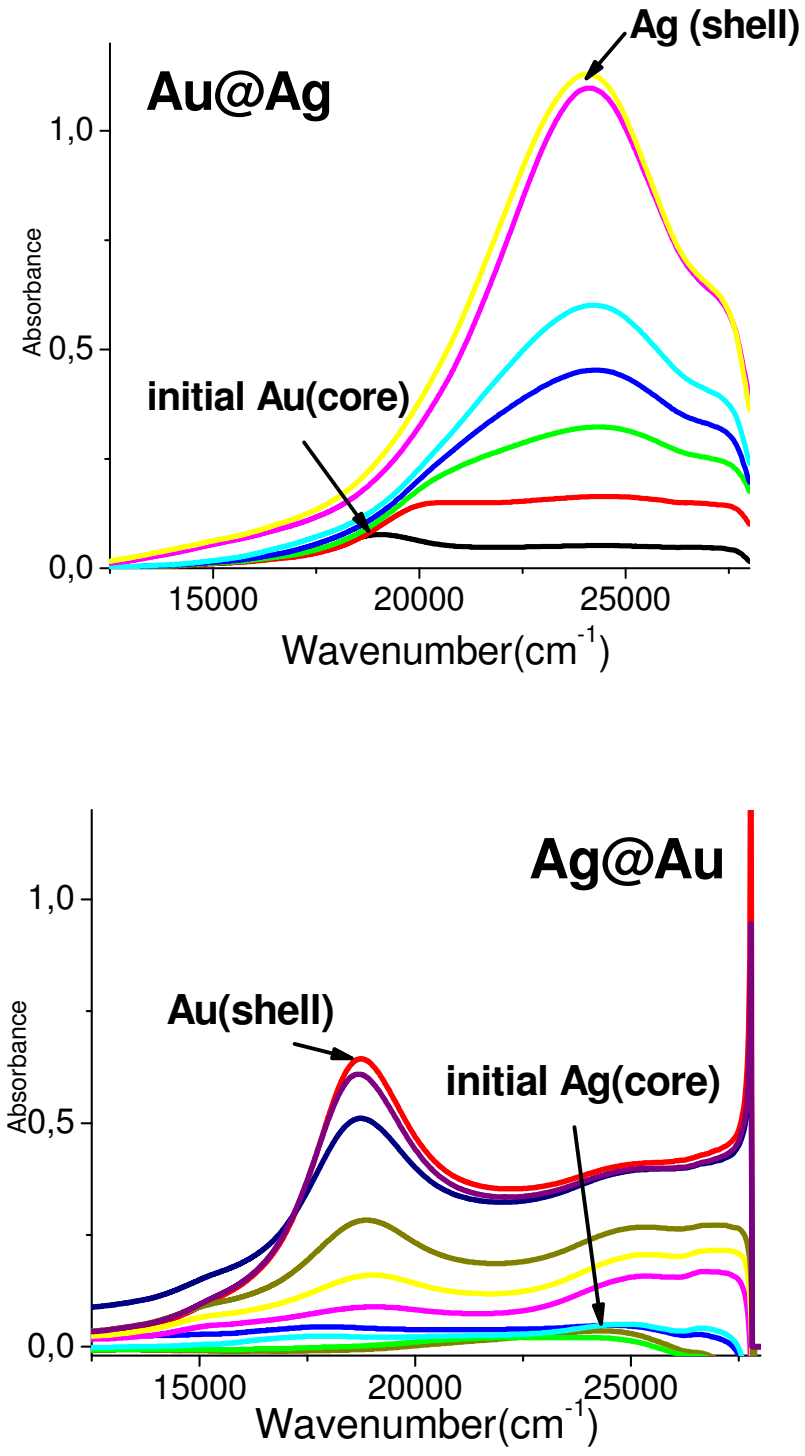


Figure 3.3 Time-evolved formation of plasmon resonance bands of Au@Ag(top) and Ag@Au nanoparticles(bottom).

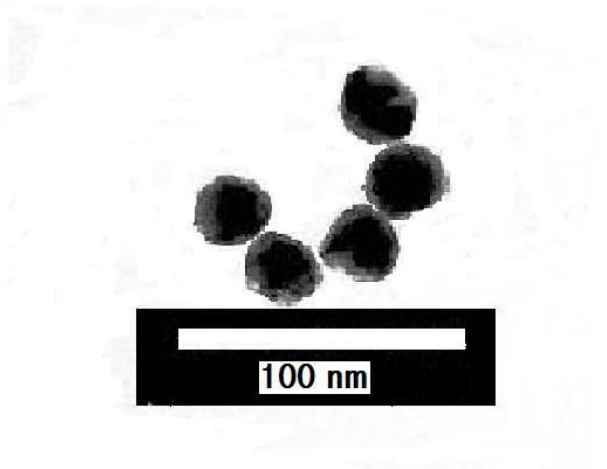


Figure 3.4. A Representative TEM Image of Au@Ag nanoparticles

It is also possible to prepare onion-like multishell Au-Ag nanoparticles by sequential reduction of the corresponding salts of Au and Ag nanoparticles, as seen in Figure 3.5. The Au@Ag nanoparticle in Figure 3.3, is used to grow Au(shell) and Ag (shell). The spectacular color change correlates with large shift of the related extinction spectra after each deposition step. The successive red and blue shifts of the plasmon band are well reproduced with sufficiently thick metal shell. The repetitive forward-backward shifts on the surface resonance band is totally a surface effect, so that deposition of second metal overlayer can completely change the resonance condition and alter the color of the colloid. By sequential deposition of Ag, Au and outer Ag color turns, yellow, blue and deep orange from wine red, respectively.

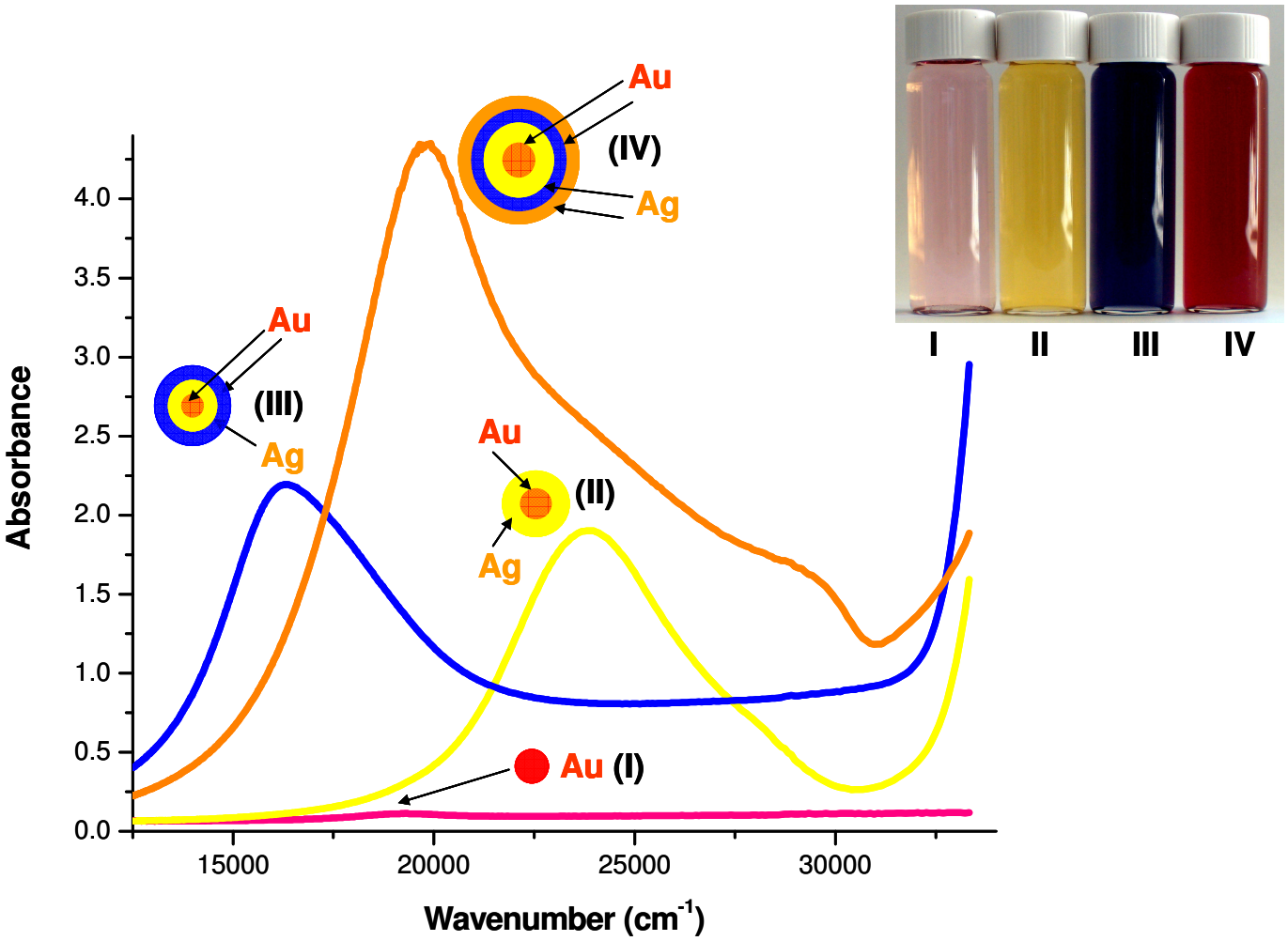


Figure 3.5 Plasmon Resonance Bands of multishell Au-Ag core-shell Nanoparticles

### *3.2. Optical Response of Ag-Au Bimetallic Nanoparticles to Electron Storage in Aqueous Medium*

Plasmon resonance band shifts also give information about charging properties of bimetallic and core-shell colloids. Namely, introduction of a reducing agent, $NaBH_4$,

causes storage of extra electrons on particles, leading to blue-shift in the SPR band due to some parameters which will be discussed below.

To study electron-storage on nanoparticles, we use the well-known oxidation of borohydride, which, upon addition to the solution, particles are polarized cathodically, by the reaction;[57]

$$BH_4^- + Ag_n + 3H_2O \rightarrow BO_3^{3-} + Ag^{8-}_n + 10H^+$$

In the case of nanoalloys, additional electrons are stored in the nanoparticles, sharing between Au and Ag atoms which can be represented as follows;

$$Ag_{1-x}Au_x\,(n.p) + BH_4^- \rightarrow Ag_{1-x}Au_x\,(n.p)^{m-}$$

Even though, additional electrons lead to red-shift in molecules, electron injection results in spectral shift due to the plasmon resonance band of the metal nanoparticles.

To understand origin of the charge injection in particles, it should be started from Mie Theory. As shown by numerous workers, the plasmon frequency as well as its extinction coefficient are both related to the electron density (n). The electron effective mass ($m_{eff}$) and dielectric function ($\varepsilon_2$) of the medium through the relation;[3]

$$\omega_{\max} = \frac{ne^2}{\varepsilon_0 m_{eff}\sqrt{1+\varepsilon_2}} \qquad (3.1)$$

As seen in the equation 3.1, plasmon frequency is directly proportional with the density of the electron particles and inversely proportional with $m_{eff}$. Since Au and Ag have almost the same $m_{eff}$, plasmon frequency is directly affected by the density of electron. Therefore, negatively charged particles show blue-shift in the plasmon band due to the increased electron density on their surface, whereas electron addition generally leads to a red-shift in the absorption bands of molecules.

*3.2.1. Effect of Composition on Electron Storage*

In Figure 3.6, the spectra are shown before and after addition of $NaBH_4$ to a solution containing both Ag and Au nanoparticles, having similar size and concentration, mixed after separate preparation. Link et al. reported that even thought theoretical effective mass and the electron densities of Au and Ag are close to each other, both position and extinction coefficient of them are widely different.[22] Furthermore, by using experimentally derived optical parameters from the thin films of gold-silver alloys, they also calculated the optical spectrum of the gold-silver nanoalloy which closely matched the experimental data.[22, 26] In what follows, we will use the finding that, when compared to gold, silver either has a larger electron density or a smaller effective mass to cause

both a larger shift in the position of frequency of the plasmon band and also its extinction coefficient, to guide us in the understanding, qualitatively, the spectral shift we observe.

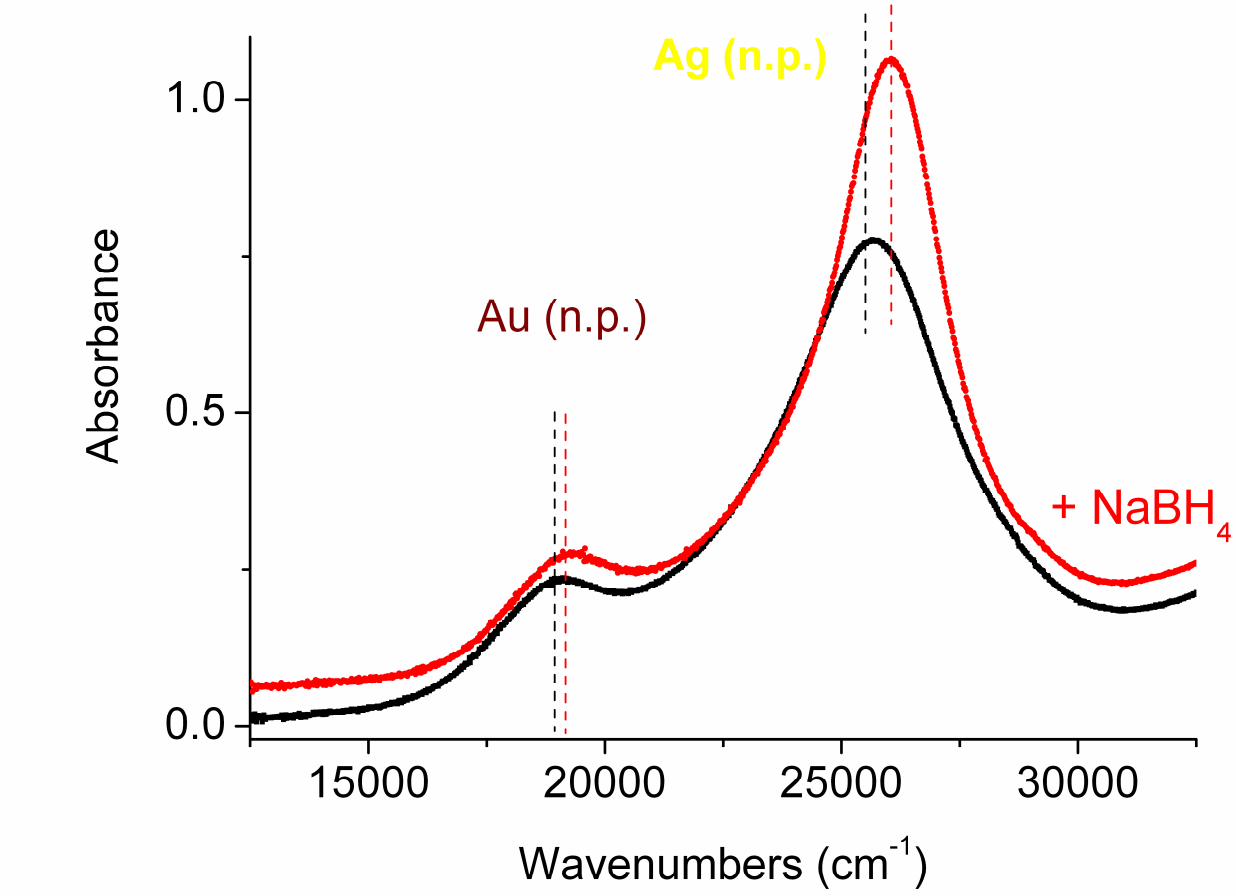


Figure 3.6. The spectra before and after addition of $NaBH_4$ to a solution containing both Ag and Au nanoparticles

Accordingly, the extinction coefficient of Ag nanoparticles is 4 times higher than that of Au nanoparticles. Upon electron injection, both extinction coefficient increment and spectral shifts are observed. The blue-shift in pure Ag nanoparticles as a result of the electron storage is always larger (ca. 600 $cm^{-1}$) than that of pure Au (ca. 200 $cm^{-1}$), as obviously seen. The spectral blue-shift and extinction coefficient enhancement in the SPR bands are obviously larger in pure Ag nanoparticles due to electron injection compared to Au nanoparticles. In a similar way one can also monitor electron storage in the nanoalloys.

In Figure 3.7, the spectral shifts are marked in the SPR bands of pure Ag, pure Au and a representative Au-Ag nanoalloy with 15% Au content having similar size and concentration in aqueous solution, after addition of exactly the same amount of $NaBH_4$. In all case extent of spectral shifts as a result of stored electrons in the particles is always somewhere in between those of pure Ag and Au nanoparticles. When the measured spectral shift is plotted with Au content, a quasi-linear dependence is obtained, as seen in the Figure 3.8. Thus, an increase of Ag content within the alloy, leads to a more extensive blue-shift, in agreement with our practical guideline introduced above.

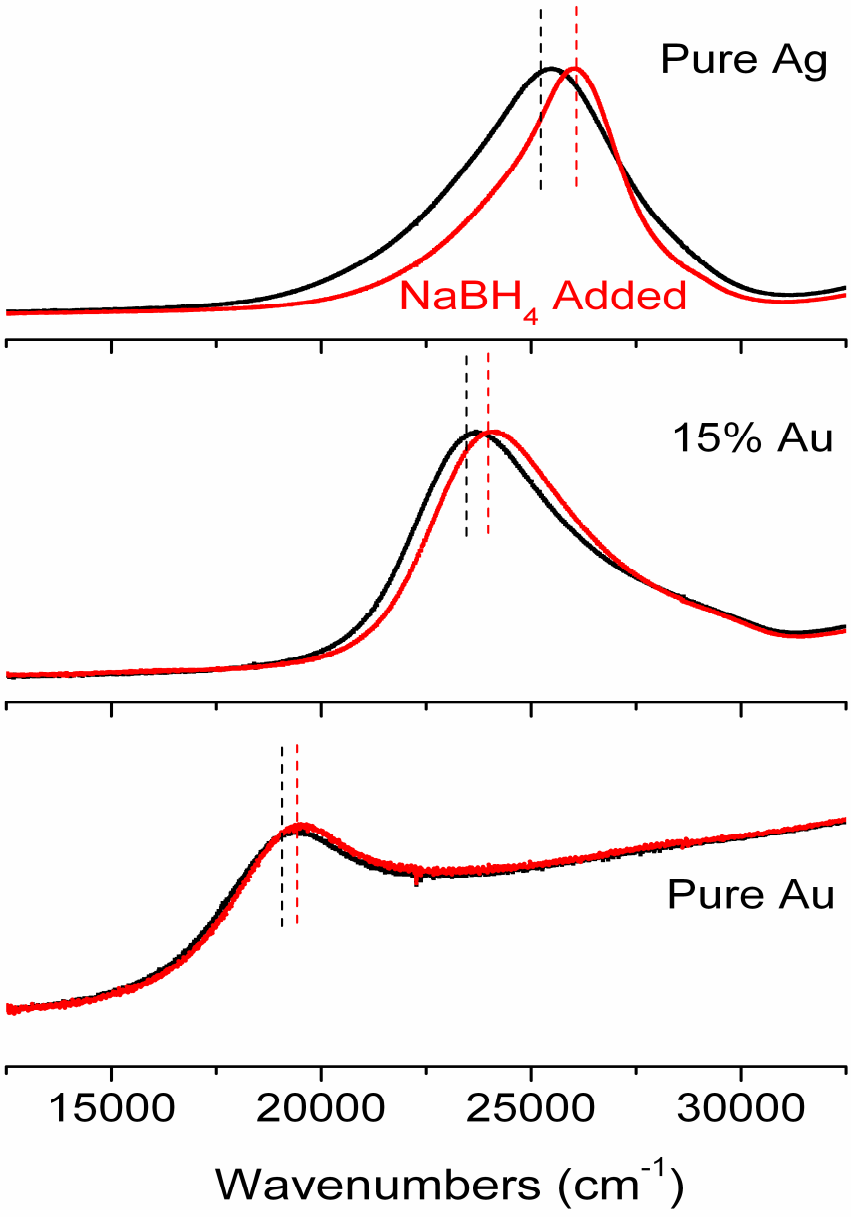


Figure 3.7. Spectra (plotted in wavenumbers) of pure Ag, pure Au and 15% Au alloy before and after addition of $NaBH_4$ for electron storage.

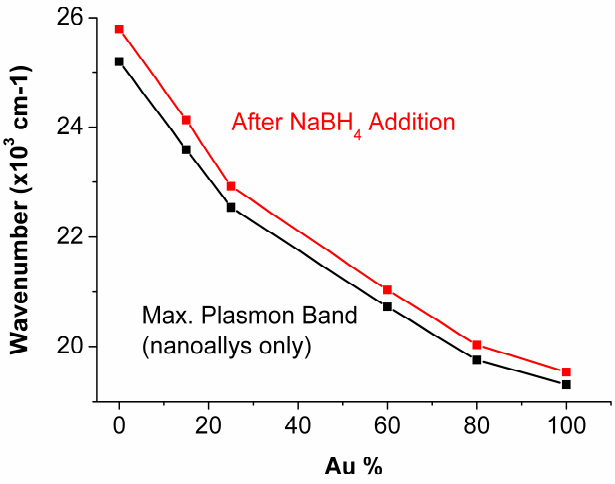


Figure 3.8. Variation of the maximum position of the SPR bands with Au content, before and after addition of $NaBH_4$.

### *3.2.2. Effect of Structure on Electron Storage*

Optical response of bimetallic nanoparticles depends on the relative amounts of both metals, as well as the actual distribution within the particles.[15] Accordingly, it is also expected that the effect of charge storage should also depend on the structure of Au-Ag nanoparticles. Comparison of the optical effects observed upon charge injection on Au-Ag nanoalloys versus core-shell nanoparticles is presented in Figure 3.9 for monitoring the SPR band shift of Au-Ag nanoalloy, as compared to that of Au(core)@Ag(shell), both with a nominal 25% Au content. The plasmon bands of the alloy and the core-shell are blue-shifted in different extents (300 $cm^{-1}$ and 1000 $cm^{-1}$, respectively). Such a large dissimilarity is certainly related with the difference in allocation of Ag and Au within

these nanoparticles. Spectral blue-shift of Au-Ag nanoalloy and core-shell with a nominal 15% Au content, are also monitored. In this case, recorded extents of spectral shift are 400 $cm^{-1}$ and 700 $cm^{-1}$ respectively. Compared to the particles with a nominal 25% Au content, the reason of smaller spectral-shift difference between alloy and core-shell is again certainly related with the larger Ag content of the particles.

Although conduction electrons of the Ag and Au atoms move freely within the whole cluster in the alloy, those in the core-shell particles are restricted to their part, either nucleus or shell.[3] In the case of the alloy, both Au and Ag contribute to the plasmon absorption frequency. However, in the core-shell case it is the silver shell which contributes most, and in agreement with our assessment earlier in the text, causes a larger spectral shift. (Particle size effect is omitted, assuming the TEM images given above are reliable.)

Ung and coworkers reported that pure Ag particles of 11 nm of average size showed ca. 600 $cm^{-1}$ blue-shift when they were cathodically polarized by combining electrochemistry with spectroscopy, and using the change in the electrode potential they stated that this corresponded ca. 2000 electrons stored per nanoparticle.[122] Using a different approach and by titrating with a stronger electron capturer, thionine, Kamat et al. reported a more than 1000 $cm^{-1}$ blue-shift in the band position of the Ag(core)@$TiO_2$(shell) particles when subjected to photoinduced electron transfer to the silver core of ca. 4 nm size. They claimed that this spectral shift corresponded to ca. 66 electrons stored in the silver core.[54-56] Another spectroelectrochemical study reports ca. 80 $cm^{-1}$ spectral shift corresponding to only 1 additional electron of ca. 2 nm gold particles.[27]

It should be underlined that the reported shifts in these 3 studies due to electron storage in the nanoparticles are very similar to our experimental findings (ca. 200 $cm^{-1}$ and 600 $cm^{-1}$ shifts for Au and Ag, respectively). However, the reported number of electrons differ significantly from 1 to 2000. Therefore, although we can not estimate the number of electrons stored in the pure Au and Ag nanoparticles, our findings point out that the chemical nature of the nanoparticle is the dominating factor for the extent of spectral shifts.

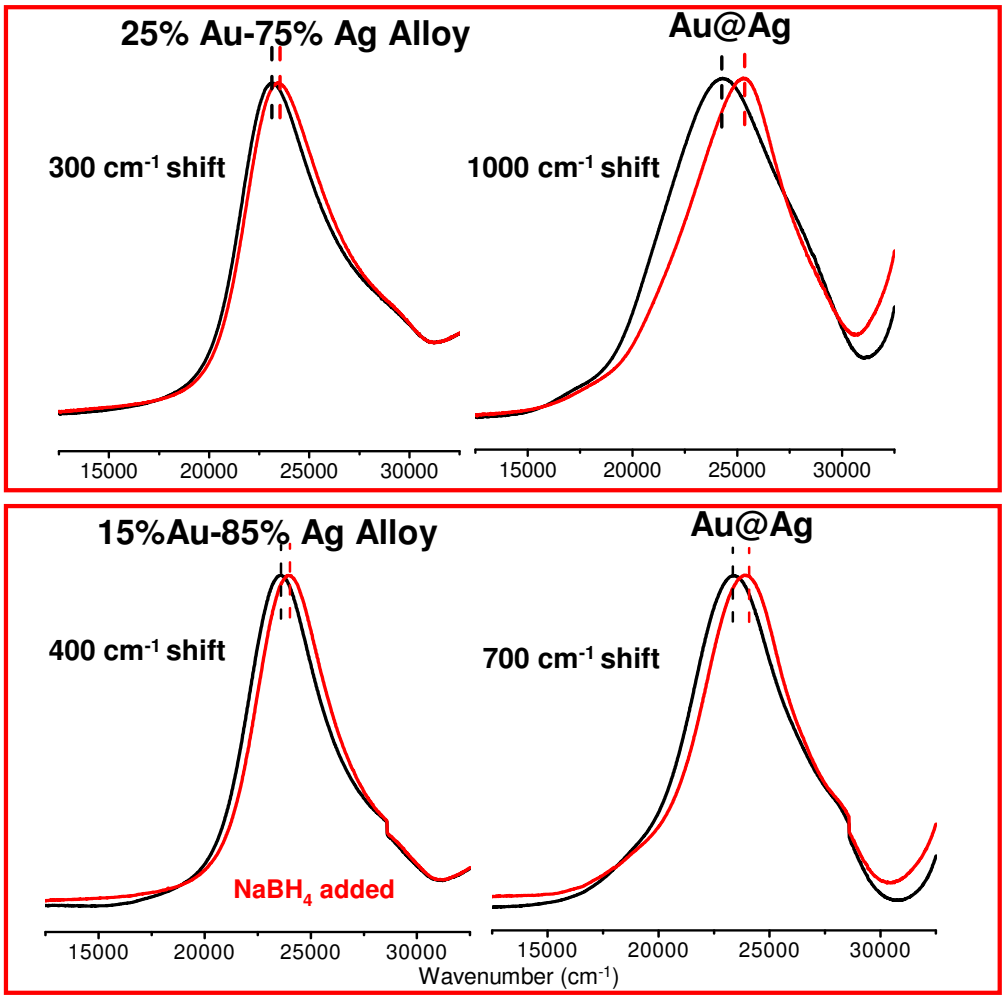


Figure 3.9. Spectral blue-shifts for alloy versus core-shell nanoparticles with different Au content by addition of $NaBH_4$.

### *3.3. Kinetics of Electron Storing/Releasing Process of Au and Ag Nanoparticles*

Kinetic investigation on electron storing/releasing abilities of Au and Ag nanoparticles by following the spectral shifts of the respective absorption bands after sequential addition of electron donor and acceptor species further our basic understanding of the contributing factors to the process.

To study the kinetic of charge storing and releasing of Au and Ag nanoparticles, time resolved response of the particles are measured by recording UV-Vis spectra of aqueous solution of an equal concentration of pure Au and Ag solution at each 0.6 second intervals, upon addition of $NaBH_4$ and thionine. Thionine is an organic dye molecule, which is widely used in following charge transfer and/or electron donor-acceptor reactions, since it exists as a monovalent cation in near-neutral pH values, and captures the electrons strongly by the following reaction:

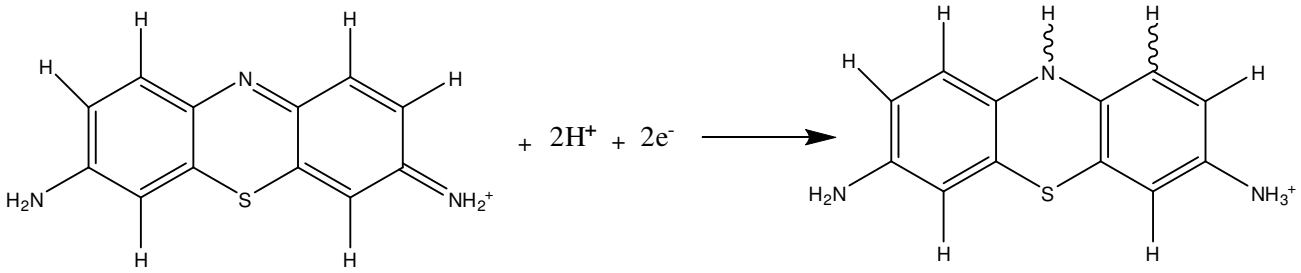


Accordingly, when thionine is introduced to the medium with negatively charged nanoparticles, it leads to the discharging process and the SPR bands start shifting back to their original positions (red-shift). As shown in Figure 3.10, red and yellow curves show

the directions of maximum position of SPR bands shifts of the Au and Ag nanoparticles aqueous mixture. The maximum blue-shift in the SPR bands is reached when particles are saturated by extra electrons within a minute. In the second part of the study, electrons are captured by thionine immediately after injected to the particle solution. The process can be followed by the back-shifting in the SPR bands which was previously blue-shifted owing to the stored electrons.

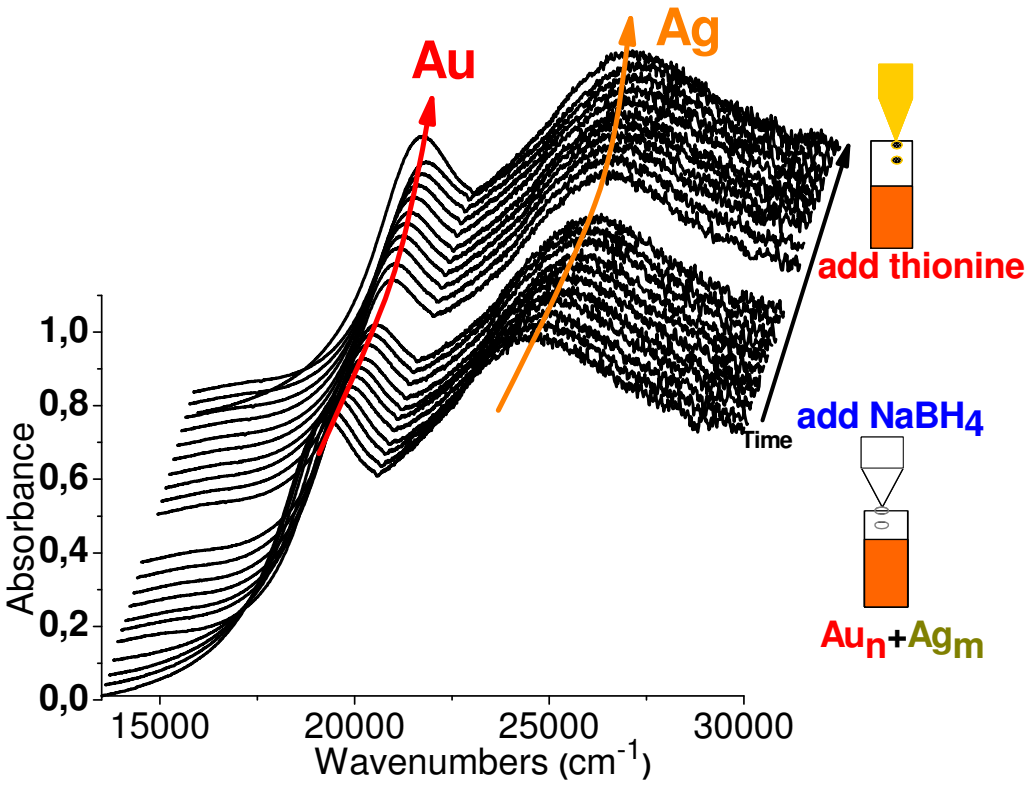


Figure 3.10. Spectral shifts in a sequence of spectra recorded in time of the pure Au and Ag nanoparticles aqueous mixture solution, following by addition of i) $NaBH_4$ and ii) Thionine

In Figure 3.11, exponential fits to the data of spectral shifts versus time reveal relative time constants (T.C.) of both electron capturing and releasing processes for pure Ag and Au nanoparticles separately (a and c, respectively), as well as their mixture (b). As was mentioned above, the Ag nanoparticles exhibit a larger spectral blue-shift upon electron addition when compared to Au nanoparticles, both separately, as well as a mixture in the same solution. However, surprisingly, Ag nanoparticles display slower kinetics. It is clearly seen that time constants of Au nanoparticles for both electron storing/capturing processes are smaller than those of Ag nanoparticles.

As a next step, kinetic study on the oxidation of Au and Ag nanoparticles by complexation with KI, is investigated by addition of KI aqueous solution. The maximum positions of the SPR band are red-shifted upon chemisorption of $I^-$ anions, due to oxidation of surface atoms of the Au/Ag nanoparticles. The proposed structure is $Ag^{\delta+}\ I^-$ for the silver complex.[123] These anodically polarized particles are then exposed to $NaBH_4$ to reverse the process, the schematic representation is as follows;

$$Ag_n + xI^- \longrightarrow Ag_{n-x}{}^{x\delta-} Ag_x{}^{x\delta+} x\, I^-$$

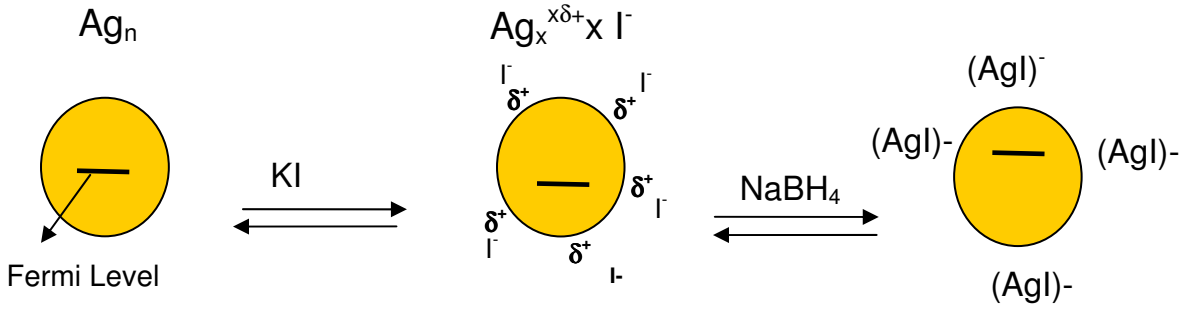

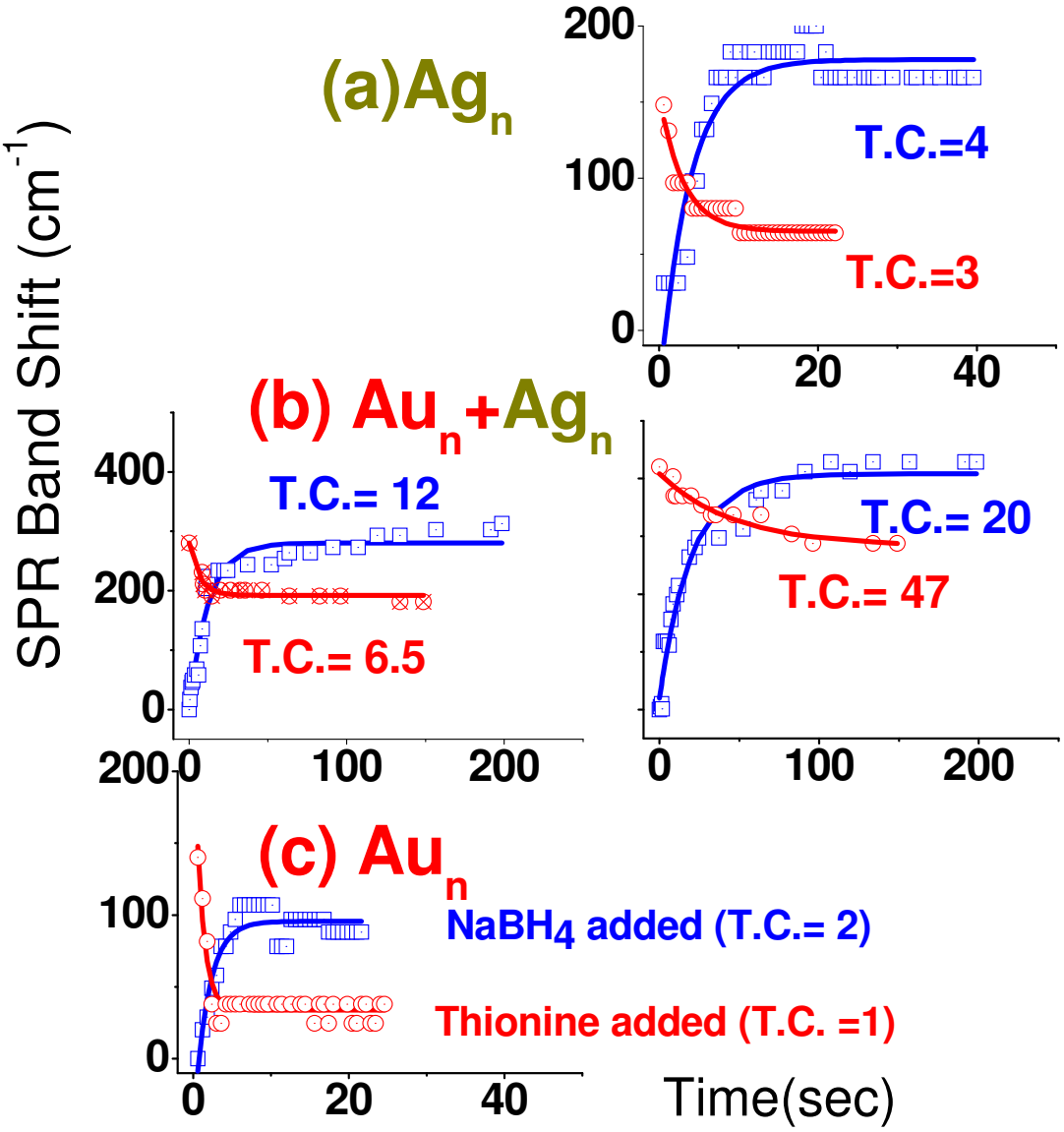


Figure 3.11. Recorded SPR band shifts with respect to time by addition of $NaBH_4$ (blue) and Thionine (red) for a) Pure Ag nanoparticles b) Au and Ag nanoparticles in equally concentrated aqueous mixture and c) pure Au nanoparticles.

The spectral shifts accompanying addition of KI and $NaBH_4$ respectively are given in Figure 3.12. The sequence of spectra recorded in time displays red-shift as a result of oxidation, later on back shifting (blue-shift) is observed due to the injection of extra electrons.

Figure 3. 13 shows the exponentially fitted maximum positions of the SPR bands of Au and Ag nanoparticles with respect to time as a result of addition of KI and $NaBH_4$. Time constants of both oxidation of Au and Ag nanoparticles by complexation of $I^-$ and electron storing rate of these complexes are also displayed.

Although there is no distinct difference between time constants for oxidation of Au and Ag nanoparticles by complexation of $I^-$, electron storing rate of Au nanoparticles complexed with $I^-$ is similar with that of pure Au nanoparticles, which is higher than that of Ag nanoparticles as seen in Figure 3.13. Pure Au and Ag nanoparticles complexes with $I^-$ also show similar behavior in electron storing process and again, kinetics of the Au nanoparticles' complexation is faster than those of the Ag nanoparticles. But, in oxidation process by $I^-$ ions, our finding is that the Au nanoparticles are slower.

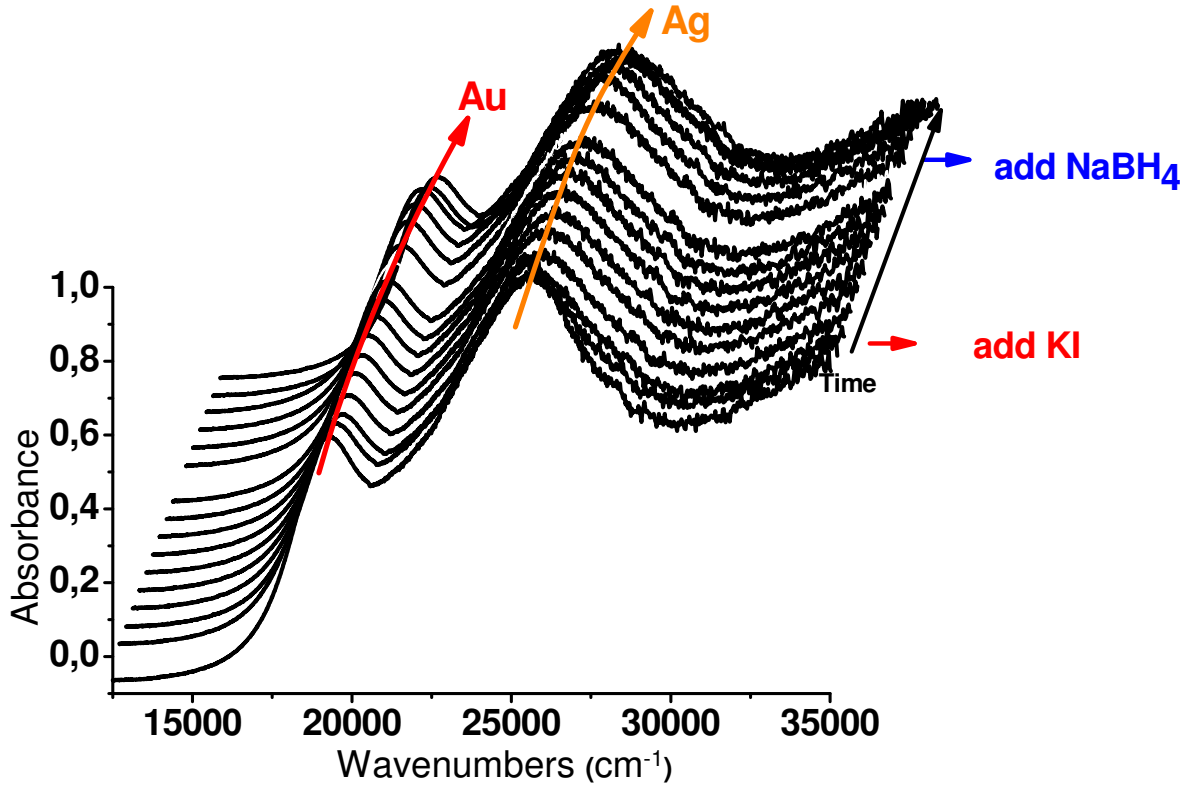


Figure 3. 12. Spectral shifts in the sequence of spectra recorded in time of the pure Au and Ag nanoparticles aqueous mixture solution, following by addition of i) KI and ii) $NaBH_4$.

Both the gas-phase electron affinity and the ionization potential of small clusters of the same size are higher for Au than Ag.[124] When the ionization energies and electron affinities in gaseous phase are extrapolated to the aqueous medium, it is expected that Au nanoparticles are better and faster for capturing electrons (reduction), and slower towards oxidation, in agreement with our findings. Therefore, we demonstrate that kinetic data is a better tool for evaluating the charging/discharging abilities of the nanoparticles in aqueous medium.

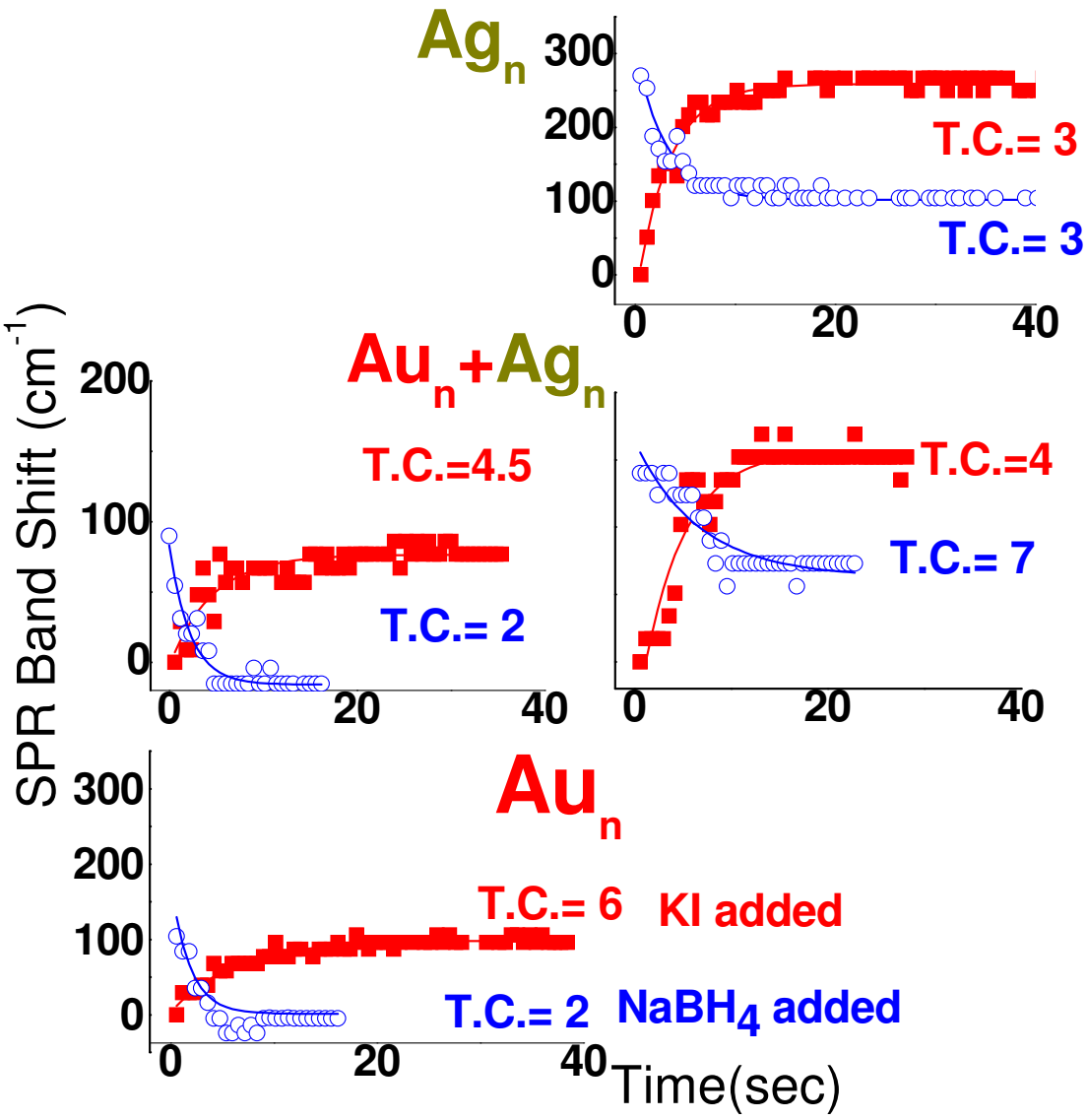


Figure 3.13. Recorded spectral shifts for SPR band shifts with respect to time of equally concentrated aqueous mixture of Au and Ag nanoparticles by addition of i) KI (red) and ii) $NaBH_4$ (blue).

### *3.4. Spectral Characterization of Metal(core)@Dielectric(shell) Nanoparticles*

To study both qualitative and quantitative characterization of Metal@Dielectric nanoparticles we used optical spectroscopy and XPS, as discussed below extensively. This part is divided into two sections as Metal(core)@$SiO_2$(shell) and Metal(core)@$TiO_2$(shell) nanoparticles.

#### *3.4.1. Metal(core)@$SiO_2$(shell) nanoparticles*

In Figure 3.14, a representative TEM image of the synthesized Au nanoparticles with an average diameter of ca. 15 nm embedded into 6 nm thick silica shell, is shown. It is clearly seen that, the particles display nearly monodisperse distribution, and core-shell structure is easily recognizable.

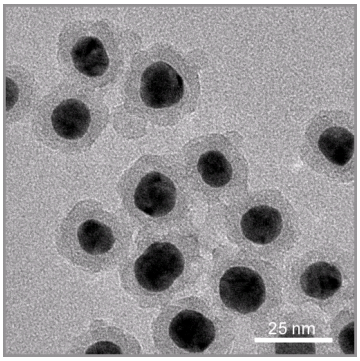


Figure 3.14. TEM image of the Au(core)@$SiO_2$(shell) nanoparticles

Figure 3.15a shows the XRD pattern of $Au@SiO_2$ nanoparticles. The pattern only shows a diffraction peak at $38^o$. The slightly broad diffraction peak corresponds to fcc Au(111) plane ( $\Delta\Phi>0.8^o$) which is an indication of crystalline gold core. Also, the SPR bands of the nanoparticles in aqueous solution are depicted in Figure 3.15b. The strong SPR bands of citrate capped gold nanoparticles and $Au@SiO_2$ nanoparticles are both around 520 nm. The slight red-shift in the plasmon band with respect to the citrate-capped gold colloid is an optic confirmation of Au(core), as has been previously discussed.[88]

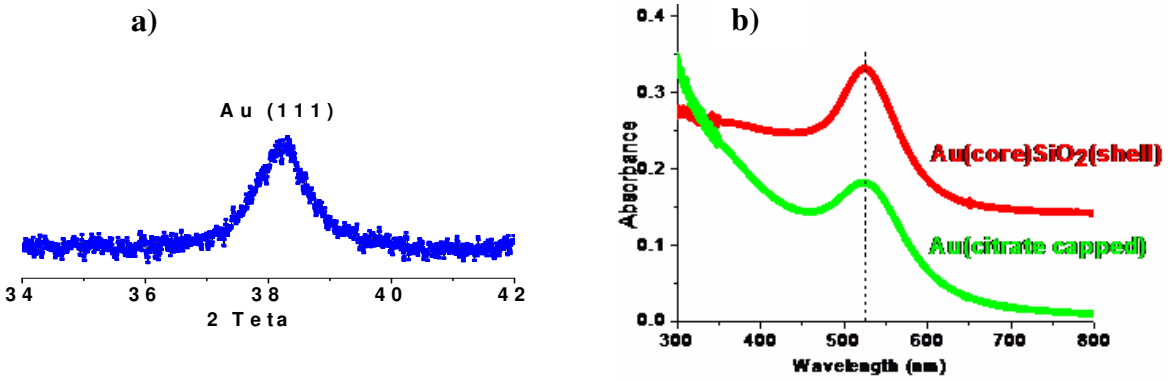


Figure 15.a. XRD pattern of $Au@SiO_2$ and 15.b UV-Vis Absorption Spectrum of $Au@SiO_2$

The angle-dependent XPS analysis of the $Au@SiO_2$ nanoparticles with respect to a gold thin film on silicon substrate containing 4 nm thermally-growth $SiO_2$ layer were carried out to further our understanding of the core-shell structure. Figure 3.16i displays the XPS spectra of the region corresponding to the binding energy range of 110-70 eV,

which includes the Si2p, Au4f, and Cu3p peaks recorded at 90° and 30° electron take-off angles, respectively.

Experimental composition of any sample is correlated to intensity ratios of each species, when elemental XPS cross section of the species and kinetic energies of the emitted photoelectrons generated from different species at different electron take-off angle are taken into account (equation 3.2).[94]

$$\frac{[C]_x}{[C]_y} = \frac{A_x}{A_y}\frac{\sigma_y}{\sigma_x}\left(\frac{E_y^k}{E_x^k}\right)^{\frac{3}{2}} \qquad (3.2)$$

where A is area underneath XPS peak, σ is the XPS cross section and $E_k$ is the kinetic energy of emitted photoelectrons. Using the expression given above, the calculated atomic ratios are $Si_1Au_{0.2}$, and $Si_1Au_{0.19}$ at 90° and 30° take-off angle respectively. According to the calculated intensity ratios at different take-off angle, it can be concluded that composition of spherical nanoparticles is angle-independent, compared to that of gold clusters deposited from the vapor phase (PVD) onto a silicon surface containing ca. 4 nm oxide layer, which is displayed in Figure 3.16ii.

Figure 3.16 shows the intensity ratios of XPS peaks of the gold deposited from the vapor phase on the $SiO_2$/Si system and those of Au@$SiO_2$ at 90° and 30° take-off angle. It is expected that the intensities of the peaks of the elements stemming from regions close to the surface increase comparative to those of peaks away from the

surface, when the XPS spectrum of sample is recorded at lower electron take-off angle. Regarding to this expression, the intensity of the Si2p peak stemming from the oxide ($Si^{IV}$) increases, while that of the silicon ($Si^{0}$) decreases for the sample of gold on $SiO_2$/Si system produced by vapor-deposition at $30^{o}$. Moreover, the intensity of Au4f peak increases relative to both of the silicon peaks, as it belongs to outermost surface species. In the case of the core-shell nanoparticles the intensities of the Si2p and Au4f peaks increase with respect to that of Cu3p substrate peak at the lower take-off angles. However, the Au/Si atomic ratio is constant within the experimental uncertainty limits. Similarly, Piyakis et al. discussed in detail the analysis of spherical Cu nanoparticles, using angle-resolved XPS, they showed that if the radius of the particle is larger than the attenuation length of the photoelectron, the intensity is roughly angle independent.[107] In our case the particle size is ca. 15-20 nm but the attenuation length of the electrons are ca. 1.5-2 nm i.e. 10 times smaller. Hence, it can be concluded that the ratio of the intensity of the XPS peak of the element which belongs to the core and the shell is also angle-independent, not only verifies their findings but also extends it to core-shell nanoparticles.

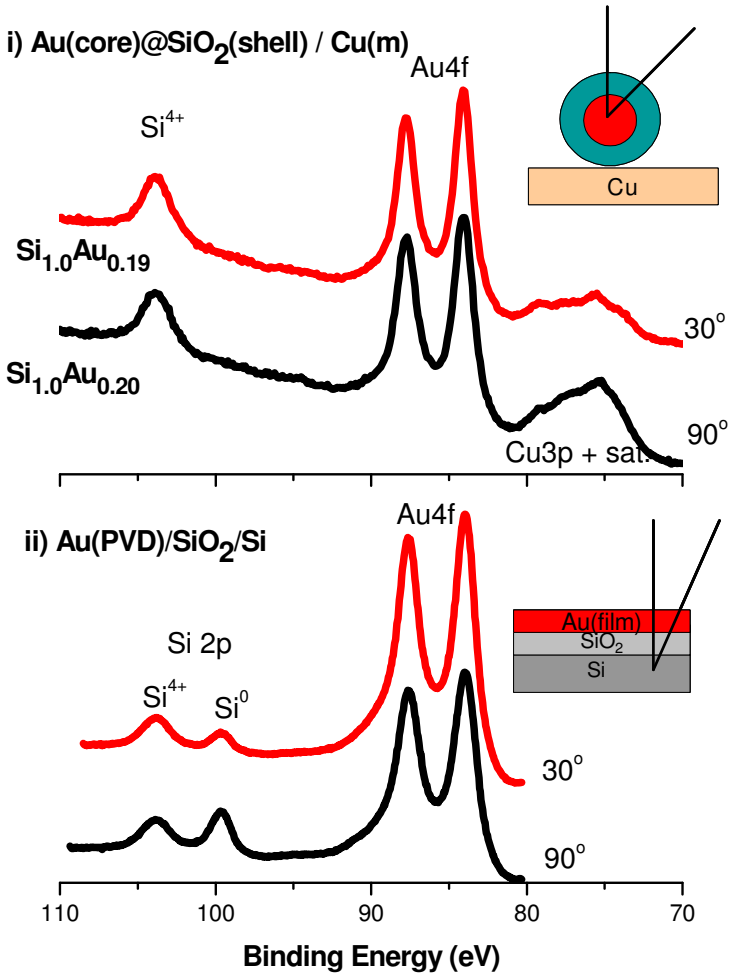


Figure 3.16. The 110-70 eV region of the XPS spectrum recorded at 90° and 30° electron take-off angles corresponding to; i) Au(core)@$SiO_2$(shell) nanoparticles deposited on copper tape; ii) gold particles vapor deposited (PVD) onto a silicon substrate containing ca. 4 nm oxide layer.

Experimental composition determined by XPS can also be related to the geometry of the core-shell nanoparticles, by taking into account the attenuation of the photoelectrons through the core and then the shell, and also the theoretical densities of

the Si in the shell and Au atoms in the core are 0.0383 mol/cm$^3$ and 0.098 mol/cm$^3$ respectively.

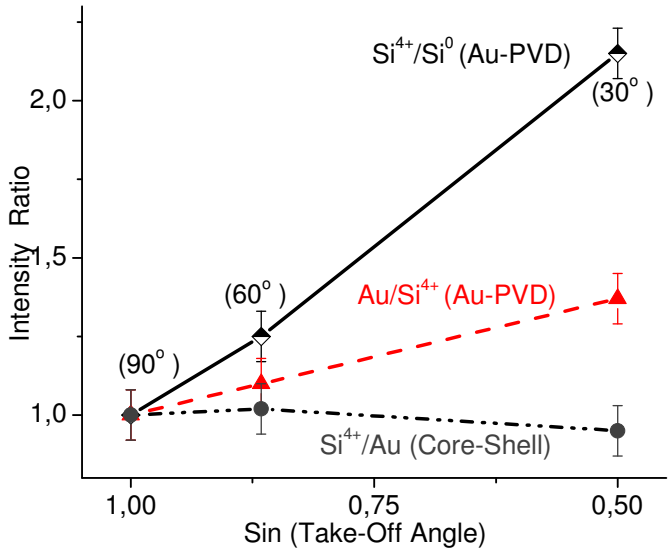


Figure 3.17. Intensity ratio of XPS peaks for $Si(2p)^{IV}/Si(2p)^0$ and $Au4f/Si(2p)^0$ from the PVD sample and $Au4f/Si(2p)^{IV}$ from the $Au@SiO_2$ sample, at 3 three different take-off angles, normalized to the ratio at 90°, and plotted against the sin of the angle.

The formula $\boldsymbol{I = I_0\,(e^{-d/\lambda})}$ gives attenuation of photoelectron intensity, where d is the finite thickness of medium photoelectrons emitted and, λ is the mean free path or attenuation length. The attenuation of photoelectron intensity strongly depends on the kinetic energy of the photoelectrons, and as well as the density of the medium.[125] Since the kinetic energies of the Au4f and the Si2p photoelectrons are very close to each other, the first factor is eliminated. However, the densities of the gold core and the silica shell, and also their scattering powers need to be taken into account. The intensity of a

photoelectron peak given by the formula derived by Wertheim and Dicenzo[108] is as follows;

$$S = \pi\lambda^3\{x^2 + [\{2x+1\}e^{-2x} - 1]/2\} \quad (3.3)$$

where, $x = r/\lambda$, as r is the radius of the nanoparticles which is the 7.5 nm in this case. This formula can be altered to calculate the intensity of the concentric silica shell by first taking the radius as 13.5 nm which is the sum of the core radius and the shell thickness and 7.5 nm which is core radius separately, and subtracting from each other. The difference gives intensity of the concentric silica shell. For the gold core we have to consider the attenuation through the silica shell. One way is to use a simple attenuation factor through the shell;

$$S_{(core)} = e^{-d/\lambda_S} * \pi\lambda_C^3\{x^2 + [\{2x+1\}e^{-2x} - 1]/2\} \quad (3.4)$$

where, d is the thickness of the silica shell, and $\lambda_S$ and $\lambda_C$ are the attenuation length of the core and the shell, respectively. The extended formula derived by Yang et al. is similar to eqn 3.4 but also comprises some additional terms;

$$S(core) = [\{\kappa\{x\}d + \lambda\}/\{d + \lambda\}] * e^{-d/\lambda_S} * \pi\lambda^3\{x^2 + [\{2x+1\}e^{-2x} - 1]/2\} \quad (3.5)$$

where, κ(x) is another function including several other terms. Two points are related to our argument below; i) the additional term in eqn.3.5 is always smaller than 1, and ii) when d=0 eqn.3.5 yields eqn.1. An additional significant point is that in our case it is not appropriate to use a single attenuation length for the core and the shell, as Yang et al. used to derive the equation given above.[109]

**Table I.** Calculated Au/Si atomic ratio for the Au(core)@Silica(shell) nanoparticles using different parameters by XPS together with the experimentally determined ratio.

| | λ-Core (nm) | λ-Shell (nm) | Shell Density (mol/cm$^3$) | Au/Si Ratio | |
|---|---|---|---|---|---|
| Experimental | | | | 0.20 | |
| | | | | Eqn.4 | Eqn.5 |
| Calculated | 1.44 | 2.74 | 0.0383 | 0.07 | 0.05 |
| | 1.44 | 3.50 | 0.0383 | 0.08 | 0.06 |
| | 1.44 | 3.50 | 0.0200 | 0.16 | 0.12 |
| | 1.44 | 3.50 | 0.0160 | 0.20 | 0.16 |
| | 2.50 | 3.50 | 0.0270 | 0.20 | 0.18 |
| | 3.50 | 3.50 | 0.0383 | 0.19 | 0.14 |
| | 3.50 | 3.50 | 0.0270 | 0.27 | 0.20 |

With $MgK_\alpha$ X-rays, practical attenuation lengths for the Au4f peak in the gold metal and the Si2p peak in the silicon oxide are given in the literature as 1.44 and 2.74 nm, respectively.[126] When these are used in eqn.3.4 and 3.5 for gold attenuation through

the silica shell, the calculated Au/Si atomic ratios are obtained as 0.07 and 0.05 respectively, which are too low compared to experimental value of 0.20. Then, the following statements arise. Assuming that the TEM data are reliable, as the calculated data are lower than experimental Au/Si ratio; i) there are extra gold particles without the shell besides core-shell nanoparticles, ii) the silica shell is less dense, resulting in a smaller concentration. iii) the attenuation lengths are different from their bulk values.

Based on other experimental data (shown in Figure 3.19), both Si2p and the Au4f peaks exhibit similar differential charging, which means that they are within close proximity, then the first point can be omitted. The second point is a more dominant contribution, since the silica shell was prepared through precipitation of sodium silicate from solution, oligomers formation in solution prior to the aggregation, is possible. Thus, the porosity is slightly higher than that of organo-silica as was shown by studying chemical reactions on metal cores.[84] On the other hand, though the thickness of the silica shells seems uniform, from TEM we can also see some cases with thinner shells or shells with less uniform thickness, which may influence through the first point. Since the gold shows the characteristic of Au (111) diffraction peak in the XRD studies, the metallic density must be used. The third point is also closely related to the second one since density is an important parameter contributing to the attenuation of the photoelectrons. Yang et al. used the attenuation length as 3.5 nm for the silicon oxide layer for relating their XPS intensities to the silicon oxide-silicon core-shell nanoparticles and justified the use of bulk densities for nanoparticles.[109] As given in Table I, using both eqn. 3.4 and eqn. 3.5 we have calculated a number of possible cases by means of different values for the densities and attenuation lengths. When we analyze the data given in the table, we

realize that we can reproduce the experimentally derived Au/Si atomic ratio only by reducing the density of the silica layer significantly. Other combinations can also be found for the corresponding attenuation length and density to match the experimental ratio, which calls for further theoretical and experimental studies. It can be concluded that densities of bulk and nanoclusters are not identical and also a new mathematical model taking into account different attenuation through the core and the shell must be developed by modifying bulk data.

#### *3.4.1.1. Charging Properties of Metal@$SiO_2$ Core-Shell Nanoparticles*

In order to get deeper information on charging properties of Au@$SiO_2$ nanoparticles, XPS measurements under external bias were recoded compared to pure Au nanoparticles. Binding energy shifts as a function of the external bias and its polarity were monitored.

Figure 3.18 depicts the part of the XPS spectra corresponding to Au 4f (stemming from nanoparticles), Cu 3p (belonging to substrate), and Na 2s (capping agent counter-ion) peaks of the only citrate-capped gold nanoparticles deposited on the copper surface. The spectra were recorded when the sample was (i) grounded, (ii) under -10 V (dc) bias, and (iii) under+10 V (dc) bias. On a conducting substrate such as copper tape, by application of a negative bias, leads to shifts all of the peaks to lower binding energy, and positive bias performs in the opposite direction, as shown in the figure. In the case of nonconducting substrate or regions of the sample with poor electrical conductivity, unsymmetrical shifts are recorded, since under a negative bias, the neutralization caused

by low-energy electrons supplied by stray electrons or a filament within the vacuum system, is prevented. [98, 125] This is illustrated by the Na 2s peak shift, because of differently charging behavior with respect to others. The differential charging shifts of the Na 2s peak with polarity become much more obvious when the spectra are back-shifted by exactly the same amount as the bias (bias correction), as shown in the right side of the figure. After bias correction, Au4f and Cu3p peaks have no binding energy shifts, because of charge compensation. In other words, no charge accumulation on Au nanoparticles on conductive copper surface is observed.

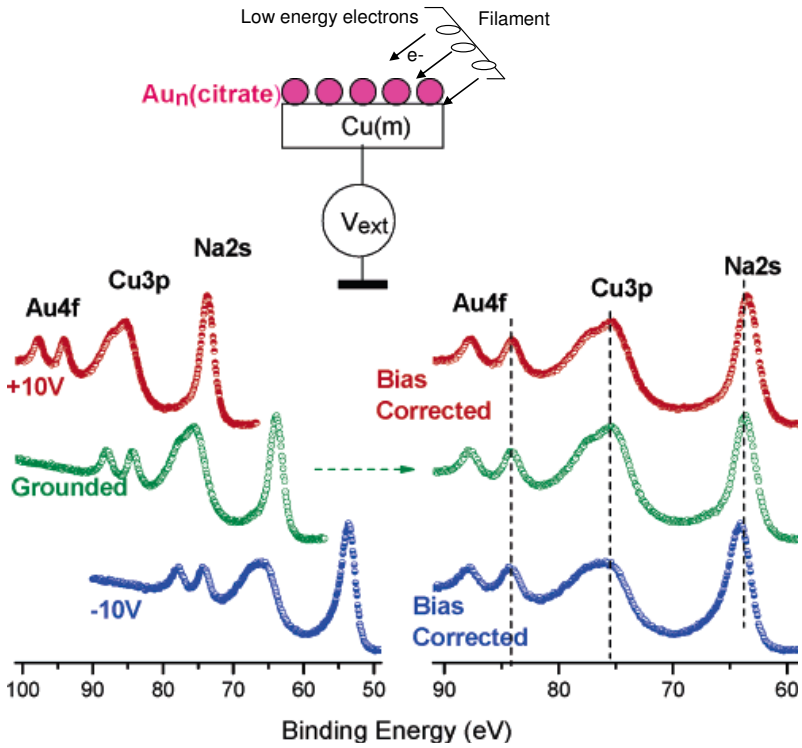


Figure 3.18. Part of the XPS spectra, corresponding to Au 4f, Cu 3p,and Na 2s peaks, of bare gold nanparticles deposited on copper substrate, recorded when the sample was (i) grounded (middle), (ii) under -10 V dc bias (bottom), (iii) and under +10 V dc bias (top).

In the second half of the figure, the same spectra are displayed after being corrected for the bias shift. The inset shows schematically application of the external voltage stress to the sample (via the sample rod).

Figure 3.19 shows the XPS analysis of Au(core)@$SiO_2$(shell) nanoparticles under ± 10 V external bias. The spectra represent Si 2p, Au 4f, and Cu 2p regions before and after bias correction. The core-shell nanoparticles have a 15-nm-diameter gold core and a 6-nm shell as determined from their TEM images as shown in Figure 3.14. The measured differential charging of the core-shell particles as verified with the shift in the measured binding energies regarding to the polarity of the external bias, is displayed in Figure 3.19. When XPS data is recorded under -10 V external bias, because of enhanced positive charging of the nanoparticles Au4f and Si2p shift to higher binding energies, whereas the Au 4f peak is not shifted in the case of bare gold nanoparticles due to the discharging to the conducting substrate. One should be noted that the Cu 2p peak does not shift at all because of discharging through ground. The shift is undoubtly related to charge trapping inside the silica shell, the extent of the differential charging can be increased by the magnitude and the polarity of the biasing voltage. Around *0.5 eV* differential charging was recorded for Au@$SiO_2$ core-shell nanoparticles deposited on copper tape under -10V and +10V external voltage stress.

The positive charges are obtained during photoemission process by creation of holes very fast ($<10^{-12}$ s) and filling of these created holes by the outer electrons consequently. The holes are transferred to the valence band are stabilized in the large band gap of the silicon dioxide. Eventually, these holes are neutralized by low energy

electrons falling onto sample when a positive external voltage stress is applied to control the flux of them. The stored charge within this silica shell of the nanocapacitor can be assessed from the measured *0.5 eV* binding energy difference in the Au4f peak and capacitance is calculated through the following expression;

$$\Delta V = Ne/C_{cs.} \qquad (3.6)$$

and capacitance of the core-shell nanoparticles are given the following expression;[127]

$$C_{cs=} 4\pi\varepsilon_{shell}\varepsilon_0/\{(1/R_{core})-(1/R_{shell}) \qquad (3.7)$$

where dielectric constant of silica shell is taken as 3 and estimated capacitance of the particles is found *10 aF* from expression 3.7, putting to this data on expression 3.6, we can estimate approximately 30 holes remained not neutralized on each particle while -10 V stress is applied, and under +10V stress they become neutralized.

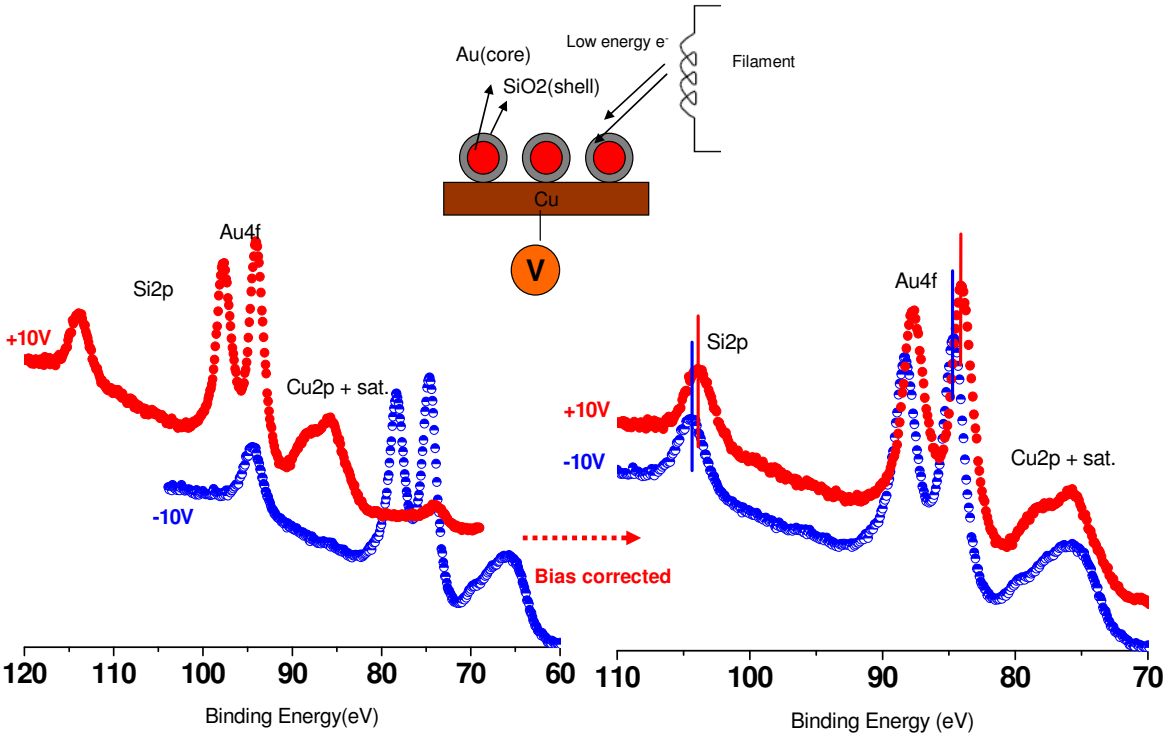


Figure 3.19 The 110-70 eV region of the XPS spectrum corresponding to; Au@$SiO_2$ core-shell nanoparticles on Cu tape under ±10V external bias

In order to analyze charging properties of Ag@$SiO_2$ core-shell nanoparticles on a dielectric substrate, the particles are deposited on a silicon surface containing ca. 5 nm oxide layer. Normally Si surface has native oxide layer on it. But since, the thickness of native oxide is not controlled, it is first removed by etching in HF, then the oxide is grown by controllable heating. Figure 3.20 displays the bias-corrected spectra illustrating Ag3d and Si2p regions in the range of 385-350 eV and 112-96 eV, respectively. Since, $Si^{0}2p$ (A) is chosen as the reference two kinds of $Si^{IV}$ 2p of $SiO_2$, are well-separated

under external bias. One of which belongs to substrate surface (peak B) and other stems from the shell (peak C) covering Ag nanocore. The bias-induced shifts are observed for both $Si^{IV}$ 2p peaks. Even though peak B shows around 3.5 eV differential charging, peak C has a larger shift displaying same differential charging with the Ag3d peak around 15 eV. This large difference is likely related with usage of dielectric substrate comparing to $Au@SiO_2$ on conductor Cu substrate. It is clearly seen that a dielectric substrate increases drastically charging capability of the sample under external biasing.

One issue should be discussed here is that more than one type of silver appear in the spectra. Accordingly, the smaller peak is separated by application of +10V providing either complete neutralization or overneutralization leading to negative charging. But the second one is definitely negatively charged and shifts as much as 15 eV. To understand we formulate the following points; i) nonuniform thickness of the silica shell ii) the presence of bare Ag nanoparticles. The first one requires that there are Ag nanoparticles with different silica shell thicknesses, if so, the additional $Si^{IV}$2p should be further split since it is expected that different $Si^{IV}$2p peaks shift in different manner. Hence the first point is ruled out. The second one is more likely, since it shows less negative charge under +10V. In fact, if the bare Ag nanoparticles exist in direct contact with the $SiO_2$ substrate, it should show less differential charging as expected (around 3.5 eV). Assuming that small amount of bare Ag nanoparticles are present, we again demonstrate one of the advantageous of XPS measurement under external biasing, since by this method bare versus core-shell nanoparticles can be distinguished from each other.

Additionally, angle-independency of core-shell nanoparticles is also obtained for the $Ag@SiO_2$ particles. Namely, the calculated ratio of intensities Ag3d of stemming

from core to Si2p from shell at 90 and $30^0$ take-off angle are *0.07* and *0.09* respectively (almost the same), in agreement with our above findings that the majority of Ag is in the core-shell geometry. The calculated ratio of intensities Ag3d to Si2p allows estimating size of the core-shell nanoparticles using the equation 3.5 assuming almost all Ag nanoparticles have uniform silica shell. Evaluation of the equation 3.5 requires knowledge of attenuation length (λ) of Ag(core) and $SiO_2$(shell) and bulk densities of Ag and silica. Attenuation length is proportional to kinetic energy of photoemmited electrons. The relation is given by Smith[128] as follows;

$$\lambda = 0.016E_k^{0.7608} \qquad (3.8)$$

The calculated $\lambda_{Ag}$ and $\lambda_{SiO2}$ are 2.8 nm and 3.4 nm respectively. Hence, taking into account the densities of Ag and $SiO_2$ as 0.097 and 0.0383 mol/$cm^3$ and putting all into the $S_{core}/S_{shell}$ equation results two-unknown equation which was solved by MATLAB computer program. Figure 3.21a shows the 3-dimensional plots of the thickness of $SiO_2$ ($d_s$), radius of the Ag(core) ($r_s$) and the calculated intensity atomic ratio of Ag to $SiO_2$. Since experimental ratio is 0.07 as a result of XPS measurement, Figure 3. 21b. displays $d_s$ versus $r_c$ plots which corresponds to this experimental ratio. In this regard, the radius of the Ag(core) and the thickness of the $SiO_2$(shell) are evaluated as 6-6.5 nm and 7-7.5 nm, respectively. Since by this method the average size of the citrate-capped Ag nanoparticles is well-known to the 10-15 nm,[67] thus the estimated core radius is reasonable.

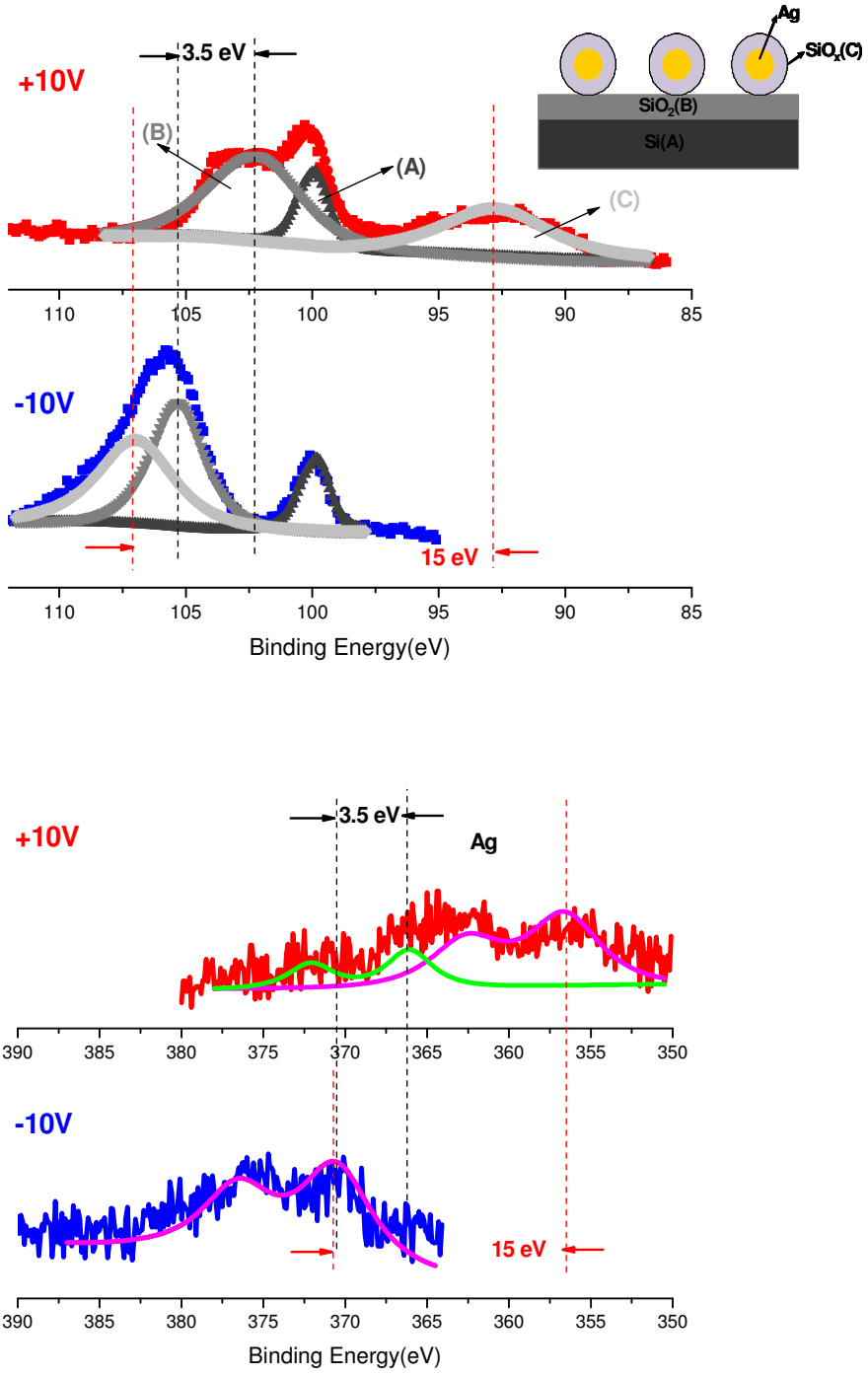


Figure 3.20 The regions 112-96 and 385-350 eV of XPS Spectra corresponding to Ag@$SiO_2$ core-shell nanoparticles deposited on $SiO_2$/Si surface at -10V and +10V external bias.

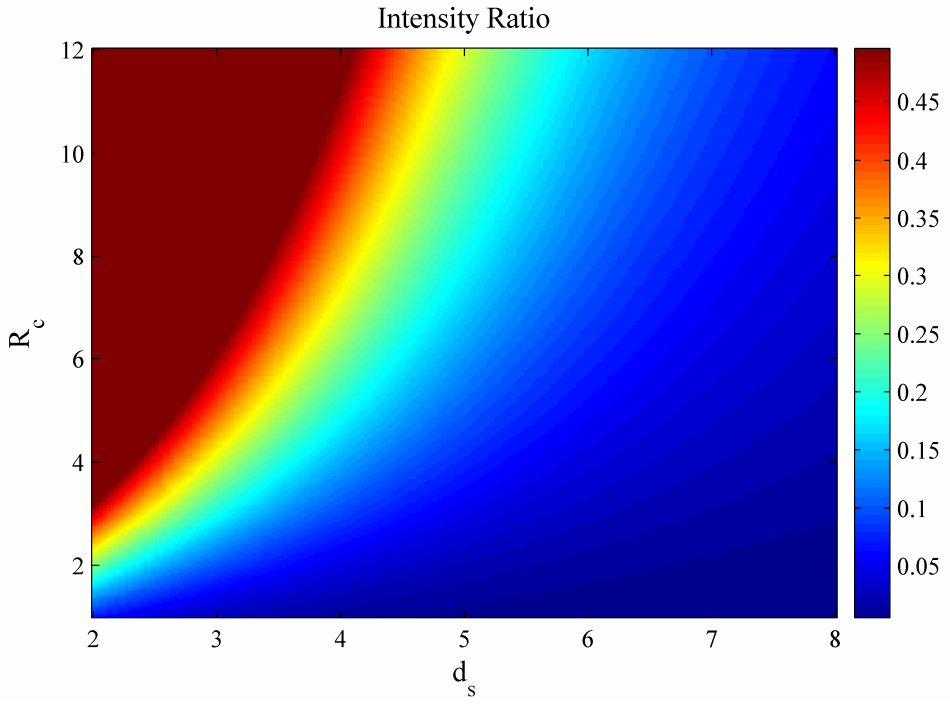


Figure 3. 21a A representative plot of the thickness of $SiO_2$ ($d_s$), radius of Ag(core) ($r_s$) and calculated intensity atomic ratio of Ag to $SiO_2$.

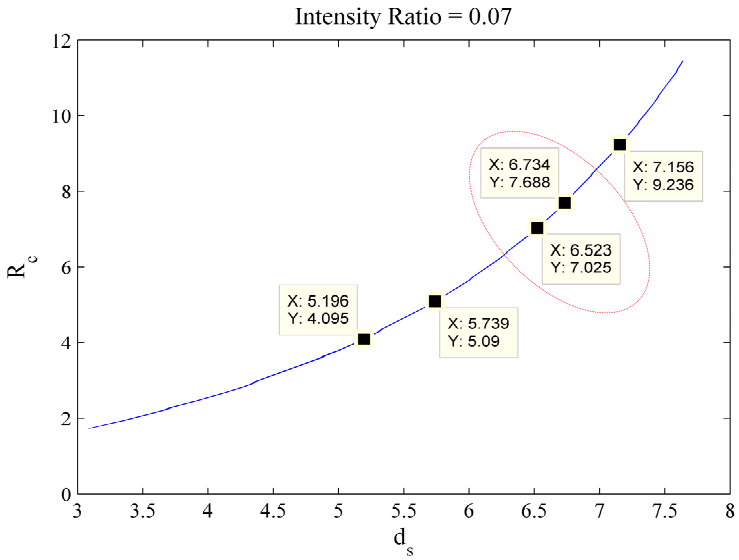


Figure 3. 21b Plot of the thickness of $SiO_2$ ($d_s$) versus the radius of Ag(core) ($r_s$) corresponding to experimental intensity ratio of Ag to $SiO_2$ (0.07).

### *3.4.2. Metal@$TiO_2$ Core-shell Nanoparticles*

#### *3.4.2.1. Optical Characterization of Ag(core)@$TiO_2$(shell) Nanoparticles*

$Ag@TiO_2$ displays strong SPR band in the visible region. This visible absorption arises from silver core which is strongly affected by the oxide shell. As shown in Figure 3.22, whereas the surface plasmon absorption of citrate-capped Ag nanoparticles is around 25300 $cm^{-1}$ (395 nm), that of $Ag@TiO_2$ (21000 $cm^{-1}$, 475 nm) is strongly red-shifted.

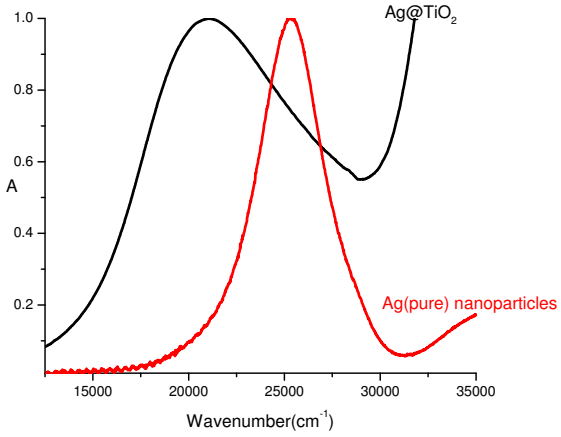


Figure 3.22 SPR band of citrate-capped Ag nanoparticles versus $Ag@TiO_2$.

As reported earlier,[3, 15] spectral shift strongly depends on the refractive index of the surrounding medium, high refractive index of titania shell bring about large red-shift in the SPR band of Ag(core), since $n_{TiO2}$ (2.5) for shell is much higher than $n_{EtOH}$ (1.359).

Capping with $TiO_2$ shell is also verified by checking the stability in acidic solution ($HNO_3$ at pH=2). Whereas Ag nanoparticles are dissolved in acidic solution, $Ag@TiO_2$ nanoparticles are quite stable evidenced by the SPR bands.[73] The stability test

verifies that Ag(core) is surrounded by uniform $TiO_2$(shell) providing protection against acids. In Figure 3.23 stability test of Ag@$TiO_2$ nanoparticles is depicted compared to citrate Ag nanoparticles.

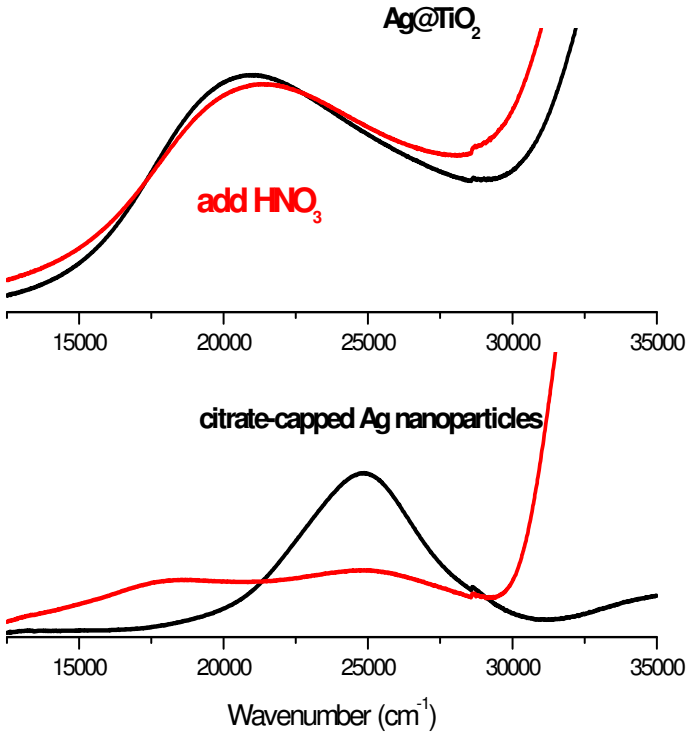


Figure 3.23 The stability test of Ag@$TiO_2$ colloids versus citrate-capped Ag nanoparticles against $HNO_3$ acid (at pH=2).

### *3.4.2.2. Photoactivity of Ag@$TiO_2$*

Figure 3.24 displays the change in absorption band with time following the UV-Irradiated Ag@$SiO_2$ and Ag@$TiO_2$ colloids in deaerated ethanol. Before subjecting Ag@$TiO_2$ colloids to UV-irradiation the absorption band is observed at 21000 $cm^{-1}$ (475

nm). As the colloids are UV-irradiated for 30 min, the absorption band is shifted to 23000 $cm^{-1}$ (435 nm). The large spectral-blue shift reflects the increased electron density on the Ag core as a result of photoactivity of $TiO_2$. Since $TiO_2$ undergoes charge separation under UV irradiation until charge equilibration is carried out between $TiO_2$ and Ag. The photogenerated electrons are transferred to the Ag core with a favorable Fermi level. ($E_f$=0.4 eV) The process was extensively discussed in section *1.3.2.1.* On the other hand, Ag@$SiO_2$ does not show any shift on its SPR band, due to the lack of such a photoactivity of Ag@$SiO_2$ nanoparticles, when UV-irradiated.

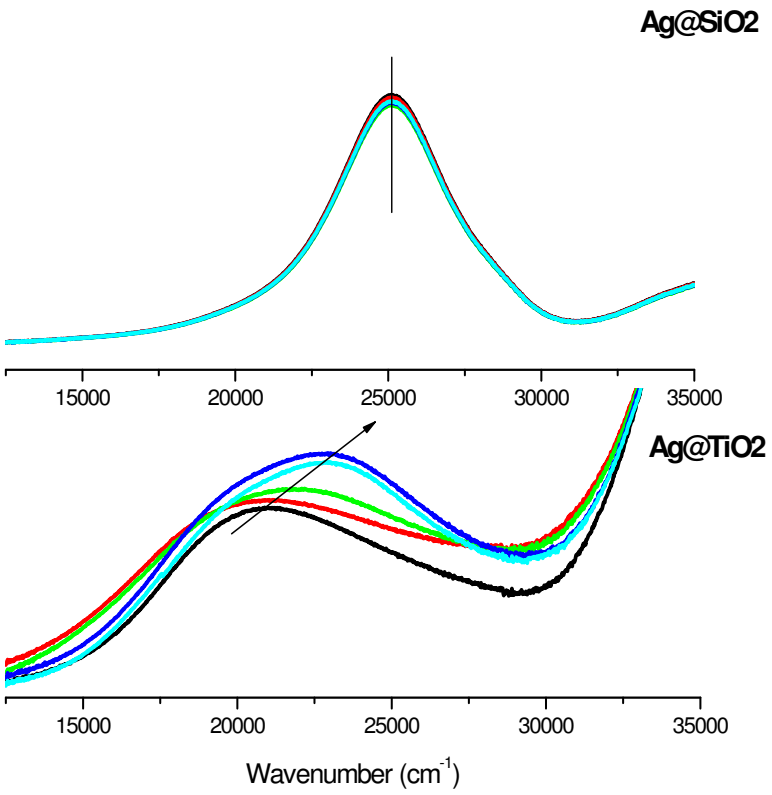


Figure 3.24 Absorption spectra of UV-Irridiated Ag@$SiO_2$ and Ag@$TiO_2$ colloids in ethanol by time.

As discussed above in detail, another way to follow charging of the colloids, is adding $NaBH_4$. Hence, to compare spectral shifts as a result of electron storage, both $Ag@TiO_2$ and $Ag@SiO_2$ solutions are treated with $NaBH_4$. Figure 3.25 shows the spectral blue-shifts of $Ag@SiO_2$ and $Ag@TiO_2$ colloids by adding the same amount of $NaBH_4$. Although, there is no shift in the SPR band of $Ag@SiO_2$, as much as 2000 $cm^{-1}$ blue-shift is observed in the case of $Ag@TiO_2$ colloids. The large blue-shift is exactly the same with the one obtained by UV irradiation. It can be inferred that similarity between behavior of $Ag@TiO_2$ in Figure 3.24 and 3.25, is the characteristic of $TiO_2$ nanoshell which is also closely related with the photocatalytic activity of $TiO_2$.

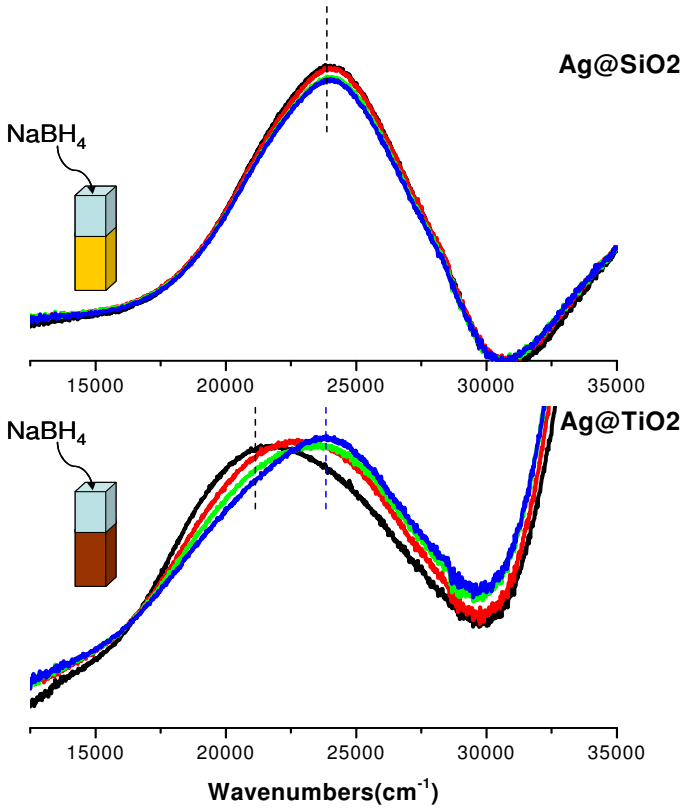


Figure 3.25 Absorption spectra of $Ag@SiO_2$ and $Ag@TiO_2$ colloids in ethanol recorded at different time after adding $NaBH_4$.

Figure 3.26 is an illustration of the combined process of electron storage of $Ag@TiO_2$ nanoparticles by UV-radiation and $NaBH_4$ introduction, respectively. The charged $Ag@TiO_2$ nanoparticles by UV radiation discharge within five minutes when exposed to air, as a second step, addition of $NaBH_4$ to the nanoparticles leads to similar behavior as a result of increased electron density. The particles discharge, and then absorption band displays back shifting to the starting point. Thus, both UV radiation and addition of $NaBH_4$ processes work in a similar manner, leading to increase of electron density at Ag particles embedded in $TiO_2$ and do not interfere each other when sequentially applied.

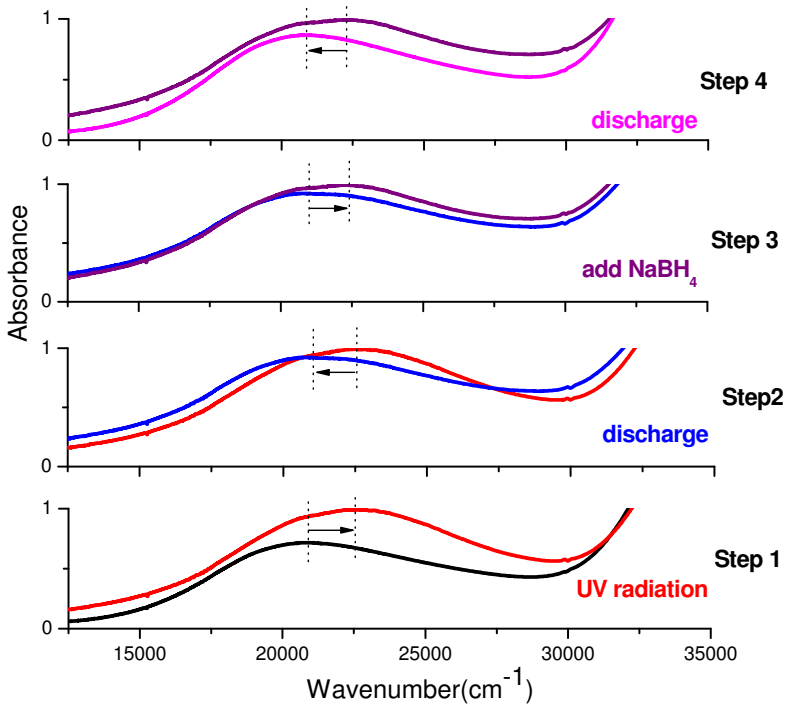


Figure 3.26 Spectral shifts of the absorption band of $Ag@TiO_2$ in ethanol by UV radiation and adding $NaBH_4$ sequentially.

*3.4.2.3 XPS Characterization of Ag@$TiO_2$*

Figure 3.27 displays the regions of 375-360 eV, 475-450 eV and 105-90 eV bias-corrected XPS Spectra of Ag@$TiO_2$ deposited on $SiO_2$/Si system, corresponding to Ag(3d), Ti(2p), and Si(2p) respectively under ± 10V external bias. According to the spectra, Ag core shows same differential charging with $TiO_2$ shell (around 2 eV), although $Si^{4+}$(2p) stemming from substrate has less differential charging (1.27 eV). The external bias was ± 10 V which causes the samples to be negatively and positively charged, respectively.

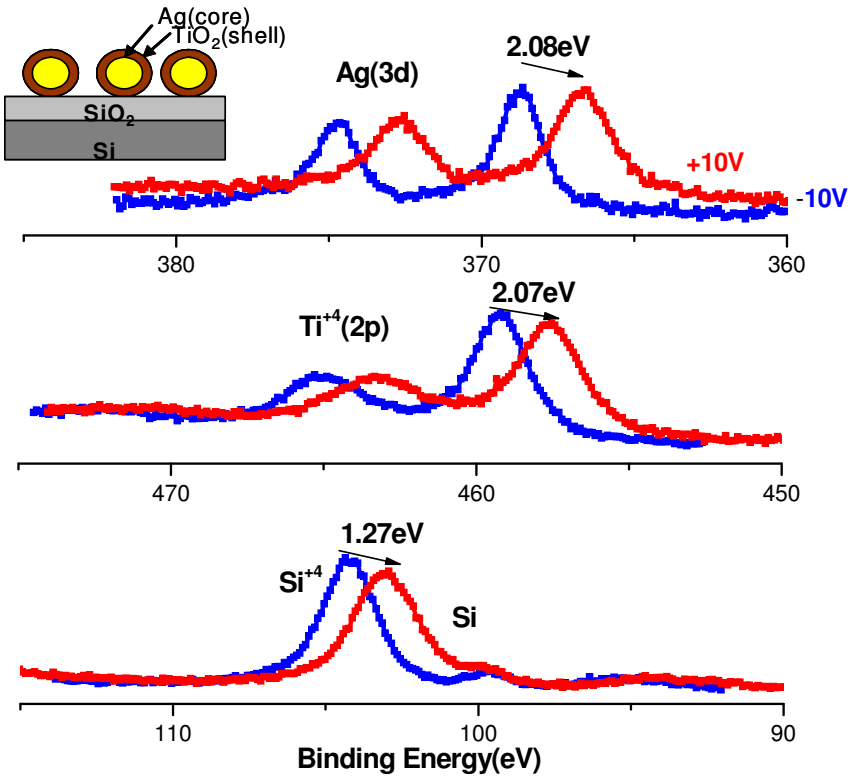


Figure 3.27 The regions 375-360 eV, 475-450 eV and 105-90 of XPS Spectra of Ag@$TiO_2$ deposited on $SiO_2$/Si corresponding to Ag(3d), Ti(2p), Si(2p ) under ± 10V external bias.

Ag(core) has less differential charging (2 eV) compared to that of Ag(core) incorporated within $SiO_2$ shell (around 15 eV) which is discussed above (in Figure 3.20) owing to characteristic of the dielectric shell. Differential charging is inversely proportional to dielectric constant and since the dielectric constant of $TiO_2$ is larger, charging is proportionally less when compared with $SiO_2$ which has a dielectric constant of around 3.

The structure of core-shell nanoparticles can also be identified by angle-dependent XPS by changing the take-off angle, as discussed earlier. There is no significant change in composition at different take-off angle for $Ag@TiO_2$ nanoparticles. Hence, the core-shell structure of the corresponding nanoparticles is once more verified by angle-independency.

The particle size is estimated by the same way discussed for $Ag@SiO_2$ nanoparticles. Figure 28a shows the plots of thickness of the $TiO_2$(shell) ($d_s$), radius of the Ag(core) ($r_s$) and the calculated intensity ratio of Ag to $TiO_2$. Since experimental ratio calculated as 0.34 as a result of XPS measurement, Figure 3. 28b. displays $d_s$ versus $r_c$ plots which corresponds to this experimental ratio. According to this calculation assuming that 5nm Ag nanoparticles are surrounded by ca. 3 nm $TiO_2$ shell. Capacitance of these particles is estimated to be around 130 aF taken into account dielectric constant of $TiO_2$ is around 80. Furthermore charge on the particles using also the binding energy difference (2 eV) is assessed as approximately *1600 holes* which remains not neutralized when -10 V external bias is applied.

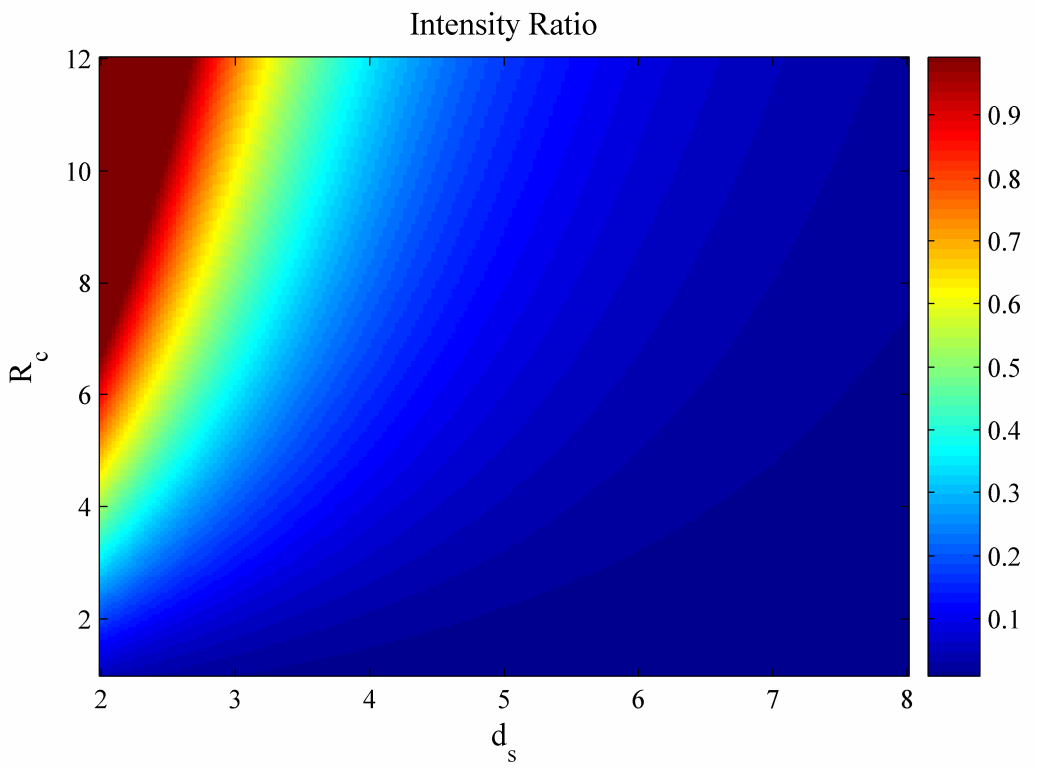


Figure 28a. A representative plot of thickness of the $TiO_2$(shell) ($d_s$), radius of the Ag(core) ($r_s$) and the calculated intensity ratio of Ag to $TiO_2$.

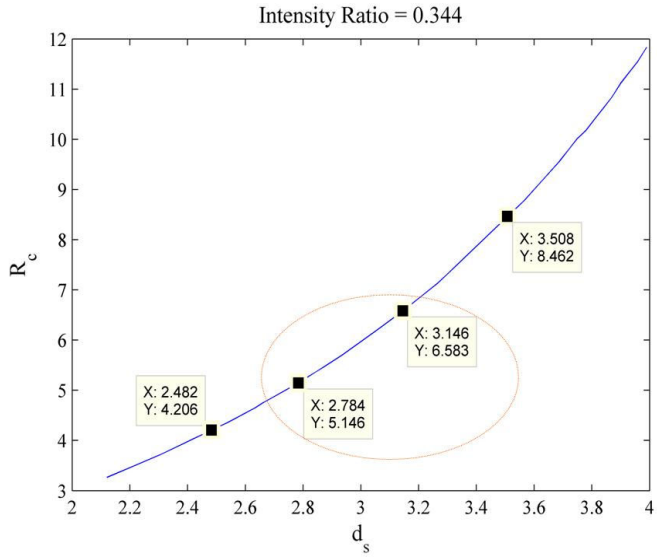


Figure 3. 28b. Plot of the thickness of $TiO_2$ ($d_s$) versus the radius of Ag(core) ($r_s$) corresponding to experimental intensity ratio of Ag to $TiO_2$.

## 4. CONCLUSION

In this thesis, Firstly, I presented preparation and characterization of bimetallic Ag and Au nanoalloys and core-shell nanoparticles. It is possible to synthesize Au-Ag alloy nanoparticles with any desired composition leading to tune the SPR band in between those of pure Au and Ag nanoparticles. On the other hand, by sequential reduction Au-Ag and/or Ag-Au core-shell nanoparticles are synthesized, the SPR bands of which depend strongly on the shell. Alternatively, in order to tune the plasmon resonance band the gold content in Au-Ag alloy nanoparticles and the geometry (in core-shell) are changed. Additionally, electron storage capacities of these nanoparticles due to composition and geometry are discussed by introducing $NaBH_4$. The spectral blue shift as a function of electron storage is followed to probe the kinetics of the process. The kinetics of electron capturing/releasing process allowed us to determine that Au is better and faster in both electron capturing and releasing processes, as expected.

Second, preparation, optical characterization of ca. 5-7.5 nm Au and Ag core surrounded by ca. 3-7.5 nm $SiO_2$ and $TiO_2$ shell nanoparticles is also carried out in order to investigate charging abilities both in solution and under external stimuli by XPS. Since silica doe not have a large dielectric constant, the SPR band is not affected strongly. However, the large dielectric constant of titania, leads to large red-shift in the SPR band. Silica and titania capping of metal nanoparticles is vital for both protection and surface modification. Characterization of geometry, charging properties, and composition of these silica-coated nanoparticles are also carried out by a highly surface sensitive technique, XPS. The XPS intensity ratios of the peaks from elements stemming from core

and from shell, is an important source of information to extract geometrical information at different take-off angles. Accordingly, the core-shell nanoparticles do not exhibit any angle-dependency.

Application of external bias during XPS measurement is important for determining charging properties of these particles and chemical composition of elements in nanoparticles as well. In this contribution, Au@$SiO_2$ on Cu, Ag@$SiO_2$ on $SiO_2$/Si and Ag@$TiO_2$ on $SiO_2$/Si are analyzed by XPS under ± 10V external bias. Binding energy shifts are correlated with usage of different dielectricity of the shells and substrates. $SiO_2$ shows larger differential charging compared to $TiO_2$ shell which is easily explained due to the differences in dielectric constants.

Titania deposition on metal nanoparticles is also important for surface modification leading to an increase in the photocatalytic activity. Ag@$TiO_2$ nanoparticles are characterized optically and photoinduced charging properties as well as their electron storage capacities are investigated optically by UV-radiation and addition of $NaBH_4$ respectively.

## 5. REFERENCES


1. Harden, D., Glass of the Caesars, exh. cat. *London, The British Museum Press* **1988**.

2. Tait, H., Five thousand years of glass. *London, The British Museum Press* **1991**.

3. Kreibig, U.; Vollmer, M., *Optical Properties of Metal Clusters*. Springer: Berlin, **1995.**

4. Liz-Marzan, L. M., Tailoring surface plasmons through the morphology and assembly of metal nanoparticles. *Langmuir* **2006**, 22, (1), 32-41.

5. Alvarez, M. M.; Khoury, J. T.; Schaaff, T. G.; Shafigullin, M. N.; Vezmar, I.; Whetten, R. L., Optical absorption spectra of Nanocrystal Gold molecules. *Journal of Physical Chemistry B* **1997**, 101, (19), 3706-3712.

6. Chen, S. W.; Ingram, R. S.; Hostetler, M. J.; Pietron, J. J.; Murray, R. W.; Schaaff, T. G.; Khoury, J. T.; Alvarez, M. M.; Whetten, R. L., Gold nanoelectrodes of varied size: Transition to molecule-like charging. *Science* **1998**, 280, (5372), 2098-2101.

7. El-Sayed, M. A., Some interesting properties of metals confined in time and nanometer space of different shapes. *Accounts of Chemical Research* **2001**, 34, (4), 257-264.

8. Heath, J. R.; Knobler, C. M.; Leff, D. V., Pressure/temperature phase diagrams and superlattices of organically functionalized metal nanocrystal monolayers: The influence of particle size, size distribution, and surface passivant. *Journal of Physical Chemistry B* **1997**, 101, (2), 189-197.

9. Henglein, A., Electronics of colloidal nanometer particles. *Berichte Der Bunsen-Gesellschaft-Physical Chemistry Chemical Physics* **1995**, 99, (7), 903-913.

10. Henglein, A., Radiolytic preparation of ultrafine colloidal gold particles in aqueous solution: Optical spectrum, controlled growth, and some chemical reactions. *Langmuir* **1999**, 15, (20), 6738-6744.

11. Henglein, A.; Meisel, D., Radiolytic control of the size of colloidal gold nanoparticles. *Langmuir* **1998**, 14, (26), 7392-7396.

12. Kim, S. H.; Medeiros-Ribeiro, G.; Ohlberg, D. A. A.; Williams, R. S.; Heath, J. R., Individual and collective electronic properties of Ag nanocrystals. *Journal of Physical Chemistry B* **1999**, 103, (47), 10341-10347.

13. Link, S.; El-Sayed, M. A., Size and temperature dependence of the plasmon absorption of colloidal gold nanoparticles. *Journal of Physical Chemistry B* **1999**, 103, (21), 4212-4217.

14. Mirkin, C. A.; Letsinger, R. L.; Mucic, R. C.; Storhoff, J. J., A DNA-based method for rationally assembling nanoparticles into macroscopic materials. *Nature* **1996**, 382, (6592), 607-609.

15. Mulvaney, P., Surface plasmon spectroscopy of nanosized metal particles. *Langmuir* **1996**, 12, (3), 788-800.

16. Pileni, M. P., Optical properties of nanosized particles dispersed in colloidal solutions or arranged in 2D or 3D superlattices. *New Journal of Chemistry* **1998**, 22, (7), 693-702.

17. Schaaff, T. G.; Shafigullin, M. N.; Khoury, J. T.; Vezmar, I.; Whetten, R. L.; Cullen, W. G.; First, P. N.; GutierrezWing, C.; Ascensio, J.; JoseYacaman, M. J., Isolation of smaller nanocrystal au molecules: Robust quantum effects in optical spectra. *Journal of Physical Chemistry B* **1997**, 101, (40), 7885-7891.

18. Liu, J.-H.; Wang, A.-Q.; Chi, Y.-S.; Lin, H.-P.; Mou, C.-Y., Synergistic effect in an Au-Ag Alloy Nanocatalyst: CO Oxidation *Journal of Physical Chemistry B* **2005**, 109, (1), 40-43.

19. Liz-Marzan, L. M.; Philipse, A. P., Stable hydrosols of metallic and bimetallic nanoparticles immobilized on imogolite fibers. *Journal of Physical Chemistry B* **1995**, 99, (41), 15120.

20. Zhang, Q.; Lee, J. Y.; Yang, J.; Boothroyd, C.; Zhang, J., Size and composition tunable Ag-Au alloys nanoparticles by replacement reactions. *Nanotechnology* **2007**, 18, 1-8.

21. Kittel, C., *Introduction to Solid State Physics*. Wiley New York, **1996**.

22. Link, S.; Wang, Z. L.; El-Sayed, M. A., Alloy formation of Gold-Silver nanoparticles and the dependence of the plasmon absorption on their composition. *Journal of Physical Chemistry B* **1999**, 103, (18), 3529-3533.

23. Papavassiliou, G. C., *J. Phys. F: Met. Phys.* **1976,** 6, 103-107.

24. Teo, B. K.; Keating, K.; Kao, Y.-H., Observation of plasmon frequency in the optical spectrum of Au18Ag20 cluster: the beginning of the collective phenomenon characteristics of the bulk? *Journal of American Chemical Society* **1987**, 109, (11), 3494-3495.

25. Sato, T.; Kuroda, S.; Takami, A.; Yonezawa, Y., Photochemical formation of silver-gold (AgAu) composite colloids in solutions containing sodium alginate. *Applied Organometalic Chemistry* **1991**, 5, 261-268.

26. Mallin, M. P.; Murphy, C. J., Solution-Phase Synthesis of Sub-10 nm Au-Ag Alloy Nanoparticles. *Nano Lett.* **2002**, 2, (11), 1235-1237.

27. Rodriguez-Gonzalez, B.; Sanchez-Iglesias, A.; Giersig, M.; Liz-Marzan, L. M., AuAg bimetallic nanoparticles: formation, silica-coating and selective etching. *Faraday Discussions* **2004**, 125, 133-144.

28. Rodriguez-Gonzalez, B.; Burrows, A.; Watanabe, M.; Kiely, C. J.; Marzan, L. M. L., multishell bimetallic AuAg nanoparticles: synthesis, structure and optical properties. *Journal of Materials Chemistry* **2005**, 15, (17), 1755-1759.

29. Jin, R. C.; Cao, Y. W.; Mirkin, C. A.; Kelly, K. L.; Schatz, G. C.; Zheng, J. G., Photoinduced conversion of silver nanospheres to nanoprisms. *Science* **2001**, 294, (5548), 1901-1903.

30. Morriss, R. H.; Collins, L. F., A Simple method for the production of a two-dimensional, ordered array of small latex particles *Journal of Chemical Physics* **1964**, 41, 3357.

31. Mulvaney, P.; Giersing, M.; Henglein, A., Surface chemistry of colloidal gold: deposition of lead and accompanying optical effects. *Journal of Physical Chemistry* **1992**, 96,(25), 10419.

32. Mulvaney, P.; Giersig, M.; Henglein, A., Electrochemistry of multilayer colloids: preparation and absorption spectrum of gold-coated silver particles. *Journal of Physical Chemistry* **1993**, 97, (27), 7061.

33. Rivas, L.; Sanchez-Cortes, S.; Garcia-Ramos, J. V.; Morcillo, G., Mixed silver/gold colloids: A study of their formation, morphology, and surface-enhanced Raman activity. *Langmuir* **2000**, 16, (25), 9722-9728.

34. Srnova-Sloufova, I.; Lednicky, F.; Gemperle, A.; Gemperlova, J., Core-shell (Ag)Au bimetallic nanoparticles: Analysis of transmission electron microscopy images. *Langmuir* **2000**, 16, (25), 9928-9935.

35. Lu, L.; Wang, H.; Zhou, Y.; Xi, S.; Zhang, H.; Hu, J.; Zhao, B., Seed-mediated growth of large, monodisperse core-shell Gold–Silver nanoparticles with Ag-like optical properties. . *Chemical Communications* **2002**, 2, 144.

36. Kamat, P. V.; Flumiani, M.; Dawson, A., Metal-metal and metal-semiconductor composite nanoclusters. *Colloids and Surfaces a-Physicochemical and Engineering Aspects* **2002**, 202, (2-3), 269-279.

37. Sun, Y.; Xia, Y., Multiple-Walled Nanotubes Made of Metals. *Advanced Materials* **2004**, 16, 264-268.

38. Sanedrin, R. G.; Georganopoulou, D. G.; Park, S.; Mirkin, C. A., Seed-mediated growth of bimetallic prisms. *Advanced Materials* **2005**, 17, 1027-1031.

39. Oldenburg, S. J.; Jackson, S. B.; Westcott, S. L.; Halas, N. J., Infrared extinction properties of gold nanoshells. *Applied Physics Letters* **1999**, 75, (19), 2897-2899.

40. Schierhorn, M.; Liz-Marzan, L. M., Synthesis of bimetallic colloids with tailored intermetallic separation. *Nano Letters* **2002**, 2, (1), 13-16.

41. Sinzig, J.; Quinten, M., Scattering and absorption by spherical multilayer particles. *Applied Physics a-Materials Science & Processing* **1994**, 58, (2), 157-162.

42. Abid, J. P.; Girault, H. H.; Brevet, P. F., Selective structure changes of core-shell gold-silver nanoparticles by laser irradiation: homogeneisation vs. silver removal. *Chemical Communications* **2001**, (9), 829-830.

43. Hodak, J. H.; Henglein, A.; Hartland, G. V., Photophysics of nanometer sized metal particles: Electron-phonon coupling and coherent excitation of breathing vibrational modes. *Journal of Physical Chemistry B* **2000**, 104, (43), 9954-9965.

44. Thomas, K. G.; Zajicek, J.; Kamat, P. V., Surface binding properties of tetraoctylammonium bromide-capped gold nanoparticles. *Langmuir* **2002**, 18, (9), 3722-3727.

45. Kamat, P. V., Photophysical, photochemical and photocatalytic aspects of metal nanoparticles. *Journal of Physical Chemistry B* **2002**, 106, (32), 7729-7744.

46. Underwood, S.; Mulvaney, P., Effect of the Solution Refractive-Index on the Color of Gold Colloids. *Langmuir* **1994**, 10, (10), 3427-3430.

47. Hughes, A. E.; Jain, S. C., Metal Colloids in Ionic-Crystals. *Advances in Physics* **1979**, 28, (6), 717-828.

48. Templeton, A. C.; Wuelfing, M. P.; Murray, R. W., Monolayer protected cluster molecules. *Accounts of Chemical Research* **2000**, 33, (1), 27-36.

49. Templeton, A. C.; Pietron, J. J.; Murray, R. W.; Mulvaney, P., Solvent refractive index and core charge influences on the surface plasmon absorbance of alkanethiolate monolayer-protected gold clusters. *Journal of Physical Chemistry B* **2000**, 104, (3), 564-570.

50. Lin, S. T.; Franklin, M. T.; Klabunde, K. J., Nonaqueous colloidal gold. Clustering of metal atoms in organic media. 12 *Langmuir* **1986**, 2, (2), 259-263.

51. Henglein, A., Physicochemical properties of small metal particles in solution: "microelectrode" reactions, chemisorption, composite metal particles, and the atom-to-metal transition *Journal of Physical Chemistry* **1993**, 97, (21), 5457-71.

52. Pileni, M. P., Nanocrystal Self-Assemblies: Fabrication and collective properties *Journal of Physical Chemistry B* **2001**, 105, (17), 3358-3378.

53. Strelow, F.; Henglein, A., Time-resolved chemisorption of I- and Sh- on colloidal Silver particles (a Stopped-Flow Study). *Journal of Physical Chemistry* **1995**, 99, (31), 11834-11838.

54. Hirakawa, T.; Kamat, P. V., Photoinduced electron storage and surface plasmon modulation in Ag@$TiO_2$ clusters. *Langmuir* **2004**, 20, (14), 5645-5647.

55. Hirakawa, T.; Kamat, P. V., Charge separation and catalytic activity of Ag@$TiO_2$ core-shell composite clusters under UV-irradiation. *Journal of the American Chemical Society* **2005**, 127, (11), 3928-3934.

56. Jakob, M.; Levanon, H.; Kamat, P. V., Charge distribution between UV-irradiated $TiO_2$ and Gold nanoparticles: determination of shift in the fermi level. *Nano Lett.* **2003**, 3, (3), 353-358.

57. Ung, T.; Liz-Marzan, L. M.; Mulvaney, P., Redox catalysis using Ag@$SiO_2$ colloids. *Journal of Physical Chemistry B* **1999**, 103, (32), 6770-6773.

58. Mulvaney, P.; Linnert, T.; Henglein, A., Surface chemistry of colloidal silver in aqueous solution: observations on chemisorption and reactivity *Journal of Physical Chemistry* **1991**, 95, (20), 7843-7846.

59. Alivisatos, A. P., Semiconductor clusters, nanocrystals, and quantum dots. *Science* **1996,** 271, (5251), 933-937.

60. Lieber, C. M., One-dimensional nanostructures: Chemistry, physics & applications. *Solid State Communications* **1998**, 107, (11), 607-616.

61. Foss, C. A.; Hornyak, G. L.; Stockert, J. A.; Martin, C. R., Template-synthesized nanoscopic Gold particles - Optical-Spectra and the Effects of Particle-Size and Shape. *Journal of Physical Chemistry* **1994**, 98, (11), 2963-2971.

62. Esumi, K.; Matsuhisa, K.; Torigoe, K., Preparation of rodlike Gold particles by Uv irradiation using cationic micelles as a template. *Langmuir* **1995**, 11, (9), 3285-3287.

63. Jana, N. R.; Gearheart, L.; Murphy, C. J., Wet chemical synthesis of silver nanorods and nanowires of controllable aspect ratio. *Chemical Communications* **2001**, (7), 617-618.

64. Yu, Y. Y.; Chang, S. S.; Lee, C. L.; Wang, C. R. C., Gold nanorods: electrochemical synthesis and optical properties. *Journal of Physical Chemistry B* **1997**, 101, (34), 6661-6664.

65. Belloni, J.; Mostafavi, M.; Remita, H.; Marignier, J. L.; Delcourt, M. O., Radiation-induced synthesis of mono- and multi-metallic clusters and nanocolloids. *New Journal of Chemistry* **1998,** 22, (11), 1239-1255.

66. Ahmadi, T. S.; Wang, Z. L.; Green, T. C.; Henglein, A.; El-Sayed, M. A., Shape-controlled synthesis of colloidal platinum nanoparticles. *Science* **1996**, 272, (5270), 1924-1926.

67. Turkevich, J.; Stevenson, P. L.; Hillier, J., A study of the nucleation and growth processes in the synthesis of colloidal gold. *Discuss. Faraday Soc.* **1951**, 11, 55-75.

68. Teranishi, T.; Hosoe, M.; Tanaka, T.; Miyake, M., Size control of monodispersed Pt nanoparticles and their 2D organization by electrophoretic deposition. *Journal of Physical Chemistry B* **1999**, 103, (19), 3818-3827.

69. Taleb, A.; Petit, C.; Pileni, M. P., Synthesis of highly monodisperse Silver nanoparticles from AOT reverse micelles: A Way to 2D and 3D self-organization. *Chemical Materials* **1997**, 9, (4), 950-959.

70. Stremsdoerfer, G.; Perrot, H. M., J. R.; Clechet, P. J., Autocatalytic deposition of Gold and Palladium onto n-GaAs in acidic media *Electrochemical Society* **1988**, 135, (11), 2881-2885.

71. Pillai, Z. S.; Kamat, P. V., What factors control the size and shape of silver nanoparticles in the citrate ion reduction method? *Journal of Physical Chemistry B* **2004**, 108, (3), 945-951.

72. Koshkin, V.; Slezov, V., Doping Nanoparticles. *Technical Physics Letters* **2004,** 30, (5), 367-369.

73. Pastoriza-Santos, I.; Koktysh, D. S.; Mamedov, A. A.; Giersig, M.; Kotov, N. A.; Liz-Marzan, L. M., One-pot synthesis of Ag@$TiO_2$ core-shell nanoparticles and their layer-by-layer assembly. *Langmuir* **2000**, 16, (6), 2731-2735.

74. Ito, T.; Sun, L.; Crooks, R. M., Simultaneous determination of the size and surface charge of individual nanoparticles using a carbon nanotube-based coulter counter. *Analytical Chemistry* **2003**, 75, (10), 2399-2406.

75. Oregan, B.; Gratzel, M., A Low-cost, High-efficiency Solar-cell based on dye sensitized colloidal $TiO_2$ films. *Nature* **1991**, 353, (6346), 737-740.

76. Micheletto, R.; Fukuda, H.; Ohtsu, M., A Simple method for the production of a two-dimensional, ordered array of small latex particles *Langmuir* **1995**, 11, (9), 3333-3336.

77. Bedja, I.; Hotchandi, S.; Kamat, P. V., Photoelectrochemistry of quantized tungsten trioxide colloids: electron storage, electrochromic, and photoelectrochromic effects *Journal of Physical Chemistry* **1993**, 97, (42), 11064-70.

78. Dance, I. G.; Choy, A.; Scudder, M. L., Syntheses, properties, and molecular and crystal structures of (Me4N)4[E4M10(SPh)16] (E = sulfur or selenium; M = zinc or cadmium): molecular supertetrahedral fragments of the cubic metal chalcogenide lattice *Journal of American Chemical Society* **1984**, 106, (21), 6285-90.

79. Hayes, D.; Micic, O.; Nenadovic, M. T.; Swayambunathan, V.; Meisel, D., Radiolytic production and properties of ultrasmall cadmium sulfide particles *Journal of Physical Chemistry* **1989**, 93, (11), 4603-4608.

80. Brust, M.; Fink, J.; Bethell, D.; Schiffrin, D. J.; Kiely, C., Synthesis and reactions of functionalized Gold nanoparticles. *Journal of the Chemical Society-Chemical Communications* **1995**, (16), 1655-1656.

81. Giersig, M.; Mulvaney, P., Preparation of Ordered Colloid Monolayers by Electrophoretic Deposition. *Langmuir* **1993,** 9, (12), 3408-3413.

82. Resch, U.; Eychmuller, A.; Haase, M. W., H., Absorption and Fluorescence Behavior of Redispersible Cds Colloids in Various Organic-Solvent *Langmuir* **1992,** 8, (9), 2215-2218

83. Badia, A.; Gao, W.; Singh, L.; Demers, L.; Cuccia, L.; Reven, L., Structure and Chain Dynamics of Alkanethiol-Capped Gold Colloids *Langmuir* 1996, 12, (5), 1262-69.

84. Ung, T.; Liz-Marzan, L. M.; Mulvaney, P., Controlled method for silica coating of silver colloids. Influence of coating on the rate of chemical reactions. *Langmuir* **1998,** 14, (14), 3740-3748.

85. Furlong, D. N., *In The Chemistry of Colloidal Silica*. American Chemical Society: Washington, DC, **1994.**

86. Kawahashi, N.; Matijevic, E., Preparation and properties of uniform coated colloidal particles : V. Yttrium basic carbonate on polystyrene latex. *J. Colloid Interface Sci.* **1990**, 138, (2), 534-542.

87. Philipse, A. P.; van Bruggen, M. P. B.; Pathmamanoharan, C., Magnetic silica dispersions: preparation and stability of surface-modified silica particles with a magnetic core *Langmuir* **1994**, 10, (1), 92-99.

88. LizMarzan, L. M.; Giersig, M.; Mulvaney, P., Synthesis of nanosized gold-silica core-shell particles. *Langmuir* **1996**, 12, (18), 4329-4335.

89. Kamat, P. V., Photochemistry on nonreactive and reactive (semiconductor) surfaces *Chemical Review* **1993**, 93, (1), 267-300.

90. Pastoriza-Santos, I.; Liz-Marzan, L. M., Formation and stabilization of Silver nanoparticles through reduction by *N*,*N*-Dimethylformamide *Langmuir* **1999**, 15, (4), 948-951.

91. Scolan, E.; Sanchez, C., Synthesis and characterization of surface-protected nanocrystalline Titania particles *Chemical Materials* **1998**, 10, (10), 3217-23.

92. Dawson, A.; Kamat, P. V., Semiconductor- Metal Nanocomposites. photoinduced fusion and photocatalysis of Gold-capped $TiO_2$ /Gold nanoparticles. *Journal of Physical Chemistry B* **2001,** 105, 960-966.

93. Kamat, P. V.; Hirakawa, T., Photoinduced charge separation in semiconductor-metal and chromophore-metal nanoassemblies. *Abstracts of Papers of the American Chemical Society* **2004,** 228, U24-U24

94. Briggs, D.; Seah, M. P., *Practical Surface Analysis*. Chichester, **1996**; Vol. 1.

95. Birer, O.; Sayan, S.; Suzer, S.; Aydinli, A., XPS investigation of thin SiOx and SiOxNy overlayers. *Journal of Molecular Science* **1999**, 480, 611-614.

96. Ishizaka, A.; Iwata, S., Si-$SiO_2$ interface characterization from angular dependence of X-Ray Photoelectron Spectra. *Applied Physics Letters* **1980**, 36, (1), 71-73.

97. Barr, T. L., Studies in Differential Charging. *J. Vac. Sci. Technol. A* **1989**, 7, (3), 1677-1683.

98. Ulgut, B.; Suzer, S., XPS studies of $SiO_2$/Si system under external bias. *Journal of Physical Chemistry B* **2003**, 107, (13), 2939-2943.

99. Boyen, H. G.; Kastle, G.; Weigl, F.; Koslowski, B.; Dietrich, C.; Ziemann, P.; Spatz, J. P.; Riethmuller, S.; Hartmann, C.; Moller, M.; Schmid, G.; Garnier, M. G.; Oelhafen, P., Oxidation-resistant gold-55 clusters. *Science* **2002**, 297, (5586), 1533-1536.

100. Cao, Y. W.; Din, R. C.; Mirkin, C. A., Ag/Au coreshell nanocrystal as a biological marker. *Abstracts of Papers of the American Chemical Society* **2001**, 222, U312-U313.

101. Dabbousi, B. O.; RodriguezViejo, J.; Mikulec, F. V.; Heine, J. R.; Mattoussi, H.; Ober, R.; Jensen, K. F.; Bawendi, M. G., (CdSe)ZnS core-shell quantum dots: Synthesis

and characterization of a size series of highly luminescent nanocrystallites. *Journal of Physical Chemistry B* **1997**, 101, (46), 9463-9475.

102. Hoener, C. F.; Allan, K. A.; Bard, A. J.; Campion, A.; Fox, M. A.; Mallouk, T. E.; Webber, S. E.; White, J. M., Demonstration of a shell-core structure in layered cadmium selenide-zinc selenide small particles by x-ray photoelectron and Auger spectroscopies *Journal of Physical Chemistry* **1992**, 96, (9), 3812-3817.

103. Katari, J. E. B.; Colvin, V. L.; Alivisatos, A. P., X-Ray Photoelectron-Spectroscopy of Cdse nanocrystals with applications to studies of the nanocrystal surface. *Journal of Physical Chemistry* **1994**, 98, (15), 4109-4117.

104. Koktysh, D. S.; Liang, X. R.; Yun, B. G.; Pastoriza-Santos, I.; Matts, R. L.; Giersig, M.; Serra-Rodriguez, C.; Liz-Marzan, L. M.; Kotov, N. A., Biomaterials by design: Layer-by-layer assembled ion-selective and biocompatible films of $TiO_2$ nanoshells for neurochemical monitoring. *Advanced Functional Materials* **2002**, 12, (4), 255-265.

105. Liu, S.; Ma, Y.; Armes, S. P.; Perruchot, C.; Watts, J. F., Direct verification of the core-shell structure of shell cross-linked micelles in the solid state using X-Ray Photoelectron Spectroscopy *Langmuir* **2002**, 18, 7780-7784.

106. Liu, Y. C.; Chuang, T. C., Synthesis and characterization of Gold/Polypyrrole core-shell nanocomposites and elemental gold nanoparticles based on the gold-containing nanocomplexes prepared by electrochemical methods in aqueous solutions. *Journal of Physical Chemistry B* **2003**, 107, (45), 12383-12386.

107. Piyakis, K. N.; Yang, D. Q.; Sacher, E., The applicability of angle-resolved XPS to the characterization of clusters on surfaces. *Surface Science* **2003**, 536, (1-3), 139-144.

108. Werthein, G. K.; DiCenzo, S. B., Cluster growth and core-electron binding energies in supported metal clusters *Physical Review B* **1988**, 37, (2), 844-847.

109. Yang, D. Q.; Gillet, J. N.; Meunier, M.; Sacher, E., Room temperature oxidation kinetics of Si nanoparticles in air, determined by x-ray photoelectron spectroscopy. *Journal of Applied Physics* **2005**, 97, (024303), 1-6.

110. Yang, D. Q.; Meunier, M.; Sacher, E., The surface modification of nanoporous SiOx thin films with a monofunctional organosilane. *Applied Surface Science* **2005,** 252, (5), 1197-1201.

111. Cao, Y. W.; Banin, U., Growth and properties of semiconductor core/shell nanocrystals with InAs cores. *Journal of the American Chemical Society* **2000**, 122, (40), 9692-9702.

112. Ertas, G.; Demirok, U. K.; Atalar, A.; Suzer, S., X-Ray Photoelectron Spectroscopy for resistance-capacitance measurements of surface structures. *Applied Physics Letters* **2005**, 86, (18), 183110-183113.

113. Tunc, I.; Demirok, U. K.; Suzer, S.; Correa-Duatre, M. A.; Liz-Marzan, L. M., Charging/discharging of Au (core)/silica (shell) nanoparticles as revealed by XPS. *Journal of Physical Chemistry B* **2005**, 109, (50), 24182-24184.

114. Tunc, I.; Suzer, S.; Correa-Duarte, M. A.; Liz-Marzan, L. M., XPS characterization of Au (Core)/$SiO_2$ (shell) nanoparticles. *Journal of Physical Chemistry B* **2005**, 109, (16), 7597-7600.

115. Iwata, S.; Ishizaka, A., Electron spectroscopic analysis of the SiO2/Si system and correlation with metal–oxide–semiconductor device characteristics. *Journal of Applied Physics* **1996**, 79, (9), 6653-7411.

116. Kobayashi, H.; Kubota, T.; Kawa, H.; Nakato, Y.; Nishiyama, N., Oxide thickness dependence of energy shifts in the Si 2p levels for the $SiO_2$/Si structure, and its elimination by a palladium overlayer. **1998,** 73, 933.

117. Seah, M. P., *Practical Surface Analysis*. Wiley: New York, **1999**; Vol. 1, p 541.

118. Chan, W. M.; Kwork, R. W. M.; Lau, W. M., Modified surface charge spectroscopy for the characterization of insulator/semiconductor structures. *Journal of Applied Physics* **1996**, 79, (7), 3635-3639.

119. Lau, W. M., Effects of a depth-dependent specimen potential on X-Ray Photoelectron spectroscopic data. *Journal of Applied Physics* **1989**, 65, (5), 2047-2052.

120. Lau, W. M., A surface charging technique in photoemission spectroscopic studies of dielectric-semiconductor structures. *Journal of Applied Physics* **1990**, 67, (3), 1504-1509.

121. Thomas, J. H. I.; Bryson, C. E. I.; Pampolone, T. R., X-Ray Photoelectron Spectroscopy surface charge buildup used to study residue in deep features on integrated circuits *Journal of Vacum Science and Technology B* **1988**, 6, (4), 1081-1087.

122. Giersig, M.; Ung, T.; Liz-Marzan, L. M.; Mulvaney, P., Direct observation of chemical reactions in silica-coated gold and silver nanoparticles. *Advanced Materials* **1997**, 9, (7), 570-575.

123. Linnert, T.; Mulvaney, P.; Henglein, A., Surface chemistry of colloidal silver: surface plasmon damping by chemisorbed iodide, hydrosulfide (SH-), and phenylthiolate *Journal of Physical Chemistry* **1993**, 97, (3), 679-682.

124. Fernandez, E. M.; Soler, J. M.; Garzon, I. L.; Balbas, L. C., Trends in the structure and bonding of noble metal clusters. *Physical Review B* **2004**, 70, (16).

125. Karadas, F.; Ertas, G.; Suzer, S., Differential charging in $SiO_2$/Si system as determined by XPS. *Journal of Physical Chemistry B* **2004**, 108, (4), 1515-1518.

126. Jablonski, A.; Powell, C. J., Comparisons of practical attenuation lengths obtained from different algorithms for application in XPS. *Surface Science* **2002**, 520, (1-2), 78-96.

127. Oldfield, G.; Ung, T.; Mulvaney, P., Au@$SnO_2$ core-shell nanoparticles. *Advanced Materials* **2000**, 12, (20), 1519-1522.

128. Smith, G. C., Evaluation of a simple correction for the hydrocarbon contamination layer in quantitative surface analysis by XPS. *Journal of Electron Spectroscopy and Related Phenomena* **2005**, 148, 21-28.

**APPENDIX:**

*MATLAB kod for the calculation of plot of thickness of the $SiO_2/TiO_2$ (shell) ($d_s$), radius of the Ag(core) ($r_s$) and the calculated intensity ratio of Ag to $SiO_2/TiO_2$:*

```
clear; close all; clc;

%%%
```

```
b2 = 0.05135;

b3 = 0.45982;


% rs1 = rc+dd;

% rs2 = rc;

%

% xc = rc/lc;

% Sc = ((b1*xc*xc + b2*xc + 1)/(b1*xc*xc + b3*xc + 1)*dd + lc)/(dd+lc);

% Sc = Sc * exp(-dd/ls) * pi*lc^3*(xc^2+0.5*((2*xc+1)*exp(-2*xc)-1));

%

% xs1 = rs1/ls;

% xs2 = rs2/ls;

% Ss = pi*ls^3*(xs1^2+0.5*((2*xs1+1)*exp(-2*xs1)-1)) -

pi*ls^3*(xs2^2+0.5*((2*xs2+1)*exp(-2*xs2)-1));

%

% (dc/ds)*(Sc/Ss)


rc = linspace(rc1,rc2,200)';

dd = linspace(dd1,dd2,200)';


for q9 = 1:length(rc)

   for r9 = 1:length(dd)

      y1(q9,r9) = hesapla(rc(q9),dd(r9),lc,ls,dc,ds);
```

```
        r1r2(q9,r9) = rc(q9) + j*dd(r9);
    end
end
imagesc(dd,rc,y1);
colorbar;
ylabel('R_c')
xlabel('d_s')
title('Intensity Ratio')

ind = find(y1>0.343 & y1<0.345);
rc2 = real(r1r2(ind));
dd2 = imag(r1r2(ind));

Cc = 4*pi*eps0*epsr./(1./rc2 - 1./(rc2+dd2))*1e-9;
Dv = 1.07;
Qq = Cc*Dv/1.6e-19;
% figure;
% plot3(rc2,dd2,Qq);
figure; plot(Qq(ind))
min(Qq)
rc2(1)
dd2(1)
figure;plot(dd2,rc2); xlabel('d_s');ylabel('R_c'); title('Intensity Ratio = 0.344')
```

```
figure(3)
set(gca,'FontSize',10);
set(gca,'FontName','times');
set(get(gca,'Xlabel'),'FontSize',12,'FontName','times');
set(get(gca,'Ylabel'),'FontSize',12,'FontName','times');
set(get(gca,'Title'),'FontSize',12,'FontName','times');
set(gcf, 'PaperPositionMode', 'manual');
set(gcf, 'PaperUnits', 'inches');
set(gcf, 'PaperPosition', [0.25 2.5 5.6 4]);
% print -depsc -r600 Figure5a

function y = hesapla(rc,dd,lc,ls,dc,ds)

b1 = 0.00289;
b2 = 0.05135;
b3 = 0.45982;

rs1 = rc+dd;
rs2 = rc;

xc = rc/lc;
Sc = ((b1*xc*xc + b2*xc + 1)/(b1*xc*xc + b3*xc + 1)*dd + lc)/(dd+lc);
```

```
Sc = Sc * exp(-dd/ls) * pi*lc^3*(xc^2+0.5*((2*xc+1)*exp(-2*xc)-1));


xs1 = rs1/ls;

xs2 = rs2/ls;

Ss = pi*ls^3*(xs1^2+0.5*((2*xs1+1)*exp(-2*xs1)-1)) -

pi*ls^3*(xs2^2+0.5*((2*xs2+1)*exp(-2*xs2)-1));


y = (dc/ds)*(Sc/Ss);
```